Design of an Electric Servo controlled Rudder pedal for an airplane simulator

Optimize the servo controller for the system

A. Damman B.Sc.

Master Thesis

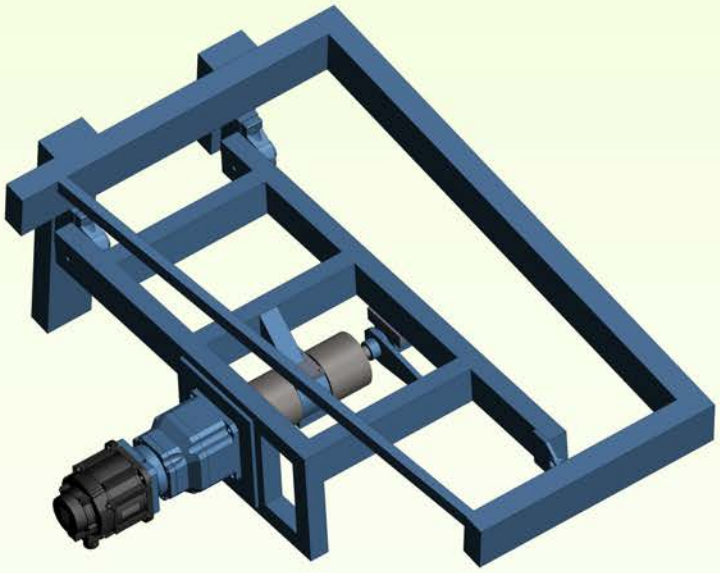

Hogeschool van Arnhem en Nijmegen
HAN University of Applied Sciences

HAN Control and Systems Engineering

Design of an Electric Servo controlled Rudder pedal for an airplane simulator

Optimize the servo controller for the system

Master Thesis

For the degree of Master in Mechatronics at HAN University of Applied Science

A. Damman B.Sc.

August 16, 2013

Faculty of Technic and Life Science · HAN University of Applied Science

The work in this thesis was supported by Yaskawa. Their cooperation is hereby gratefully acknowledged.

Copyright © Control and Systems Engineering
All rights reserved.

Summary

A Servo controlled control loading system for a fixed based simulator is converted from hydraulic to electric. In this thesis is explained how a high performed hydraulic servo system is exchanged for an electrical servo motor via EtherCAT.

The first reason is the advantage in maintenance costs and safety items when using an electrical servo motor. The second reason is noise influence on the analog signal to the servo controller. This is an advantage in comparison to the old situation. The disadvantage is the high volume-power-ratio of an electrical servo motor in comparison with a hydraulic servo system.

To reduce the load torque at the motor side, a gearing is necessary. For selecting the correct gearing, the load inertia is taken into account, that the inertia is lower than 2 times of the selected motor inertia. A backlash free gearbox will improve the results, but is this the best solution? The maximum acceleration rate of the specific motor will take effect on the total acceleration time to reach the maximum speed of the motor. A trapezium test profile is commonly used, but in our system not useful. A sinusoidal test signal is a useful solution to avoid hitting the hard end stops.

The control loop can be made in several ways, explained are: position, velocity and force (torque) control loop. The best simulated results are obtained by the force (torque) control loop. However force prediction is a problem in this situation. From a practical point of view, the signal-noise-ratio is a problem for the servo controller certainly in an extreme field of electromagnetic compatibility. Best possible grounding and shielding of the power and the sensor cables is a guidance for a reliable signal-noise-ratio.

In this specific arrangement, the signal-noise-ratio is low for the torque sensor, however the velocity control loop is a sufficient signal. Therefore a control loop based on velocity is the best practical solution to reduce the jerky effects of the system. An additional reliable torque sensor to assist the actual value is the best improvement. For now the best option is to implement the servo controller in a digital EtherCAT environment.

The implementation of a synchronized Distributed Clock will improve the results. Some disturbance in the timing during the validation tests is noticed.

The bandwidth necessary for aircraft simulation (FCS) goes up till 2 Hz or 12.6 rad/s. The FCS is commonly modeled as a second order system. For good simulation, the cut-off frequency of the actuator needs preferable 10 times higher. For an admissible simulation of hard-end stops, a cut-off frequency of 50 Hz or higher is preferable at the desired position.

The cut-off frequency of the ideal simulated hydraulic actuator (velocity loop) is 5550 rad/s or 883 Hz. The cut-off frequency of the electrical servo system is 14.7 Hz at the maximum velocity.

The signal-noise-ratio of the torque sensor is very poor. The single ended torque signal does have a signal-noise-ratio of 500/18, and this is useless for torque control loop. The differential signal has an improved signal-noise-ratio of 500/3. The accuracy is of the attached HBM torque sensor is 0.2% and the overall accuracy is 0.5%. The disappointing signal-noise-ratio of the torque sensor and the open control loop in cyclic torque mode, makes the decision to choose for a decent velocity inner loop and a torque (force) outer loop.

The mass and added mass of a human body cannot be accounted very accurate because you simply do not know anything of the reaction force of the subject in the time domain and this is far from constant in time domain. The accuracy of the position and velocity encoder is $1.9 \cdot 10^{-7}$% (within a window of 5 steps at nominal velocity) much higher than the accuracy of the torque level 0.1% of the rated torque. This torque is calculated in the servo pack as a result of the forward current to the motor. The accuracy of the servo pack torque level is 3% at the pedal side when the gear ratio is applied.

The implemented control loop meets the requirements. A simple second order mass-spring-damper system converts the required force into a velocity. The inner loop is based on velocity and the outer loop is a torque control loop. A graphical presentation is obtained from the results of the evaluation experiment.

The safety environment in the old hydraulic situation is less sufficient. In the new electric servo drive system, there is full control over the behavior of the pedals. This is satisfactory better compared to the hydraulic situation. The safety is grouped in several layers: a hardware layer (mechanical end stops), Hardware Base Block (HBB) in the servo pack and a software environment layer. In the old situation there was only a software environment layer what was actually taken care of the safety of the subject.

Please don't hesitate to contact me if you have any further questions: alwindamman@gmail.com.

Preface

This document is part of my Master graduation thesis. The idea of doing my thesis on this subject came after a discussion about maintenance costs of hydraulic systems with my colleagues F.N. Postema and H. Lindenburg.

I am very grateful that Mr. H. Lindenburg and prof. M. Mulder gave me the possibility to exchange a reliable hydraulic actuator for an unfamiliar technique with electrical servo drive system. This has never been done before in our group. The scientific staff in our work team are not so enthusiastic about electrical servo drive systems in performance respect. Hydraulic servo actuators are excellent in that respect. The high force and small volume relation is very powerful for a wide range of applications. In most cases, a hydraulic servo motor implementation is not necessary. The choice of a hydraulic servo system over an electrical servo drive system is made because of lack of space. In most cases the dimensions of an electrical drive system are in conflict with the construction environment.

In high performance point of view, a solution with a high torque motor is the ultimate solution. Due to financial restrictions, it was not possible to implement such a high torque motor for this first attempt of electrifying the system. In other situations it is preferable to select a servo drive where the inertia of the motor is at least 1/5 of the total load inertia. The system feels a little nervous when the inertia of the selected motor is more than five times of the inertia of the load. When using a backlash free gearbox, the high performance can be reached with a smaller size motor. To optimize the system, I did select the smallest motor, so that speed and torque both can be reached continuously. The challenge is to tune the system in a way that both aspects can be reached. And most important in all situations the system should "feel" smooth like a real airplane. Another challenge is to tune the system for a generic configurable airplane.

The first reason to write this report is of course a report of my master thesis in control and system engineering. The second less important reason is to order the steps that are followed to develop the rudder pedals system and this documentation is a good start for further improvement for this system. The project oriented information is moved to the appendix as much as possible. To understand these information it is recommended to read the thesis report first.

Acknowledgments

I would like to thank my HAN University of Applied Sciences (HAN University) supervisor ir. P.A.C. Ypma at the department CSE for his assistance during the writing of this thesis. Also his general and global knowledge to setup this master thesis. His knowledge about LaTeX to make this document is really an eye opener for now and the future. I can recommend everyone using LaTeX . For more information read [1]. The next person, I would like to thank is my company supervisor from the department CS at the TU Delft dr.ir. M.M. van Paassen for his assistance during the writing of this thesis, his control knowledge and the knowledge about the set up of the specifications [2].

My colleague ir. F.N. Postema was very helpful with assisting me selecting and installing the servo system. His enormous experience in building servo systems helped detailing the system step by step.

Two people who had made this thesis project possible in financial and administrating respects are Prof.dr.ir. M. Mulder and ing. H. Lindenburg. Ing. A. Muis and ing. E.H.H. Thung made the communication possible to get the drive system running via Linux Etherlab.

Last but not least, my girlfriend G.M. Fontijn. I really appreciate her incredible support during my thesis. She made a lot of improvements on the first draft of this thesis. I love you Gyselle, it's you and me together forever and never apart, maybe in distance, but never in heart.

Arnhem, HAN University of Applied Science A. Damman B.Sc.
August 16, 2013

Glossary

List of Acronyms

CSE	Control and Systems Engineering
TU Delft	Technical University of Delft
TU Twente	Technical University of Twente
HAN University	HAN University of Applied Sciences
DUECA	Delft University Environment for Communication and Activation
LQR	Linear-Quadratic Regulator
EtherCAT	Ethernet for Control Automation Technology
LaTeX	Leslie Lamport TEX typesetting language
FCS	Flight Control System
HBM	Hottinger Baldwin Messtechnik
EtherLab	open source toolkit for real time Linux using EtherCAT-Technology
IgH	Ingenieurgemeinschaft Hydraulik
AC	Alternating Current
DC	Direct Current
EMF	Electromagnetic Field
EMI	Electromagnetic Interference
EMC	Electromagnetic Compatibility
CANopen	open Controller Area Network
HF	High Frequency

EMP	Electromagnetic Pulse
PDO	Process Data Object
SDO	Service Data Object
Linux	open source operating system
SGDV	electric servo amplifier of brand Yaskawa
CS	Control and Simulation department at the TU
NASA	National Aeronautics and Space Administration
FBW	Fly-By-Wire
MIL	United States Military Standard
Compax3	electic servo controller type of brand Parker
RS422	Differential signaling protocol
AISI	American Iron and Steel Institute
DAQ	Data Acquisition
NEN	NEderlandse Norm
SGMGV	electric servo motor type of brand Yaskawa
SGMCS	electric servo motor type of brand Yaskawa
RPM	Revolutions Per Minute
RPS	Revolutions Per Second
RMS	Root Mean Square
FFT	Fast Fourier Transfer function
Twincat	Communication protocol which correspond with EtherCAT
A/D	Analog to Digital Conversion
D/A	Digital to Analog Conversion
IEEE	Institute of Electrical and Electronics Engineers
UDP	User Datagram Protocol
IP	Internet Protocol
I/O	Input / Output
MAC	Media Access Control
IEC	International Engineering Consortium

FTP	File Transfer Protocol
FPGA	Field-Programmable Gate Array
ASIC	Application-Specific Integrated Circuit
Sercos	SErial Real-time COmmunication System
OSI	Open Systems Interconnection

List of Symbols

Abbreviations

α	acceleration rate [rad/s^2]
Δp	pressure difference over piston [N/m^2]
δ	skin depth is the depth below the surface of the conductor at which the current density has fallen to 1/e of J_S [m]
η	efficiency [-]
μ	absolute magnetic permeability of the conductor [Wb/(A $\cdot$ m)]
ω	angular frequency of current [rad/s]
ω_0	$\sqrt{\frac{4 \cdot \mathrm{E} \cdot \mathrm{A_p}}{\mathrm{m_{effp}} \cdot \mathrm{S_p}}}$[-]
ω_m	motor speed [rad/s]
ρ_r	resistivity of the conductor [$\Omega\cdot$ m]
ζ_e	damping of the electric servo [-]
ζ_h	damping of the hydraulic servo [-]
A_p	area of the piston [m^2]
b_{sim}	effective damping of the simulated system [Ns/m]
c_{sim}	effective stiffness of the simulated system [N/m]
c_t	coefficient of rigid mechanical construction of the system [Nm/rad]
d	depth [m]
E	bulk modulus of the oil [N/m]
EMF_b	back EMF [mV/rpm/phase]
F_a	force connection rod [N]
F_b	force hydraulic actuator [N]
F_{pd}	force at pedal side [N]
f_{res}	resonance frequency of the electric servo drive system [Hz]
g	standard gravity [m/s^2]
i_1	gear ratio of the first force lever of at the rudder pedals [-]
i_2	gear ratio of the second force lever of at the rudder pedals [-]
i_T	total gear ratio of the force levers of at the rudder pedals [-]

I_i	motor instantaneous peak current RMS [A]
i_{max}	maximum value electrical input signal [A]
I_r	motor rated current [A]
J_S	current density at the surface [A $\cdot$ m^2]
J_{AC}	AC current density [A $\cdot$ m^2]
J_l	load inertia of the electric servo drive system [kg $\cdot m^2$]
J_m	motor inertia of the electric servo drive system [kg $\cdot m^2$]
J_r	reflected load inertia [kg $\cdot m^2$]
J_t	total inertia of the electric servo drive system [kg $\cdot m^2$]
K_v	specific velocity gain of the servo [-]
K_1	$= q_{max}/i_{max}$ gain between electrical input signal and oil flow [-]
K_2	$= \left(\frac{2\cdot\zeta}{\omega_0} - \frac{L_c \cdot m_{effp}}{Ap^2}\right) \cdot \frac{A_p}{K_1}$ gain of acceleration feedback of the servo [-]
K_3	$= \frac{K_v \cdot A_p}{K_1}$ gain between physical input and the electrical servo input [-]
K_b	back EMF constants [V/(rad/s)]
K_{ff}	feedforward gain [-]
K_m	motor torque constants [Nm/A]
L_c	leakage coefficient [m^5/Ns]
L_{hp}	inductance [mH/phase]
L_h	motor inductance constants [H]
l_{i_2}	Lever arm length from F_a to the second pedal shaft axis [m]
l_{i_2}	Lever arm length from F_a to the second pedal shaft axis [m]
m_{effp}	effective mass at the piston [kg]
M_{omd}	mass above measurement device [kg]
m_{sim}	effective mass of the simulated system [kg]
N_p	number of poles or phase [-]
P_r	motor power rated output [kW]
q_l	oil flow due to leakage [m^3/s]
q_c	oil flow due to compression [m^3/s]
q_{max}	maximum oil flow generated by the servo [m^3/s]
q_s	oil flow generated by the hydraulic servo [m^3/s]
q_{xp}	oil flow due to piston movement [m^3/s]
R	motor winding resistance [Ohm]
R_p	resistance per phase [Ohm/phase]
R_g	gear ratio of the control device [-]
R_i	inertia ratio [-]
RA_a	motor rated angular acceleration [rad/s^2]
RP_r	motor rated power rate [kW/s]
$s_{ActuatorMax}$	maximal displacement of the hydraulic actuator [m]
S_m	motor maximal speed [RPM]
S_p	stroke of the piston [m]

$s_{RudderMax}$	maximal displacement of the pedal [m]
S_r	motor rated speed [RPM]
T_2	Torque at the pedal shaft [Nm]
T_2	Torque at the pedal shaft [Nm]
T_a	acceleration torque [Nm]
T_i	motor instantaneous peak torque [Nm]
T_r	motor rated torque [Nm]
T_s	settling time [s]
V_a	supply voltage to the DC motor [VDC]
V_{bs}	supply voltage to the brushless DC motor [DC Volt]
V_{class}	voltage rated class between two phases RMS [VAC]
X_c	displacement of control device [m]
x_d	desired position [m]
'B'	breakout force ['lbs']
'M'	force at maximum travel ['lbs']
'X'	maximum travel ['in']

Table of Contents

Summary i

Preface iii

Acknowledgments v

Glossary vii

List of Acronyms . . . vii

List of Symbols . . . ix

1 Introduction 1

1-1 Background Rudder pedals HMI-Laboratory . . . 1

1-2 Process Description Rudder pedals Setup . . . 1

1-2-1 Objectives . . . 2

1-3 Sizing and Design . . . 3

1-4 Approach . . . 4

1-5 Chapter summary . . . 5

2 Flight Control System 7

2-1 Aircraft Flight Control System . . . 7

2-1-1 Primary controls . . . 7

2-1-2 Secondary controls . . . 8

2-2 Mechanical Flight Control System . . . 8

2-3 Hydraulic-mechanical Flight Control System . . . 8

2-4 Fly-by-wire control systems . . . 10

2-5 Comparison the rudder performance of 6 different vehicles . . . 10

2-6 Dynamic Force/Feel System Considerations . . . 13

2-7 Other Dynamic Effect acting on Force/Feel System . . . 14

2-8 Chapter summary . . . 15

3 Performed Solution **17**
3-1 Performed Solution . . . 17
3-2 Mechanical Identification . . . 17
3-3 Inertia of the drive system . . . 20
3-3-1 Mechanical analyses . . . 22
3-3-2 Acceleration torque . . . 23
3-4 Chapter summary . . . 23

4 Performance of the analytical models **25**
4-1 Hydraulic Servo Simulation . . . 27
4-2 Comparison of Position, Velocity and Force loop based Control Loading Architectures 28
4-2-1 Basics for Control Loading Simulation . . . 28
4-2-2 Subsystems . . . 28
4-3 Hydraulic Servo Identification . . . 32
4-3-1 Analytical performance evaluation . . . 35
4-3-2 Choice Type of Control Loop . . . 37
4-4 Electrical Servo Simulation . . . 37
4-4-1 Matlab/Simulink model . . . 38
4-4-2 Feedforward value for simulation . . . 41
4-4-3 Simplified synchronous brushless servomotor model . . . 47
4-4-4 Simulated Acceleration Bandwidth . . . 48
4-5 Comparison Hydraulic and Electrical Servo Simulation . . . 50
4-6 Implementation possibilities for the selected servo drive . . . 52
4-7 Chapter summary . . . 52

5 Performance evaluation experiment **53**
5-1 Rudder pedal Impression . . . 53
5-2 Results of the velocity control loop . . . 56
5-2-1 Start stop input response . . . 57
5-2-2 Sinusoidal cyclic signal . . . 58
5-2-3 Noise on torque signal . . . 60
5-2-4 Added mass on rudder pedal . . . 61
5-2-5 Bode plot velocity control loop . . . 64
5-3 Chapter summary . . . 68

6 Discussion **69**
6-1 Discussion . . . 69

7 Conclusions **71**
7-1 Conclusions . . . 71

A Alternative Solutions **73**
A-1 Alternative Solution 1 . . . 73
A-1-1 Mechanical solution . . . 74
A-2 Alternative Solution 2 . . . 75
A-3 Alternative Solution 3 . . . 76
A-4 Alternative Solution 4 . . . 76
A-5 Cost Analysis . . . 78
A-6 Compare 4 Alternative Solutions . . . 79
A-6-1 Energy Balance . . . 79
A-6-2 Supposed Solution . . . 79

B Installation Yaskawa Servo Drive **81**
B-1 Overview Components . . . 82
B-2 Overview Wiring . . . 85
B-3 EtherCAT State flow . . . 86
B-4 Yaskawa Drive State flow . . . 87
B-5 Modes of operation SGDV servopack . . . 87
B-5-1 Profile Position mode . . . 88
B-5-2 Interpolated Position mode . . . 89
B-5-3 Cyclic Synchronous Position mode . . . 89
B-5-4 Homing mode . . . 90
B-5-5 Profile Velocity mode . . . 90
B-5-6 Cyclic Synchronous Velocity mode . . . 91
B-5-7 Torque Profile mode . . . 91
B-5-8 Cyclic Synchronous Torque mode . . . 92

C Practical Implementation **93**
C-1 EMC . . . 93
C-1-1 Coupling mechanisms . . . 94
C-1-2 EMC control . . . 95
C-2 Skin effect . . . 96
C-3 Results Signal-Noise-Ratio after alleviation Skin effect . . . 98
C-4 Data Acquisition . . . 100
C-4-1 Oversampling factor . . . 100
C-5 EtherCAT Implementation . . . 101
C-5-1 CANopen over Ethernet (CoE) in the Yaskawa drive . . . 105
C-5-2 Linux Etherlab Communication . . . 105
C-6 CANopen . . . 106
C-6-1 Service Data Object (SDO) protocol . . . 108
C-6-2 Process Data Object (PDO) protocol . . . 108
C-7 Safety Rudder Pedal System . . . 109
C-7-1 Hardware layer . . . 109
C-7-2 Servo pack layer . . . 109
C-7-3 Software environment layer . . . 109

D Calibration **111**
D-1 Calibration setup torque transducer 111
D-2 Calibration torque transducer 113

Bibliography **115**

Chapter 1

Introduction

1-1 Background Rudder pedals HMI-Laboratory

When flying an aircraft, the feel of the rudder pedals provides feedback to the pilot about the yaw state of the aircraft. In a flight simulator this feeling needs to be simulated by the control loading device. The simulators at the Control and Simulation division are equipped with a hydraulic control loader.

At this moment a hydraulic driven controlled rudder system is installed in the research simulator Human Machine Interface Laboratory at the Delft University of Technology. The reason why this configuration does not fulfill the requirements at this moment, is the many man-hours to keep the system running. In maintenance respect this is not acceptable. The big advantage for a hydraulic driven actuator is the compact building method, the force/volume ratio for hydraulic is excellent. However it could be done electrical. This is the opinion of some colleagues working at the Faculty Aerospace Engineering, department Control and Systems.

The already installed electric servo driven motors for the side stick and also for the helicopter control do have an excellent performance. This was installed by the company Fokker Control Systems nowadays known as Moog Netherlands. To design a robust servo controller is a complicated task and a great challenge for a graduation project.

It is not an ordinary system with a fixed set-point for position or velocity, because the system should behave the same as in an airplane. Also the parameters of the mass-spring-damper system of a certain airplane are adjustable for simulation. The difficult aspect of this control model is the large operating bandwidth without oscillations.

1-2 Process Description Rudder pedals Setup

In our HMI-laboratory, there is a setup for a generic airplane simulator with side stick on the right hand side. For the rudder pedals on the right hand side, an used Fokker 50 rudder is

installed. Below is a picture of a Fokker 50 cockpit. In the pictures 1-2a, 1-2b and 1-2c the original set up in our HMI-laboratory is shown.

Figure 1-1: Rudder pedals Fokker 50

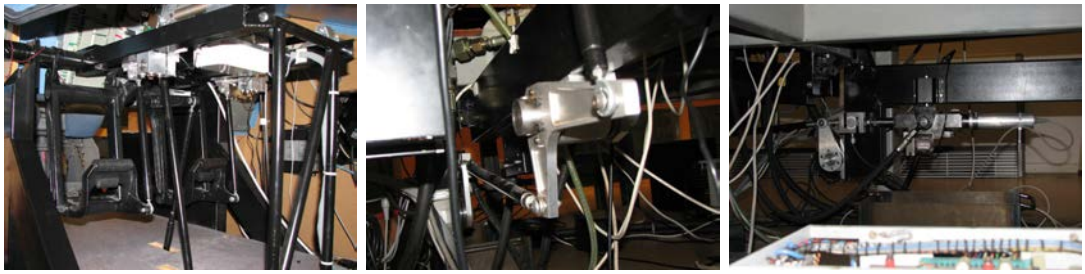

(a) First force lever **(b)** Second force lever **(c)** Hydraulic actuator

Figure 1-2: Original situation rudder pedals hinge system HMI-laboratory

1-2-1 Objectives

The described objective is the implementation of an electrical servo controlled motor that fulfill the requirements for the rudder pedals for a generic airplane based on the human factors. Develop a system that fulfills the design requirements and also "feels" realistic. Taking into account dynamic control, safety systems and human machine interface performances for research aspects like dynamic model identification.

Implement the supposed solution in the existing environment without loosing any performance of the actual system. Develop a solution what does fulfill the requirements in cost and performance. Improve the safety level at the hardware layer.

The process description is given in the Figure 1-3. The control loop of the HAN approach is used and is explained as followed: Design and implementation; Analytical analysis; Experimental Analysis. First the actual system will be identified. The implemented solution is presented and the control strategy for this particular system is explained in Chapter 4.

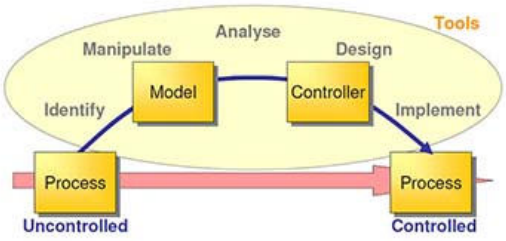

Figure 1-3: Control loop HAN

Several objectives have been defined for this graduation project:

- Literature study regarding the produced forces on the rudder. The limitations of these forces must be investigated together with the characteristics of speed of the movements.
- Human factor aspects only for the sizing of the control range.
- Research on airplane rudder pedals like damping and delay.
- Literature study regarding the defined controller. A closer look at the past might reveal similar problems and possible solutions to implement the controller well.
- Implementing developed controllers in existing hardware at HMI-laboratory to validate the conclusions drawn in this project.
- Develop a solution what does fulfill the requirements in cost and performance.
- Select the best option in consultation with the stakeholder.
- Comparison of the hydraulic system and electric system in bandwidth aspect.
- Develop a maintenance free system.

1-3 Sizing and Design

Some considerations for sizing and design of control loading devices are made by M.M. van Paassen, January 13, 2011. The units in aviation is normally expressed in US imperial units, therefore these imperial units are converted to metric units. The original literature quantities are expressed in US imperial units.

The following considerations need to be taken into account:

- Maximum force/moment level exerted by human. Pedals 150 lbf $\approx$ 667.23 N [3].
- Travel, Pedals 4 inches (measured from neutral, total travel 8 inches) $\approx$ 100 mm [3].
- Velocity, Max 2 Hz sinusoidal cycling at maximum travel of 4 inches. For a pedal; $(2 \cdot 2 \cdot \pi) \cdot 4$ (in) $\approx$ 50 (in/s) $\approx$ 1.3 m/s.

- Position bandwidth, When the simulator is configured as a position servo (simulating hard stops etc.), the maintain bandwidth is preferably 50 Hz or higher. Bandwidth should be at least 25 Hz.

- Force/moment from bandwidth, necessary for simulating hard stops. Consider effective mass of the device and add effective limb mass (some guesses: arm side stick roll 1 kg, arm side stick pitch 4 kg, arms column pitch 8 kg, arms column roll 3 kg, legs pedals 15 kg). Consider a ramp and hold input signal with half of the maximum velocity, and feed to a 2nd order system, $\zeta_e = 0.7$, ω_n as per the desired bandwidth. Calculate the acceleration at the start of the hold phase from that simulation (sufficient ramp to have achieved a constant velocity) and multiply by effective mass + limb mass to obtain required torque/force levels.

These particular values are obtained by keeping the NASA report [3] about the force/feel characteristics in mind. These conservative assumptions are taken to avoid possible compliance during the project that decrease the performance of the rudder pedal system. The required characteristic for the velocity is calculated for 2 Hz sinusoidal cycling at maximum travel. For example in an extreme situation, a human person can follow a 1 Hz cycling signal what is demanded on a sidestick. To follow such a signal by foot is not a very realistic situation.

1-4 Approach

The purpose of this thesis report is for two reasons. The first and most important goal is to document the scientific thesis information and the second reason is more relevant for further improvement in the future and report practical obstructions during the thesis process. The practical relevant implementation is moved to the appendices.

To understand the control challenge of the rudder system, some basic information is required. To tackle the control challenge, it is necessary to get a scope in a very large aspect to avoid difficulties during the engineering process. The performance of a generic rudder pedal is investigated especially for the Flight Control System.

The design specifications are set up and several options are developed to make the right decision. In total 4 alternative solutions are checked to make a decision and can be found in the Appendix A. The decision for the performed solution is based on several aspects like: costs, energy loss and performance.

An analytical performance check is executed before ordering the hardware. The acceleration rate is the most important item to predict the performance in comparison with a original hydraulic actuator.

After designing and ordering the parts, the parts are assembled properly to get the system up and running. This operation action of the motor and controller is made in 3 steps. First lets operate the motor in Windows mode, later in Linux mode and finally in the DUECA mode via EtherCAT. The second step was not easy due to different software versions inside the controller of Yaskawa.

Safety items are taken into account and are inside the controller on hardwired base block like proximity switches. Maximum torque rate, maximum velocity rate and limited positioning are also in the controller. In software there is also a limited range for these parameters to avoid emergency stops.

A performance evaluation test is executed to compare the analytical model with the realized installation.

At the end of the project, there is solved some minor difficulties concerning the adjustment of the rudder pedals in length for the well-known 95 percentile indicated human. Some EMC complications are solved to assure the robustness of the system and the quality of the acquired signal data.

The installation of an inclination transducer is used for correcting the adjustment range. The final step to use the system is the implementation into the DUECA environment. Delft University Environment for Communication and Activation (DUECA) is a middle layer real-time software package, developed in house by dr.ir. M.M. van Paassen. This software package makes it relatively easy to stream data into channels and hardware modules.

1-5 Chapter summary

Hydraulic control loading has to be changed by an electric servo controller without any loss on the performance of the bandwidth. A bandwidth check of the hydraulic model is performed to identify the bandwidth of the hydraulic actuator. The HAN approach is followed during this project. Design an electrical drive system what can meet the requirements.

- displacement 100 mm.
- velocity 1.3 m/s.
- force 667 N.
- 2 Hz sinusoidal cycling at desired velocity and desired displacement, $\zeta = 0.7$.
- hard-end stop simulation: start-up ramp to stationary velocity of 0.5 times the minimal velocity and stop immediately.
- The obtained bandwidth should be at 50 Hz or at least 25 Hz.

Additional project related information is available in the appendix for further improvement in the near future.

Chapter 2

Flight Control System

2-1 Aircraft Flight Control System

Aircraft flight control systems are classified as primary and secondary. The primary control systems consist of those that are required to safely control an airplane during flight. These include the ailerons, elevator (or stabilizer) and rudder. Secondary control systems improve the performance characteristics of the airplane, or relieve the pilot of excessive control forces.[4] Examples of secondary control systems are wing flaps and trim systems.

2-1-1 Primary controls

A control yoke (or control column), center stick or side-stick (or joystick) operate the aircraft's roll and pitch by moving the ailerons when turned or deflected left and right, and moves the elevators when the backward or forward rudder pedals are moved. The throttle controls manage the control engine speed or thrust of the powered aircraft. An explanation of the operating rudder pedals is explained in Figure 2-1.

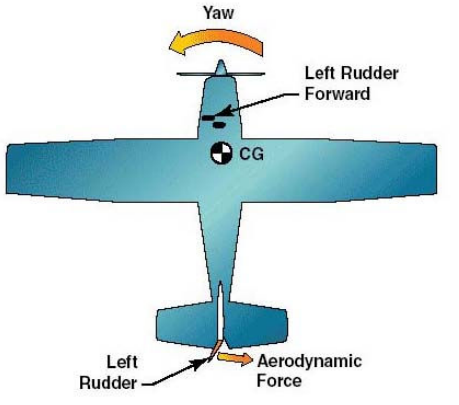

Figure 2-1: Rudder Control Aircraft [4]

2-1-2 Secondary controls

In addition to the primary flight controls for roll, pitch and yaw, there are often secondary controls available to give the pilot a more refined control over the aircraft or to ease the workload. The most commonly available control is a wheel or other device to control the elevator trim, so that the pilot does not have to maintain constant backward or forward pressure to hold a specific pitch attitude. Many aircrafts have wing flaps controlled by a switch or a mechanical lever. In some cases they are fully automatically computer controlled, which alter the shape of the wing for improved control at the slower speed used for take-off and landing. Other secondary flight control systems may be available, including slats, spoilers, air brakes and variable-sweep wings.

2-2 Mechanical Flight Control System

Mechanical or manually operated flight control systems are the most basic methods of controlling an aircraft. They were used in older aircrafts and are currently used in small aircrafts where the aerodynamic forces are not excessive.

A manual flight control system uses a collection of mechanical parts such as push rods, tension cables, pulleys, counterweights, and sometimes chains to transmit the forces applied to the cockpit controls directly to the control surfaces. Turnbuckles are often used to adjust control cable tension.

Increases in the control surface area, required by large aircraft or higher loads caused by high airspeed in small aircraft, lead to a large increase in the forces needed to move them. Consequently complicated mechanical gearing arrangements were developed to extract maximum mechanical advantage in order to reduce the forces required from the pilots. This arrangement can be found on bigger or higher performance propeller aircrafts such as the Fokker 50.

2-3 Hydraulic-mechanical Flight Control System

The complexity and weight of mechanical flight control systems increase considerably with the size and performance of the aircraft. Hydraulically powered control surfaces help to overcome these limitations. With hydraulic flight control systems, the aircraft's size and performance are limited for economic reasons rather than a pilot's muscular strength. At first, only partially boosted systems were used in which the pilot gets feedback of the feel of the aerodynamic loads on the control surfaces. The working of such a system is explained further on in this chapter, Figure 2-2 represent a hydraulic servo rudder system with load feel. The induced movement at the pedals are displaced via a stainless steel control cable to the hydraulic mechanical rudder servo system. A mechanical cantilever system with rods translate the movement to a movement in the hydraulic sliding control valve. Via a gain system in the servo valve, the hydraulic actuator starts to move. The feedback of the induced force is performed via a mechanical mass-spring-damper system. This force is limited where a human can handle these forces when the aircraft is in a controllable situation.

A hydraulic-mechanical flight control system has two parts:
The **mechanical circuit**, which links the cockpit controls with the hydraulic circuits. Like

the mechanical flight control system, it consists of rods, cables, pulleys, and sometimes chains. The **hydraulic circuit**, which has hydraulic pumps, reservoirs, filters, pipes, valves and actuators. The actuators are powered by the hydraulic pressure generated by the pumps in the hydraulic circuit. The actuators convert hydraulic pressure into control surface movements. The electro-hydraulic servo valves control the movement of the actuators.

The pilot's movement of a control causes the mechanical circuit to open the matching servo valve in the hydraulic circuit. The hydraulic circuit powers the actuators which then move the control surfaces. As the actuator moves, the servo valve is closed by a mechanical feedback linkage.

With purely mechanical flight control systems, the aerodynamic forces on the control surfaces are transmitted through the mechanisms and are felt directly by the pilot. With hydraulic mechanical flight control systems, however, the load on the surfaces cannot be felt and there is a risk of over stressing the aircraft through excessive control surface movement. To overcome this problem, artificial feel systems can be used.

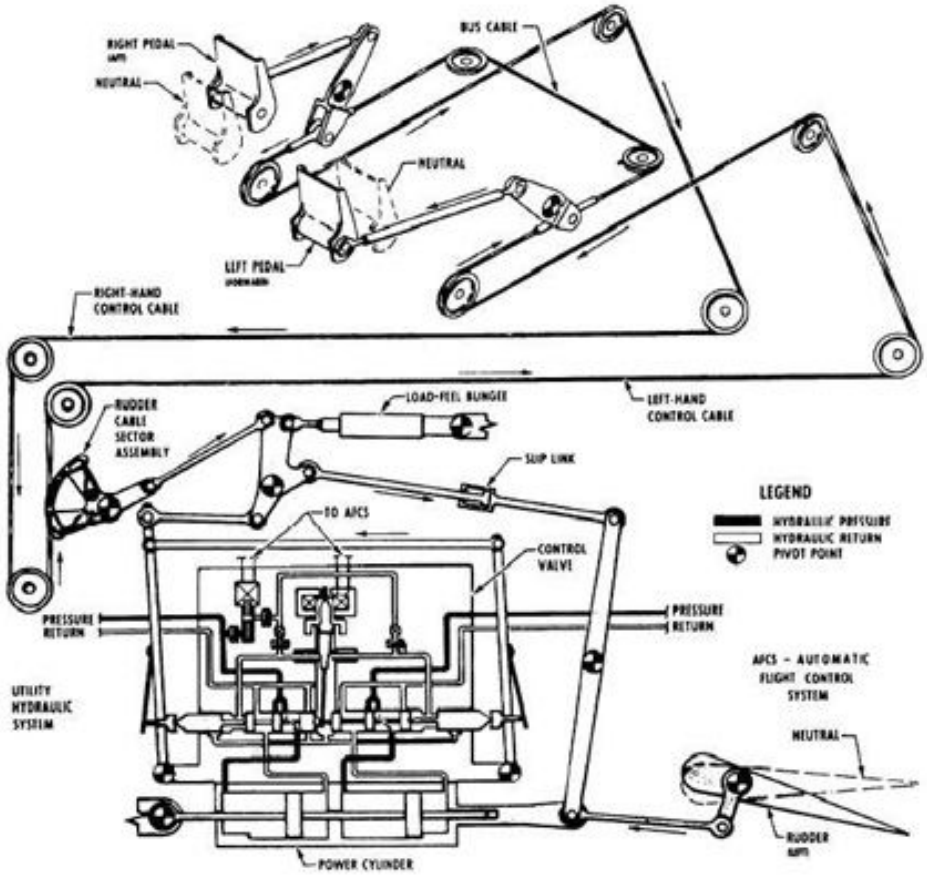

Figure 2-2: Hydraulic Servo Rudder Control Aircraft [5]

2-4 Fly-by-wire control systems

A fly-by-wire (FBW) system replaces the manual flight control of an aircraft with an electronic interface. The movements of flight controls are converted into electronic signals transmitted by wires (hence the fly-by-wire term), and flight control computers determine how to move the actuators at each control surface to provide the expected response. Commands from the computers are also input without the pilot's knowledge to stabilize the aircraft and perform other tasks. Electronics for aircraft flight control systems are part of the field known as avionics.

2-5 Comparison the rudder performance of 6 different vehicles

The pedal force/feel characteristics are defined in the Military Specification Flying Qualities of Piloted Airplanes (MIL-F-8785C). The Military Specification Flying Qualities of Piloted Airplanes (MIL-F-8785C) is very useful and defines the maximum allowable loads and deflection, however the characteristics are not completely defined. The use of a handling qualities rating scale Cooper-Harper is sensitive for different interpretation of the test pilots panel. In the past a comparison in pedal force/feel characteristics of 6 different vehicles has been done by R. Hess [6] and [7]. This a a representative method to compare the force-feel characteristics. In Figure 2-3 the double spring characteristics of the rudder pedals for a wide set of airplanes is shown. This is a typical system with three static pedal parameters ('M','B','X'), where 'M' is the Force at maximum travel 'X' and 'B' the transition point of the breakout force. Normally a stiff spring is suggested around the zero and a soft spring is suggested from the breakout force till the maximum travel.

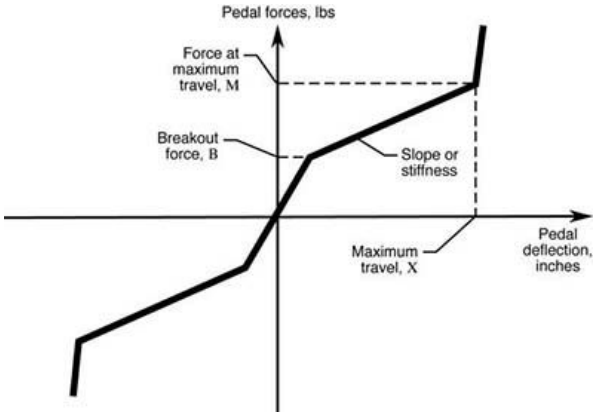

Figure 2-3: Pedal Characteristics (Force-Deflection) [6]

Pedal force/feel characteristics for the six vehicles just defined are obtained from a variety of sources by mr. R. Hess.

Table 2-1: Specific rudder pedal characteristics of 6 vehicle

Aircraft Abbreviation	Brand	Type Vehicle
A300-600	Airbus	Airplane
AH-64A	Apache	Rotorcraft
UH-60A	Blackhawk	Rotorcraft
CH-47D	Chinook	Rotorcraft
CH-53D	Sea Stallion	Rotorcraft
B-767	Boeing	Airplane
A300-B2-B4	Airbus	Airplane

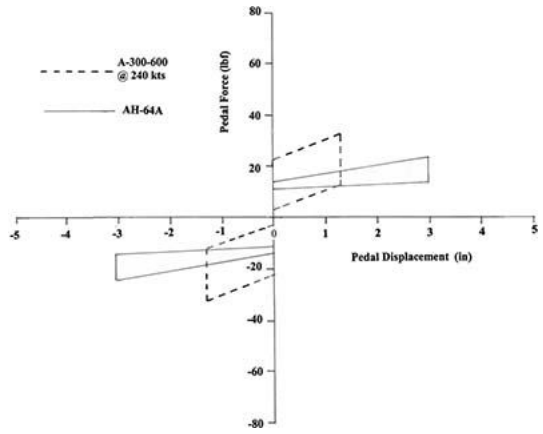

Figure 2-4: Comparison of Pedal Force/Feel Systems, AH-64A and Airbus A300-600 [6]

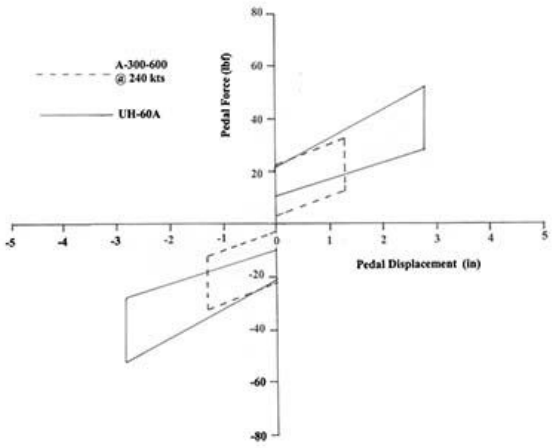

Figure 2-5: Comparison of Pedal Force/Feel Systems, UH-60A and Airbus A300-600 [6]

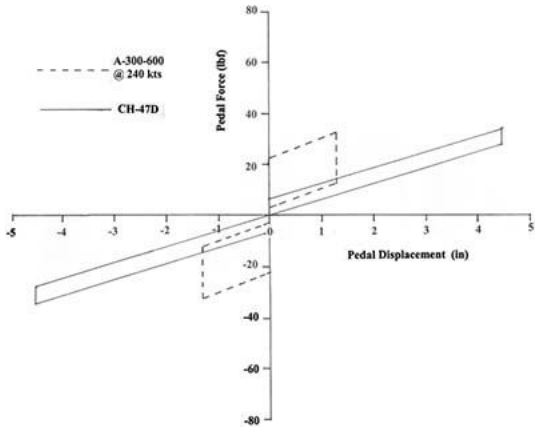

Figure 2-6: Comparison of Pedal Force/Feel Systems, CH-47D and Airbus A300-600 [6]

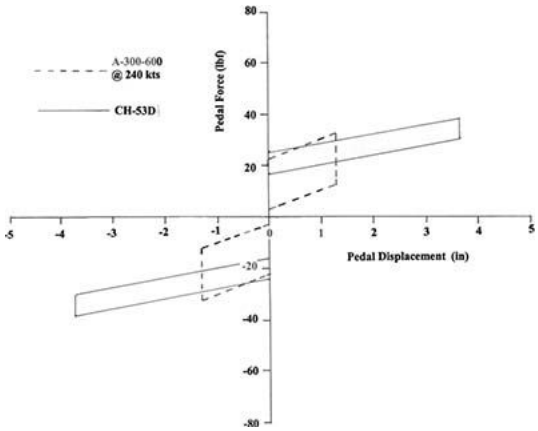

Figure 2-7: Comparison of Pedal Force/Feel Systems, CH-53D and Airbus A300-600 [6]

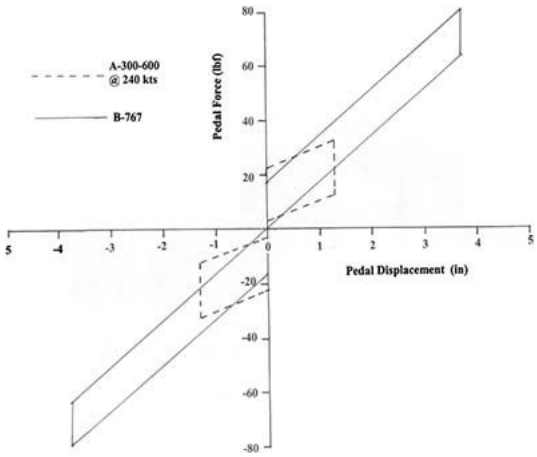

Figure 2-8: Comparison of Pedal Force/Feel Systems, B-767 and Airbus A300-600 [6]

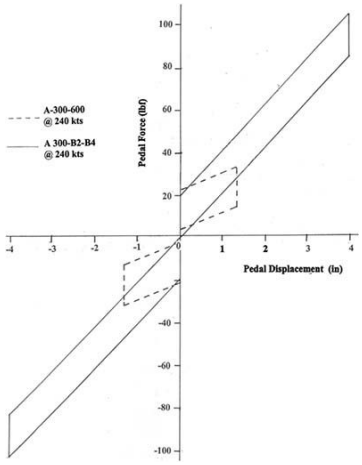

Figure 2-9: Comparison of Pedal Force/Feel Systems, Airbus A300-B2-B4 and A300-600 [6]

2-6 Dynamic Force/Feel System Considerations

The Force/Feel system is a dynamic system and behaves progressively with the airspeed floating along the rudder surface. To give an example for the dynamics, Figure 2-10 and 2-11 show two systems.

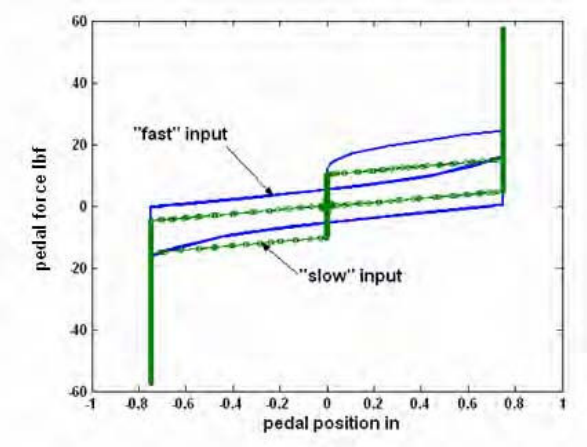

Figure 2-10: Example of the Effect Dynamic Characteristics of Force/Feel System with Sinusoidal Inputs of Different Frequency [7]

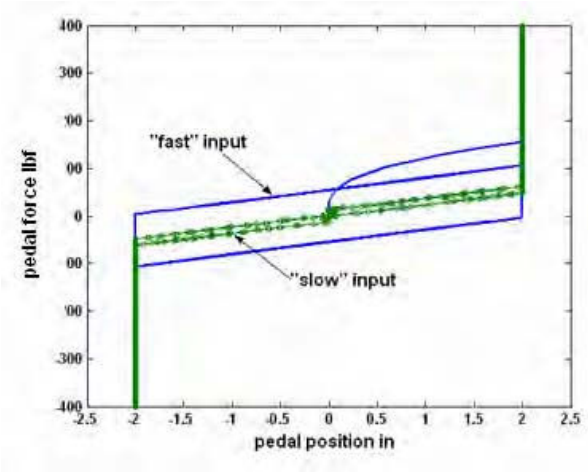

Figure 2-11: Example of the Effect Dynamic Characteristics of Force/Feel System with Sinusoidal Inputs of Different Frequency [7]

Figure 2-12 demonstrates the characteristics with force/feel System B for the vehicle analyzed here. In this figure, a sinusoidal pedal force is being applied at the frequency of the aircraft's Dutch roll mode, with an amplitude approximately creating the maximum pedal displacement. The rudder actuator rate limit was reduced by 50% to demonstrate the effect.

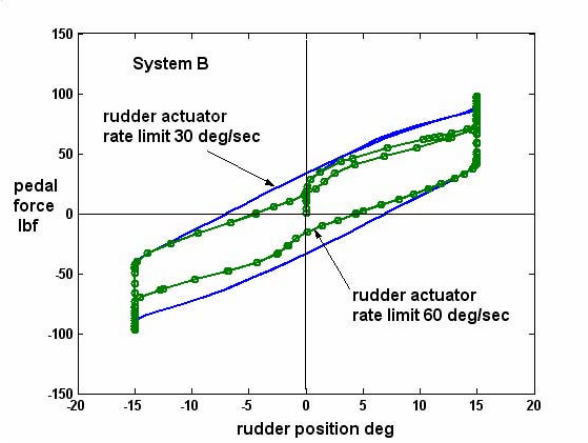

Figure 2-12: Example of the Effect of Force/Feel System Dynamics and Rudder Actuator Characteristics on Pedal Force vs Rudder Position for Force/Feel System [7]

2-7 Other Dynamic Effect acting on Force/Feel System

The dynamics of a force/feel system can be divided into: airplane dynamics, model dynamics and human dynamics. The last previous section described the airplane dynamics. The alteration of the airspeed during a simulation is the most dynamic quantity in the system. As shown in the last section, the behavior of an airplane is not linear, however the airplane part of the Force/Feel system can be described as a second order model, the unknown part of the control loading part.

A human can induce a constant force very well. The model dynamics are performed to connect the human with the airplane in a likely constant force model with limitations. The human is a complicated dynamic model. The physics can be approached by different parameters. It is hard to simulate the skin, bones, muscles and mass of the body. The human acting behavior is hard to model and can be described as a black box. The skin dynamics also need to be simulated. Skin dynamics are often simulated with a simple mass-spring-damper system, but neglected in the model simulation. The effect of a unknown human dynamics does have a significant contribution on the total system, much more than the skin dynamics.

2-8 Chapter summary

The Dynamic Force/Feel system needs to be considered in the design of an electrical rudder pedal. It is a critical issue that the system can be configured during the simulation. A simple fixed or linear setting can not be applied to the electrical rudder pedal system. The alteration of the airspeed during a simulation is the most dynamic quantity in the system. The system behaves partly linear in some cases. For the most cases, the simulated airplane system can be described as a second order system. However the dynamics of a human subject is a heavy dynamic model. A control loop at the position or equivalent of the position is a possibly a reliable solution. The torque loop is feedback in the outer loop to encounter the demanded value, so that the force/feel correspond with the real airplane.

Concluded from the literature of Hess [6], [7] a suggestion for the spring constant, 8900 N/m is taken. The maximum mass that can be applied to the rudder pedal is formulated by M.M. van Paassen as 68.04 kg.

Chapter 3

Performed Solution

3-1 Performed Solution

To get to the performed solution, four alternative solutions have been obtained. The four alternative solutions could be implemented in terms of torque and velocity specifications, however the following criteria have to be taken into account in order to make the decision of the preformed solution: communication speed, encoder accuracy, backlash, inertia, inrush current induced by the servo pack, energy consumption and costs. The implemented solution (alternative solution 4) is presented in this Chapter. For more information about the other elaborated alternative solutions, please refer to the Appendix A.

The most important difference between the three other alternative solutions and the performed solution is the gearbox which results in a reduced torque and more important a reduced inertia at the pedal side. In the formula the gear ratio is to the second power. [8] Preferred is the three phase model of the drive system, because of the experience with inrush current by switching the controller on, in one of our other laboratory. In fact the 20 bit alternative solution is maybe not really necessary, but is however very useful for accurate data to implement in the control system. The gearbox is the part that can cause some problems in our system performance. For your understanding the backlash in other parts of the rudder pedals is higher than the standard backlash in the gearbox, so this can be neglected. Furthermore, the backlash in the rudder pedals is behind the motor, and this has no consequences for our control loop. The selected motor can operate in all required conditions within the rated torque characteristics.

3-2 Mechanical Identification

To obtain the specific acting forces and moments on the drive line, an analysis is made from the current system. The current transmission is at the pedal side. This also shown in Figure 1-2 to get an impression of the situation in reality. The first gear ratio is at the pedal side (Figure 3-1) and the second gear ratio is at the drive shaft below floor level (Figure 3-2).

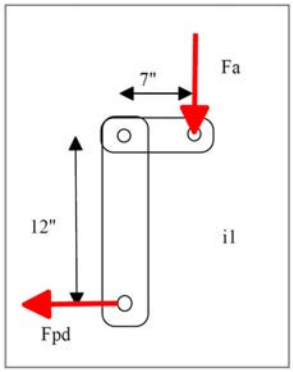

Figure 3-1: First force lever of at the rudder pedals

F_{pd} = Force at pedal side [N]
F_a = Force connection rod [N]
F_b = Force hydraulic actuator [N]
$s_{RudderMax}$ = Displacement of the pedal in meter [m]
$s_{ActuatorMax} = s_{RudderMax}/i_T$ [m]

$$i_1 = \frac{12}{7} \tag{3-1}$$

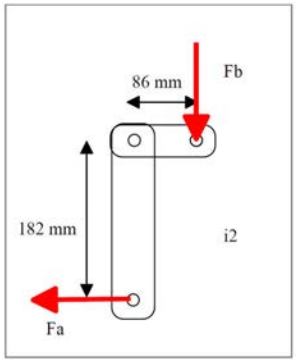

Figure 3-2: Second force lever of at the rudder pedals

The gear ratio at the pedals and the total gear ratio can be described as follow:

$$i_2 = \frac{182}{86} \tag{3-2}$$

$$i_T = i_1 \cdot i_2 \tag{3-3}$$

As a result of the considerations for sizing and design in Chapter $1-3$, the conclusion is:
Maximum rudder force continuous = 150 lbf $\approx$ 68.18 kg
$g = 9.81$ m/s^2
$F_{pd} = g \cdot 68.18 \approx 668.85$ N

$F_a = i_1 \cdot F_{pd} \approx 1146.59$ N
$F_b = i_2 \cdot F_a \approx 2456.51$ N
$s_{RudderMax} = 0.2$ m
$s_{ActuatorMax} = s_{RudderMax}/i_T \approx 0.055$ m

The torque at the drive shaft is:

$$T_2 = \frac{F_{pd} \cdot i_2}{l_{i_2}} = 208 \tag{3-4}$$

l_{i_2} = lever arm length from F_a to the second pedal shaft axis.

The choice of the selected electric motor is based on the maximum speed in revolutions per minute and the rated continuous torque. The range of the selected servo motor; SGMGV-13D [9], has a nominal rated speed of 1500 RPM, which means 157.08 rad/sec. The maximum required speed is 4.54 rad/s; the maximum gear ratio that can be applied is 34.6. The gear ratio is selected at 1:30. The maximum required torque is 208 Nm at the pedal shaft, the torque at the motor side becomes 6.93 Nm without any loss. When a value of 0.85 is taken for efficiency, the torque at the motor shaft is 8.16 Nm. The maximum introduced backlash is 3 arc minute instead of 4 with an angled gearbox. [10] The next motor in the selected range is a 8.34 Nm continuous torque motor. The following step when designing a control loading system is to design the selected drive line. The chosen components are selected to comply with difficulties in the control loop. It is important to avoid any mechanical obstruction that can cause instability of the control loop.

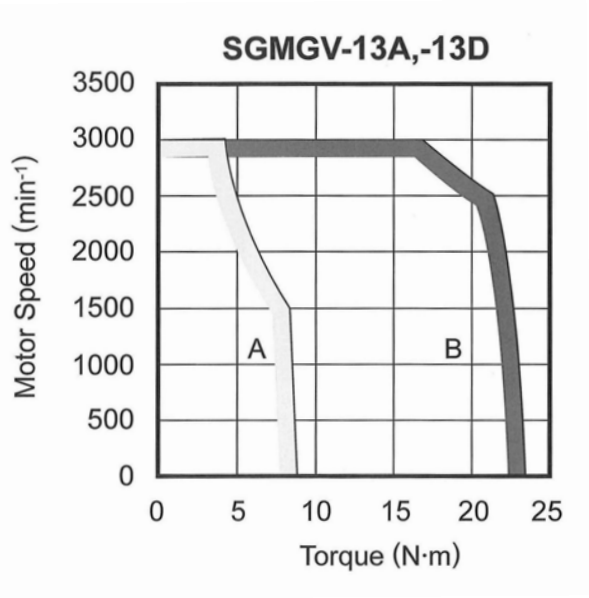

Figure 3-3: Torque characteristics of the motor SGMGV-13D

In Figure 3-3 the torque characteristics of the selected motor is shown. Graph 'A' is the characteristic of the motor for the continuous acting speed and torque. Graph 'B' is the maximum characteristic of the motor for a short-time. When the motor is heating up during

operation the characteristics increase. A dwell time can lower the ambient temperature of the motor. The maximum continuous torque and speed is 1500 RPM (or 157 rad/s) without any loss of torque. The graph is suggested as a vertical line in this situation. In Figure A-4 an artist impression of the performed solution is shown. The particular views are presented in Figure A-5.

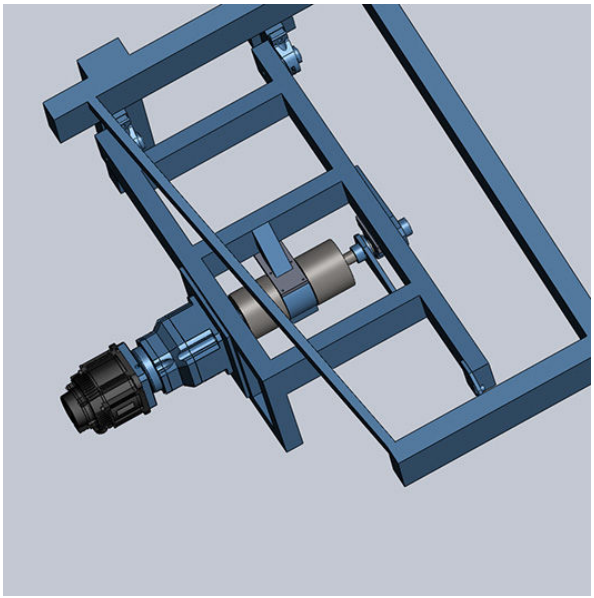

Figure 3-4: Alternative solution 4 proposed gearing via planetary gearbox on an electric servo direct drive

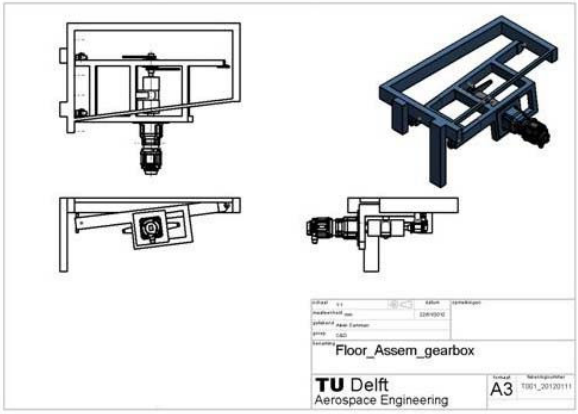

Figure 3-5: Drawing alternative solution 4

3-3 Inertia of the drive system

For higher performance of the rudder pedal system, it is important to take into account the inertia of the system. To estimate the inertia of the actual rudder pedals with levers, a solid design analysis is made by the design software Solidworks. The derived values are considerable

for this system and by scaling the values to the motor shaft scale they become more accurate. Possible miscalculation is filtered out by the gear ratio to the power of two. The inertia what is reflected at the motor shaft is called the reflected load inertia. Formula 3-5 presents the relation with the gear ratio and the load inertia.

$$J_r = \frac{J_l}{{R_g}^2} \tag{3-5}$$

The inertia of the current pedals and levers are calculated in Figure 3-7.

Figure 3-6: Inertia calculation of current pedal system

		lever length [m]	Force [N]	Torque [Nm]	mass [kg]	I [kg*m^2]	ratio	
					15	1,3935456	29,3077	0,0016224
pedalforce		0,3048	801,9231	-	3,93993132	0,20222348	29,3077	0,00023543
pedalaxis		-	-	244,4262				
		0,1778						
leverforce		0,182	1374,725	-				
leveraxis		-	-	250,2	0,875756	0,000082	30	9,1111E-08
bus		-	-	250,2	0,06288763	0,00001759	30	1,9544E-08
coupling		-	-	250,2	4	0,0072	30	0,000008
torque-transducer		-	-	250,2	2	0,0001879	30	2,0878E-07
coupling		-	-	250,2	4	0,0072	30	0,000008
bus		-	-	250,2	0,06288763	0,00001759	30	1,9544E-08
gearbox		-	-	250,2		0,000271	1	0,000271
motor	SGMGV-13D3A6F					0,00199	1	0,00199
	Load inertia without motor		Jl					0,00214517
	Total inertia		Jt					0,00413517
			load factor max 5			Jl/Jm		1,07797565

Figure 3-7: Inertia calculation of drive system

The rotor inertia of the motor seen at the motor shaft is $J_l = 0.0020$ kg $\cdot$ m^2
The load inertia of the system seen at the motor shaft is $J_l = 0.0021$ kg $\cdot$ m^2

$$J_t = J_m + J_l \tag{3-6}$$

$$R_i = \frac{J_m}{J_l} \tag{3-7}$$

The calculated inertia ratio (R_i) is 1.08 and this a good result for the expected performance of the system. A ratio till 5 is allowed for high performance, above 5 the stability of the control loop will decrease in comparison to a very low value for the ratio.

The total inertia of the system as seen at the motor shaft is $J_t = 0.0041$ kg $\cdot$ m^2
A check for the resonance frequency is important to avoid oscillations. This can be calculated when the inertia value of the load and motor are available. The most common way to check the resonance frequency is as followed. [9]:

$$f_{\text{res}} \approx \frac{1}{2 \cdot \pi} \cdot \sqrt{c_{\text{t}} \cdot \frac{J_{\text{m}} + J_{\text{l}}}{J_{\text{m}} \cdot J_{\text{l}}}} [9] \tag{3-8}$$

$c_t = 288.6$ [kNm/rad]. The result is 2661 Hz as a theoretical expected mechanical resonance frequency.

3-3-1 Mechanical analyses

Mechanical analyses derived by the servo controller. The lowest resonance frequency that has been found is 130 Hz on the total system with additional mass of $2 \cdot 7.5$ kg. The maximum revolutions that can be reached in operational function is 3450 RPM, 57.5 RPS or 361 rad/s.

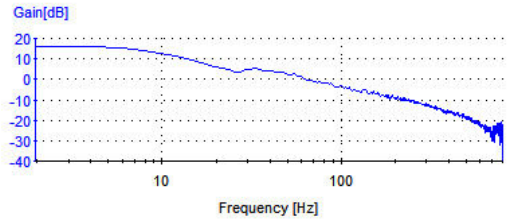

Figure 3-8: Results of measurement gainplot

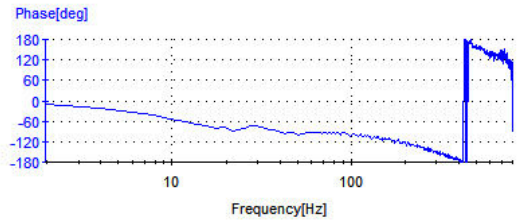

Figure 3-9: Results of measurement phaseplot

In Figure 3-8 and Figure 3-9 the results of the mechanical analysis is shown. Around 30 Hz a hollow is inspected in the gain plot, however the phase shift is not turned over dramatically. It is possible to add a notch filter to decrease this effect, but this is not executed. The system is not very useful for frequencies above 100 Hz. The vertical line in the phase plot around 130 Hz is induced by the phase shift over 180 degrees.

3-3-2 Acceleration torque

$$T_a = J_t \cdot \frac{\alpha}{\eta} \tag{3-9}$$

The maximum acceleration torque can be calculated by the Equation 3-9. The efficiency is to be considered as 0.85. The shortest acceleration time of the motor at maximum velocity is: 361 / 4190 = 0.0862 sec.

3-4 Chapter summary

The selected electric motor drive is a Yaskawa SGMDGV-13D with a 20 bit accuracy position encoder. The supply power is 3 phase 230 VAC 50 Hz to avoid high inrush current at the start-up. The setup is attached with an EtherCAT communication module to the control loop, to avoid noise on the desired control signal. Another big advantage is the synchronized timing of the control loop. A digital communication has a variety of advantages above an analog desired control signal. The signal/noise ratio of a digital communication is much higher than an analog variety of signal transfer.

The transmission is performed by a "backless free" planetary gearbox of the brand Apex Dynamics. The transmission ratio is chosen at 1:30 and this is a first stage gearing. The gearbox is used to reduce the torque and also the inertia by the second power. The maximum continuous rated torque what can be delivered by the motor is 250.2 Nm at the end of the gearbox or 820 N at the rudder pedal.

The inertia of the lever system is approximated by a drawn model. The possible error of the actual inertia and the approximated calculation is filtered out when the gear ratio is applied. For a high performance drive system a maximum J_l/J_m ratio is to be taken at 5 maximum. The realized inertia of the load/motor ratio is 1.08.

The theoretical resonance frequency of the mechanical system is 2661 Hz, this is beyond the operation frequency range of rudder pedals.

The acceleration limited by the maximum velocity and maximum acceleration rate of the free running motor is 4190 rad/s^2. The acceleration torque decreases with the acting load and the inertia of the load.

Chapter 4

Performance of the analytical models

In this chapter the modeling of the original hydraulic driven actuators in three different control loops is first explained . The second simulation is an electric driven actuator in the control loop. This is decided for several reasons. The simulation of the electric servo motor is difficult to establish with the lag of information of the servo pack. This has to be seen more as an estimation of the limitations of the servo system.

The input signal for the system identification is a sinus profile in the stationary part of the oscillation. The start up and stop of the oscillation is not acquainted with the simulation. The reason is the interference at the inrush oscillation and the abrupt stopping of the oscillation.

A sinusoidal input signal is achieved to inspect the response, the reason why there is been chosen for a sinusoidal input signal is the limitation on the travel and the mechanical system. It is not really a good solution to run a step profile or a trapezium pattern where the angle is less steep as in a step response. The jerk will have effect on the system like vibrating the rigid frame construction and so on. A sinus is maybe not the ideal identification method in terms of workload, however it is a smooth method for identification.

In the Chapter Flight Control System the dynamic behavior of the system is described. The components that are used for simulation is supposed as a linear system. The most important elements of the simulated model can be described as a second order mass-spring-damper system. In the Figure 4-1 the different elements of the mass-spring-damper system what is model for the simulation is shown. The ζ is supposed as a value of 0.7.

As concluded in Chapter 2, the value from experience of the literature of Hess [6], [7] a suggested spring constant of 8900 N/m has been taken. The maximum mass that can be applied to the rudder pedal is formulated by M.M. van Paassen as 68.04 kg. The ζ is formulated as 0.7, which mean a damping value of 886 Ns/m when the Formula 4-1 is applied.

$$\zeta = \frac{b_{sim}}{2\sqrt{m_{sim} \cdot c_{sim}}} \tag{4-1}$$

$$\omega_0 = \sqrt{\frac{k}{m}} \tag{4-2}$$

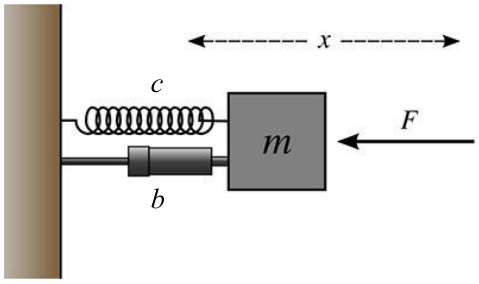

Figure 4-1: Mass Spring Damper system

$M = M_{sim} + M_{omd}$
$M_{sim} = 68.04$ kg
$M_{omd} = 15$ kg
$c_{sim} = 8900$ N/m
$b_{sim} = 886$ Ns/m
$\zeta = 0.7$
x = displacement of the rudder pedal in m

In Figure 4-1 a vibrating linear system (mass-spring-damper) with one degree of freedom is shown. Some basic principles can be recognized in a very simple linear model of a mass-spring-damper system. Such a system contains a mass 'M', a spring with spring constant 'c' that serves to restore the mass to a neutral position, and a damping element which opposes the motion of the vibratory response with a force proportional to the velocity of the system, the constant of proportionality being the damping constant 'b'. This damping force is dissipative in nature, and without its presence a response of this mass-spring system would be completely periodic.

This second order model is used to achieve the desired position and velocity. Generally, damped harmonic oscillators satisfy the second-order differential equation:

$$\ddot{x} + 2 \cdot \zeta \cdot \omega_0 \cdot \dot{x} + \omega_0^2 \cdot x = 0 \tag{4-3}$$

where ω_0 is the undamped angular frequency of the oscillator and ζ is a constant called the damping ratio. The value of the damping ratio ζ determines the behavior of the system. A damped harmonic oscillator can be:

- Overdamped ($\zeta > 1$): The system returns (exponentially decays) to equilibrium without oscillating. Larger values of the damping ratio ζ return to equilibrium more slowly.
- Critically damped ($\zeta = 1$): The system returns to equilibrium as quickly as possible without oscillating.
- Underdamped ($0 < \zeta < 1$): The system oscillates (at reduced frequency compared to the undamped case) with the amplitude gradually decreasing to zero.
- Undamped ($\zeta = 0$): The system oscillates at its natural resonant frequency (ω_0).

First a bodeplot of the maas-spring-damper system (FCS).

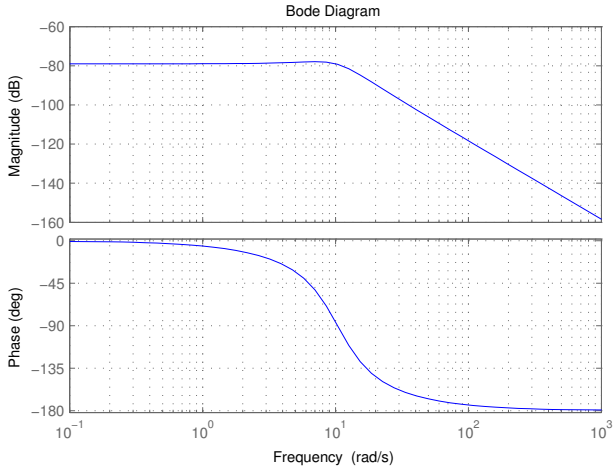

Figure 4-2: Bodeplot of the FCS mass-spring-damper model

In Figure 4-2 the defined Flight Control System is shown. The cut-off frequency is at around 10 rad/s and the magnitude reduce with 40 dB per decade. This is so to say, a nice representation of a second order mass-spring-damper system. The phase shift is also particular for a second order system and is shifted 180 degrees in total.

4-1 Hydraulic Servo Simulation

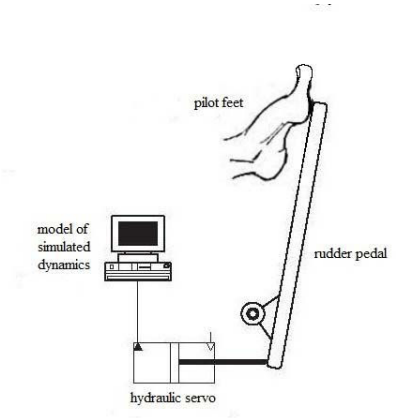

Figure 4-3: Control loading system layout

The actual control loading system is running with a hydraulic actuator. At the TU Delft, there is an enormous knowledge about these hydraulic systems. The first setup for model

simulation is taken from these basics of hydraulic driven actuators. In Figure 4-3 the schematic connection of the rudder pedal and the system is shown. There is a gear ratio necessary to obtain the force values an velocity values in the limit range of the hydraulic actuator. The gear ratio of the system is 10/3 for the hydraulic actuator. In the past Arno Gerretsen [11] compared control loops. In this chapter, the position control loop, velocity control loop and torque control loop are explained.

4-2 Comparison of Position, Velocity and Force loop based Control Loading Architectures

4-2-1 Basics for Control Loading Simulation

Three possible control loading architectures have been evaluated in the past, to find the most suitable control loading architecture for the simulators. These architectures are the position loop where the desired position of the control device is regulated, the velocity loop where the desired velocity of the control device is regulated and the force loop where the desired force of the control device is regulated.

In the position loop the difference between the position of the control column and the desired position, based on the force applied on the control column, is used as the input signal into the hydraulic servo, making it act as a position servo. In the velocity loop the desired velocity of the control column is determined, based on the position of the control column and the force applied on the control column. This desired velocity is then used as the input signal into the hydraulic servo. In the force loop the currently simulated force is determined based on the position, velocity and acceleration of the control column. The force error, the difference between this simulated force and the applied force, is used as the input signal of the hydraulic servo, making this servo act as a force servo.

Previous work showed [11] that the force loop architecture could be a promising alternative for the velocity loop, which is currently implemented in the simulators. To explain the choice for the control loading, a comparison between the three control loops will be made analytical and an experimental setup for the chosen control loop has been performed to reach our goal. First mathematical models of the subsystems of the control loading system are derived, followed by the models of the three evaluated architectures. Results of an analytical performance evaluation of these architectures are discussed next.

4-2-2 Subsystems

Specific values considered for hydraulic simulation

To compare the analytical performance of the different control loading architectures, mathematical models have been constructed of these architectures. Before the actual models are derived in the next section, the different components of the control loading system will be discussed first. The most important element of the control loading system is the "feel" that needs to be simulated.

Table 4-1: Specific values considered for hydraulic simulation

Variable		Value	Unit
M_{omd}	=	15.0	kg
m_{sim}	=	68.04	kg
b_{sim}	=	886	Ns/m
c_{sim}	=	8900	N/m
E	=	$1.38 \cdot 10^{9}$	N/m
m_{effp}	=	1	kg
S_p	=	0.06	m
i_{max}	=	0.015	A
q_{max}	=	0.0020	m^3/s
R_g	=	10/3	-
A_p	=	$3.2673 \cdot 10^{-4}$	m^2
L_c	=	$1.0 \cdot 10^{-12}$	m^5/Ns
ζ_h	=	0.70	-
K_v	=	1	-
K_1	=	q_{max}/i_{max}	-
K_2	=	$\left(\frac{2 \cdot \zeta}{\omega_0} - \frac{L_c \cdot m_{effp}}{Ap^2}\right) \cdot \frac{A_p}{K_1}$	-
K_3	=	$\frac{K_v \cdot A_p}{K_1}$	-
ω_0	=	$\sqrt{\frac{4 \cdot \mathrm{E} \cdot \mathrm{A_p}}{\mathrm{m_{effp}} \cdot \mathrm{S_p}}}$	-

Normally there are 2 elements that need to be simulated, the hydraulic actuator dynamics and the skin dynamics. For simulation is in our case, the actuator dynamics are the most important. The feeling of human feet is less sophisticated than a hand for example. The dynamics of the skin are not simulated, only added as a solid mass.

Simulated model desired behavior

The simulated model, also called Flight Control System (FCS), is the model that relates the state of the control rudder pedal with the force that should be simulated. Different elements, like the control surfaces, cables and actuators, contribute to these dynamics. When a linear model is made of the most important elements, it is possible to write the simulated model as a second order mass-spring-damper system. Based on the desired output the simulated model can be given by a transfer function.

$$X_c = \frac{F}{m_{\mathrm{sim}} \cdot s^2 + b_{\mathrm{sim}} \cdot s + c_{\mathrm{sim}}} \tag{4-4}$$

$$F = m_{\mathrm{sim}} \cdot X_c \cdot s^2 + b_{\mathrm{sim}} \cdot X_c \cdot s + c_{\mathrm{sim}} \cdot X_c \tag{4-5}$$

Hydraulic servo

The dynamics of the hydraulic servo are determined by the different oil flows inside the servo. In the mathematical model derived the following oil flows are identified:
Oil inflow q_s: This is the amount of oil that flows into the servo from the hydraulic pump. The size of this oil flow is determined by the input signal into the hydraulic servo i and it is assumed that there is a proportional relation between this signal and the oil inflow.

$$q_s = K_1 \cdot i \tag{4-6}$$

Oil flow due to movement q_{xp}: Movement of the piston will cause a change in the volume behind it and will therefore also result in a flow of oil. This flow depends on the velocity of the piston x_p and the area of the piston A_p.

$$q_{xp} = A_p \cdot \dot{x}_p \tag{4-7}$$

$$q_l = L_c \cdot \Delta p \tag{4-8}$$

Leakage oil flow q_l: No piston is perfect, therefore a certain amount of oil will leak away around the piston. It is assumed that this oil flow is proportional to the pressure difference over the piston.

Oil flow due to compression q_c: The oil that is not by the oil flows listed above will be collected behind the piston and be compressed. These four oil flows must be in equilibrium and from that equilibrium the pressure difference over the piston can be determined. Multiplied by the area of the piston this gives the force the servo generates.

The three architectures

In this section models of the three architectures that have been evaluated are constructed, using the subsystems described in the previous section.

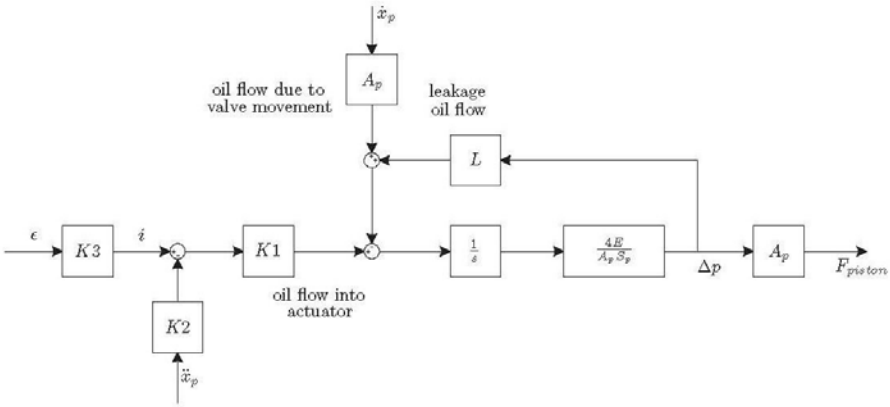

Figure 4-4: Hydraulic servo model

A. Position loop

For the position loop architecture, see Figure 4-5, the input signal of the hydraulic servo is determined by Δp, the difference between the current position and the desired position x_d. This desired position is calculated by the simulated model based on the input force of the system. As a result of the input signal the hydraulic servo will generate a force, which causes the control rudder pedal to move.

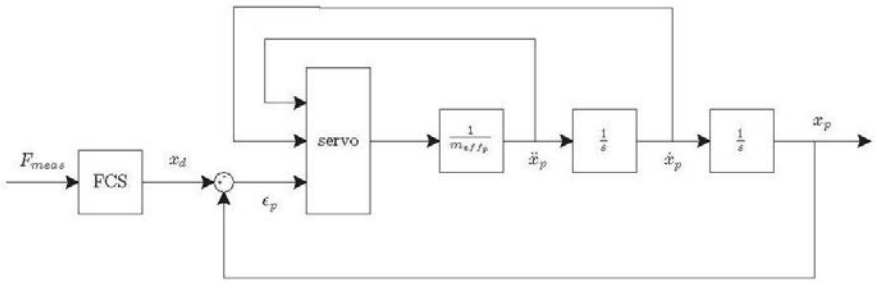

Figure 4-5: Hydraulic position loop

B. Velocity loop

For the velocity loop architecture, see Figure 4-6, the input signal of the hydraulic servo is the desired velocity x_d of the control rudder pedal. This velocity is determined by the simulated model, based on the input force of the system and the current position of the control rudder pedal. As a result of the input signal the hydraulic servo will generate a force, which causes the control rudder pedal to move.

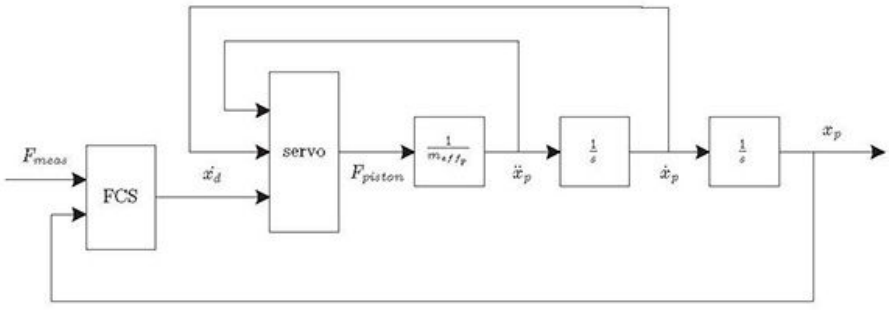

Figure 4-6: Hydraulic velocity loop

C. Force loop

For the force loop architecture, see Figure 4-7, the input signal of the hydraulic servo is determined by the force error ϵ_F, the difference between the currently simulated force and the input of the system. This currently simulated force is calculated from the acceleration, velocity and position of the control rudder pedal. As a result of the input signal the hydraulic servo will generate a force, which causes the control rudder pedal to move.

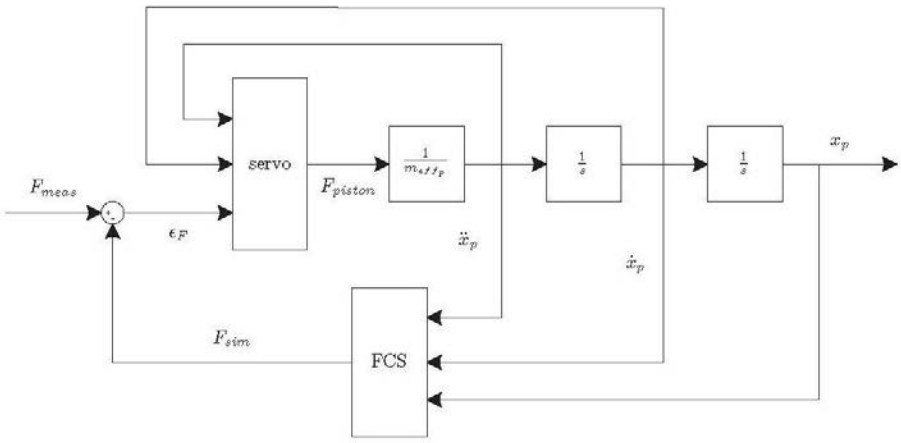

Figure 4-7: Hydraulic force loop

4-3 Hydraulic Servo Identification

The inventory of the hydraulic setup is given in Figure 4-8. In this case the behavior of the airplane is simulated by a second order model for the airplane (Cessna Citation II) of the Faculty Aerospace Engineering at the TU Delft.

The cut-off frequency of the FCS-model is around 12.6 rad/s or 2 Hz. For simulation of this model, a cut-off frequency of 126 rad/s is at least required. The bode plot of the modeled original hydraulic standard actuator is shown in Figure 4-9. This is an analytical model, and compared to the experimental setup it is not realistic, there is no gear ratio and also no inertia implemented in this simplified model. The experimental data for a bare hydraulic actuator are not available yet. In Figures 4-10 the bode plot of the bare actuator without connection with the rudder pedal. The maximum displacement of the actuator is 60 mm.

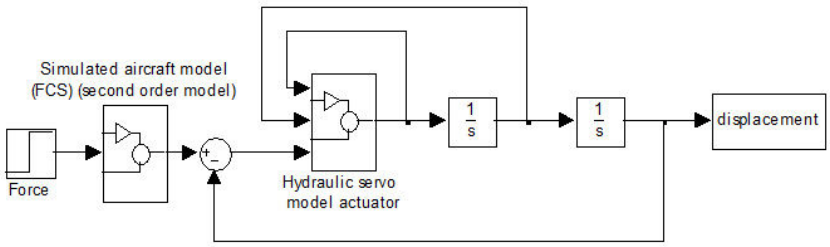

Figure 4-8: Schematic complete hydraulic control loop

In the Figures 4-11 and 4-12 the analytical results for a hydraulic control loading system is shown. The control loops that are used for simulation are explained and shown in the previous section. The Figure 4-5, 4-6 and 4-7 the fundamentals of the control loop are shown.

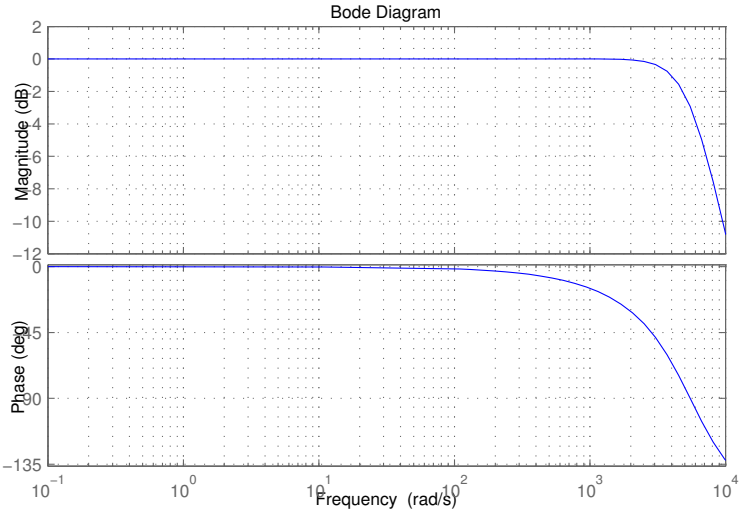

Figure 4-9: Bode plot bare hydraulic actuator model with a velocity loop

The low-pass cut-off frequency is at around 5550 rad/s or 883 Hz. The behavior of the system is a pure second order system. Two poles around 5550 rad/s.

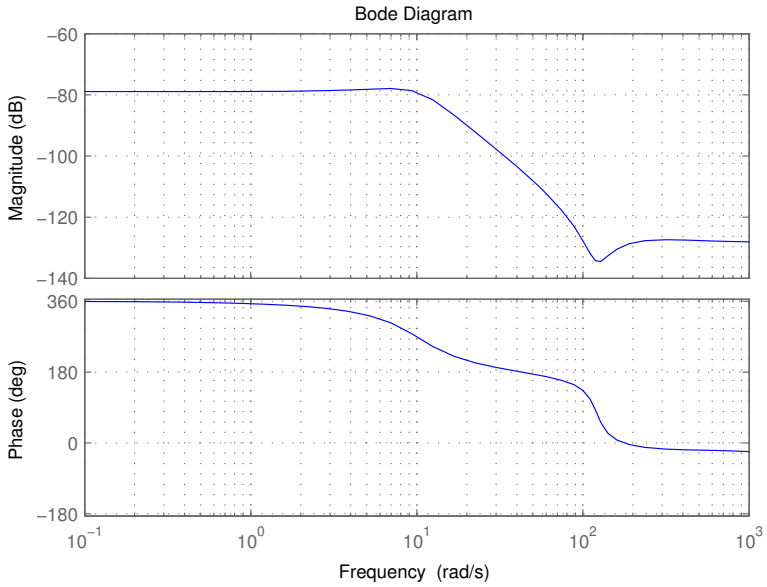

Figure 4-10: Hydraulic bode plot position loop (Simulink Result)

The low-pass cut-off frequency is at around 10 rad/s and fit more or less the mass-spring-damper system (defined FCS system). The behavior of the system is not a second order

system. It seems to be a system with two poles around 10 rad/s and two additional zero around 110 rad/s.

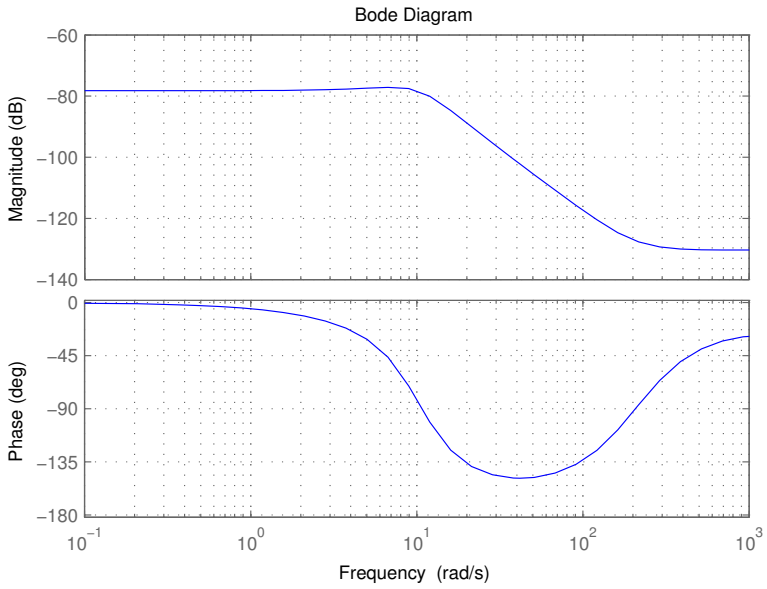

Figure 4-11: Hydraulic bode plot velocity loop (Simulink Result)

The low-pass cut-off frequency is at around 10 rad/s and fit more or less the mass-spring-damper system (defined FCS system). The behavior of the system is not a second order system. It seems to be a system with two poles around 10 rad/s and two additional zeros around 300 rad/s.

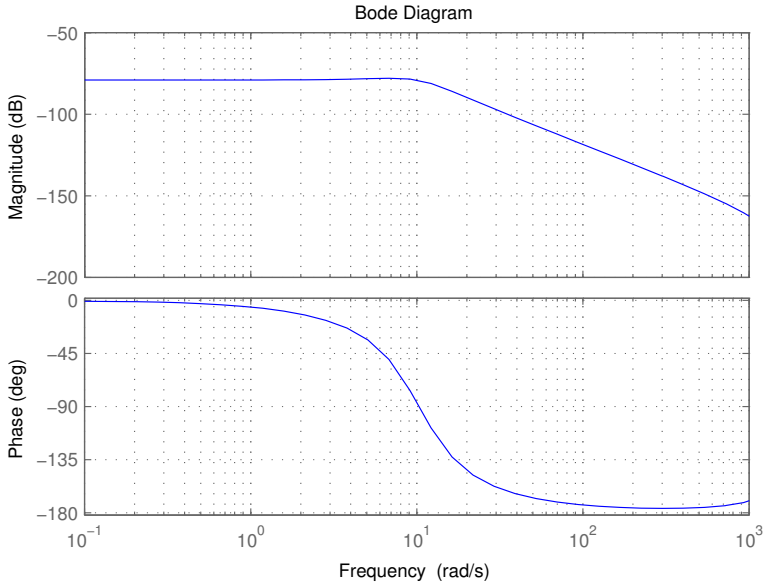

Figure 4-12: Hydraulic bode plot force loop (Simulink Result)

The low-pass cut-off frequency is at around 10 rad/s and fit more or less the mass-spring-damper system (defined FCS system). The behavior of the system is a second order system. There are two poles around 10 rad/s. The system do not show lead or lag, there is so to say less difference in the phase shift for the FCS mass-spring-damper model and the force control loop.

4-3-1 Analytical performance evaluation

To compare the response of a step input of 750 N feed to the FCS model, the following responses are obtained. The response of the three loops shows a certain settling time to become in a stationary part of the sinus. The velocity loop shows a lead response and the position loop shows a lag response. The force loop present a optimal response.

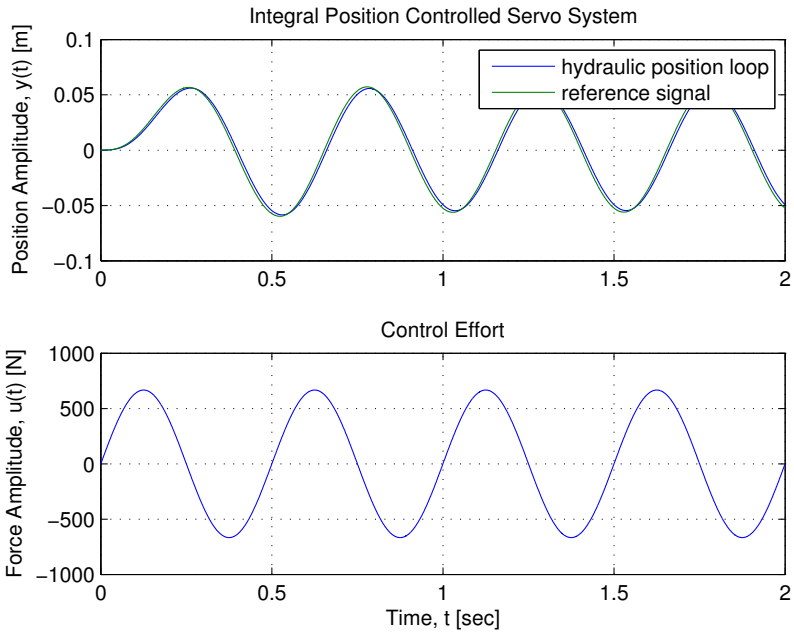

Figure 4-13: Hydraulic position loop (Simulink Result)

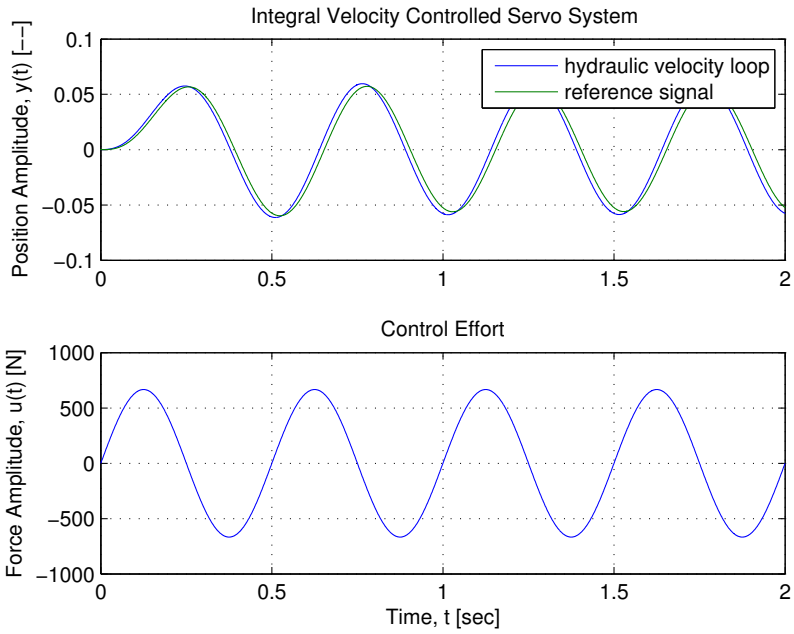

Figure 4-14: Hydraulic velocity loop (Simulink Result)

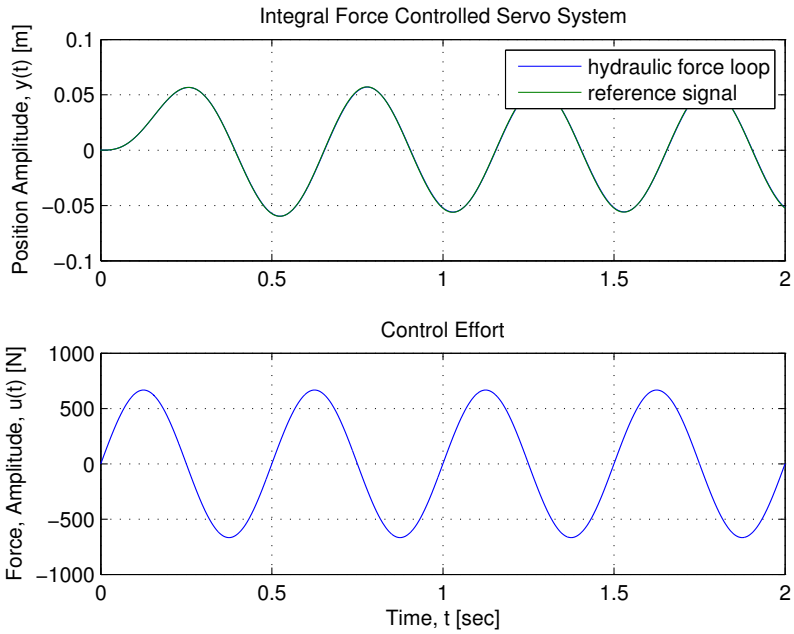

Figure 4-15: Hydraulic force loop (Simulink Result)

4-3-2 Choice Type of Control Loop

From the analytical performance evaluation of the different hydraulic architectures, it can be concluded that the force loop architecture is the best choice for a hydraulic control loader. The currently used velocity loop simulates the desired dynamics less accurate, but still provides an appropriate match. The position loop on the other hand is not suitable as control loader, it is shown in the past that this architecture becomes unstable for certain conditions.

To be implemented in the simulator, it was necessary to add an estimator to the force loop architecture. A performance evaluation conducted with these implemented models showed that the velocity loop has a slightly better performance than the force loop in the simulator, the force loop has less damping.

4-4 Electrical Servo Simulation

For the model simulation of the electrical servo drive system, a first model is made out of the bode-plot of the bare motor with the available specification. The work that is done in the past by identifying an electric motor was very helpful. [12] and [13] The literature of Riazollah Firoozian [14] and the documentation of Allen Bradley [15] was useful to set up the model. For setup of the best controller the documentation of the lectures of E. Tazelaar, Non Linear Control was used. [16]

4-4-1 Matlab/Simulink model

Simulink model

To simulate the dynamical behavior of our specific AC servo motor of Yaskawa, it is difficult to get the detailed information about the motor and the schematic detail of the electronics inside. A simplified model is proposed conform [17], see Figure 4-17. Some parts of this book are old fashioned, but many aspects have been described in a clear way and are still relevant.

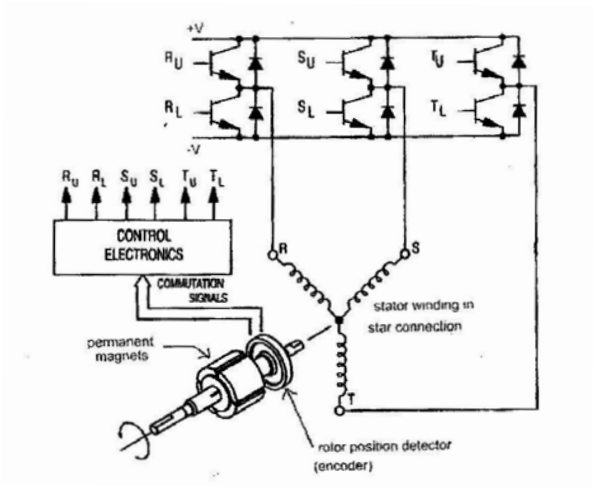

Figure 4-16: Schematic 3 phase brushless servomotor

The dynamic electrical and mechanical behavior of a servomotor, regardless what kind of motor, can be expressed by the equation:

$$V_{bs} = K_b \cdot \omega_m \tag{4-9}$$

V_{bs} = supply voltage to the brushless DC motor in Volt. Be aware that this gives a simplified representation, not suitable for the design of the motors and their power electronic supplies (servo amplifiers), but surely an appropriate for control strategy of a servo application with catalog motors and amplifiers. The received information about the motor of Yaskawa Netherlands is shown in Table 4-2:

Table 4-2: Specific values considered for electrical motor SGMGV-13D simulation

Variable		Value	Unit	Description
R	=	10.56	[Ohm]	winding resistance
L_h	=	0.064	[H]	inductance of the winding
K_m	=	1.78	[Nm/A]	motor torque constants
K_b	=	1.2544	[V/(rad/s)]	back EMF constants
J_l	=	0.021452	[kg·m^2]	inertia load
J_m	=	0.0199	[kg·m^2]	inertia motor
J_t	=	0.0041352	[kg·m^2]	inertia total
P_r	=	1300	[kW]	motor power rated output
V_{class}	=	400	[VAC]	voltage rated class between two phases RMS
T_r	=	8.34	[Nm]	motor rated torque
T_i	=	23.3	[Nm]	motor instantaneous peak torque
I_r	=	5.4	[A]	motor rated current
I_i	=	14	[A]	motor instantaneous peak current RMS
S_r	=	1500	[RPM]	motor rated speed
S_m	=	3000	[RPM]	motor maximal speed
RP_r	=	35	[kW/s]	motor rated power rate
RA_a	=	4190	[rad/s^2]	motor rated angular acceleration
EMF_b	=	58.8	[mV/rpm/phase]	back EMF
N_p	=	8	[-]	number of poles or phase
R_p	=	1.32	[Ohm/phase]	resistance per phase
L_{hp}	=	8	[mH/phase]	inductance
V_a	=	400	[VDC]	supply voltage to the DC motor

The voltage supplied to the motor (V_a) is assumed as to be a 400 VDC bus system. When simulating the maximum rotational velocity of a bare motor without load and without disturbance [18], the following simplified simulation model can be derived.

Simulink model motor without load

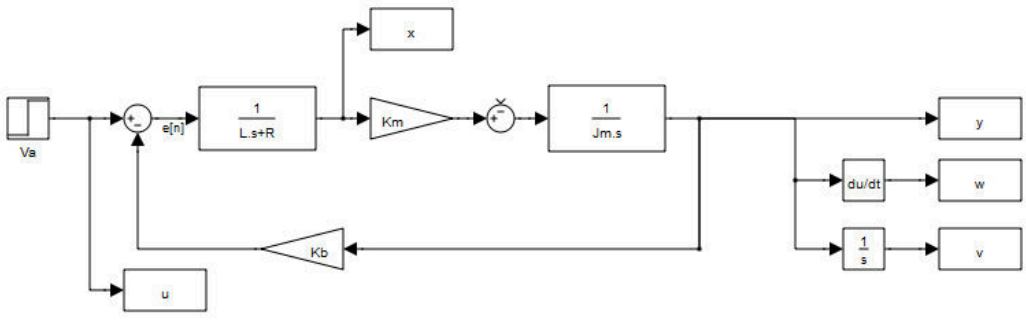

Figure 4-17: Simplified model brushless servomotor conform [17]

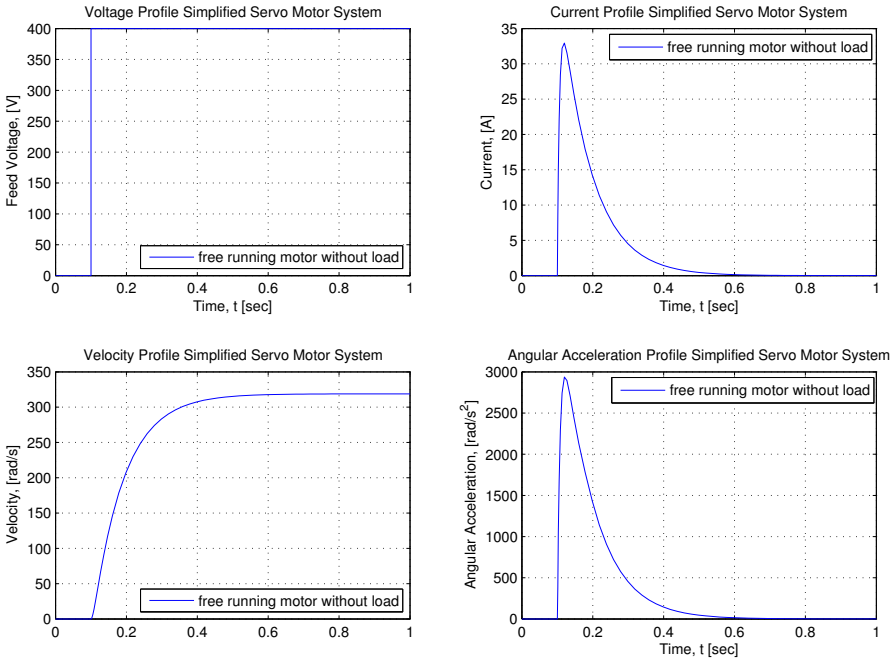

Figure 4-18: Results of 400 V step input feed to the simplified model of the servomotor

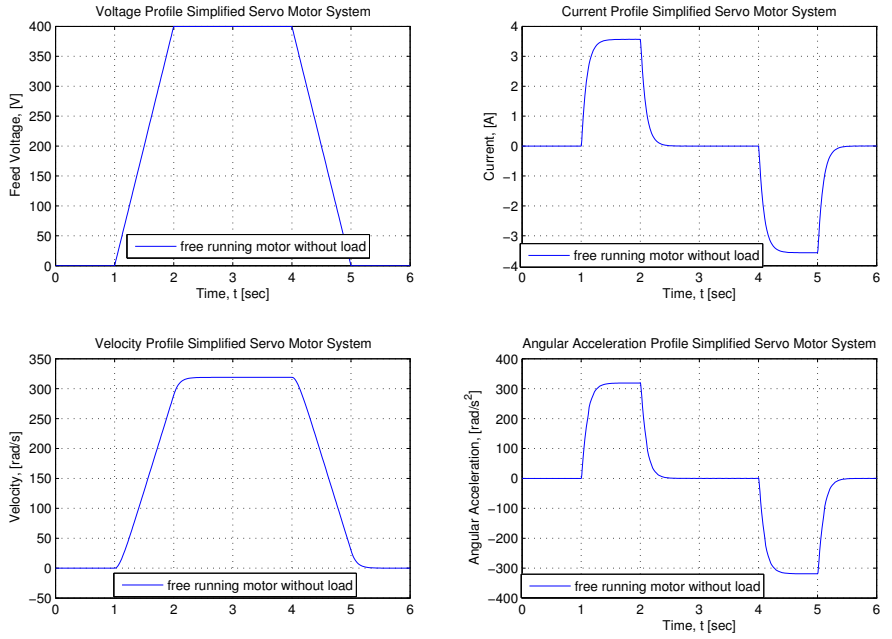

Figure 4-19: Results of 400 V profile feed to the simplified model of the servomotor

In Figure 4-19 the results: position, angular velocity, angular acceleration and current loop, are shown.

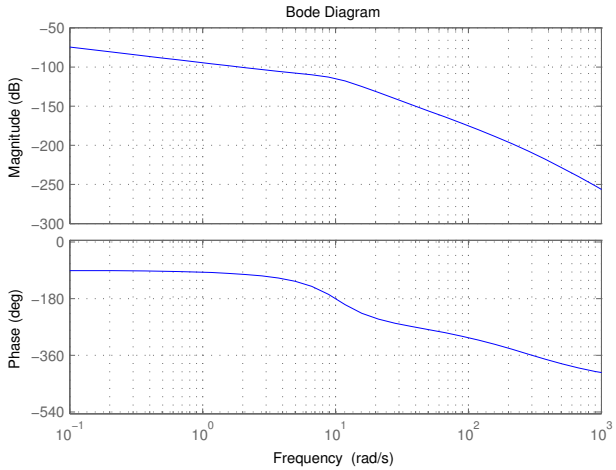

Figure 4-20: Bodeplot of design of a simplified model brushless servomotor

4-4-2 Feedforward value for simulation

A suggestion is to calculate the motor torque by a root locus method to find the optimal feedforward value K_{ff}. To do this, the control toolbox in Matlab is used. [18] On the next pages three classic methods for tracking set point and reducing sensitivity to load disturbances are compared with each other. The following three classic methods are presented:

- feedforward command (Figure 4-24)
- integral feedback control (Figure 4-26)
- LQR regulation (Figure 4-29)

The motor is suggested as a simple DC-motor with the components as shown in Figure 4-21 and 4-22. The values for the motor constants are presented in Table 4-3.

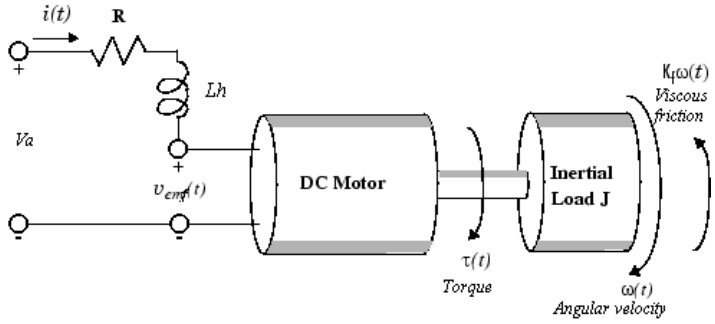

Figure 4-21: Model of a DC motor

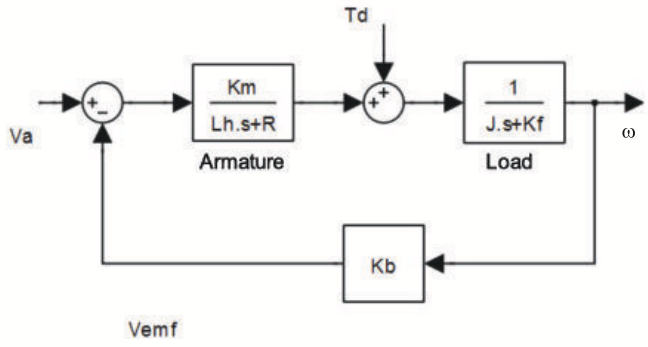

Figure 4-22: Model of voltage control loop of a DC motor

Physical motor constants:

Table 4-3: Specific constants of the Physical motor

Variable		Value	Unit	Description
R	=	10.56	Ohm	winding resistance
L_h	=	0.064	H	inductance of the winding
K_m	=	1.78	Nm/A	motor torque constant
K_b	=	1.2544	V/(rad/s)	back EMF constant
J_l	=	0.021452	$kg \cdot m^2$	inertia load
J_m	=	0.0199	$kg \cdot m^2$	inertia motor
J_t	=	0.041352	$kg \cdot m^2$	inertia total
K_f	=	1.90986	Nms	viscous friction constant

To convert the physical motor constants in the simplified model, the following transfer functions can be constructed. Closed loop of the motor with back EMF

$$H_{\mathrm{m}_{closed}} = \frac{1.78}{0.002647 \cdot s^2 + 0.5589 \cdot s + 22.4}$$

In state space representation:

$$\dot{\mathbf{x}}(t) = A\mathbf{x}(t) + B\mathbf{u}(t)$$
$$\mathbf{y}(t) = C\mathbf{x}(t) + D\mathbf{u}(t)$$

$$\begin{bmatrix} \dot{\mathbf{x_1}}(t) \\ \dot{\mathbf{x_2}}(t) \end{bmatrix} = \begin{bmatrix} -46.19 & 27.81 \\ -30.33 & -165 \end{bmatrix} \begin{bmatrix} \mathbf{x_1}(t) \\ \mathbf{x_2}(t) \end{bmatrix} + \begin{bmatrix} 0 \\ 4 \end{bmatrix} \mathbf{u}(t)$$
$$\mathbf{y}(t) = \begin{bmatrix} 6.046 & 0 \end{bmatrix} \mathbf{x}(t) + [0]\,\mathbf{u}(t)$$

The goal is to minimize the velocity variations which are induced by load disturbances. The load disturbance is shown in Figure 4-25 as a dashed line. The response of the the angular velocity step change in voltage Va is shown in Figure 4-23. The acquired T_s settling time = 0.805 sec.
The feedforward control design is shown in Figure 4-24. The feedforward gain K_{ff} should be set to the reciprocal of the DC gain from Va to ω.

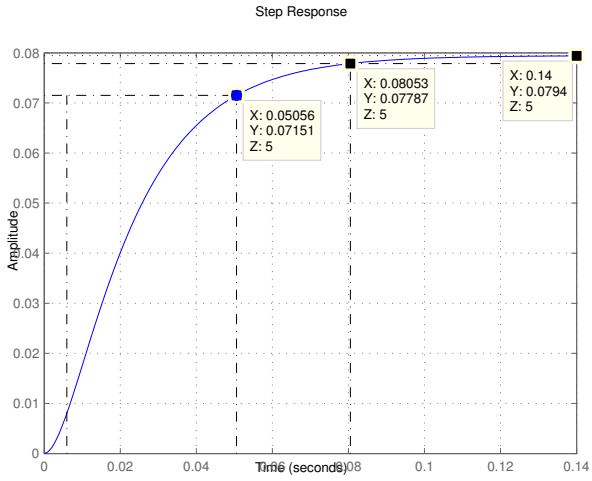

Figure 4-23: Step response of simplified model brushless servomotor

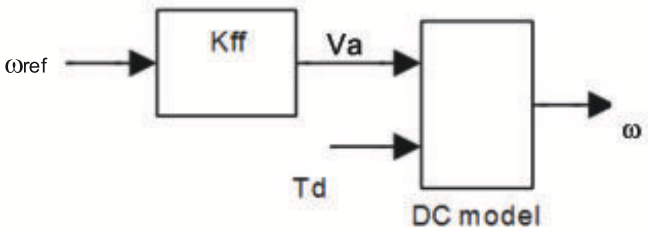

Figure 4-24: Model of feedforward control

The established value for $K_{ff} = 12.585$. The feedforward control design is a simple gain to reach the steady state value.

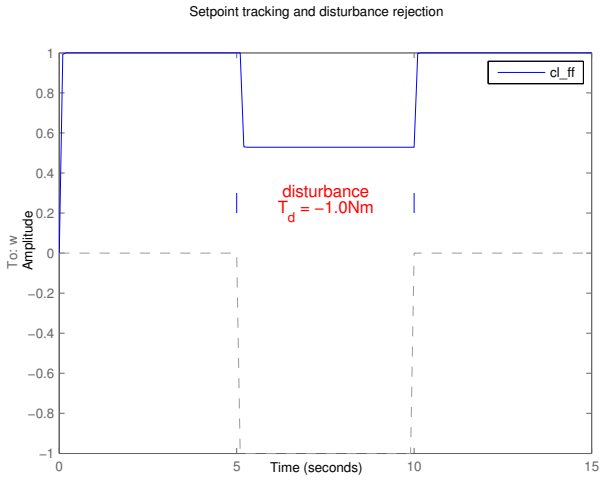

Figure 4-25: Plot of disturbance on a simplified model brushless servomotor closed loop

The feedback control Design is shown in Figure 4-26.

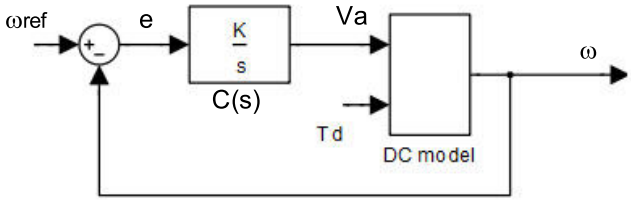

Figure 4-26: Model of feedback control

To enforce zero steady-state error, the integral control form $C(s) = K/s$ is used to determine the gain K. The root locus technique is applied to the open-loop and K=500 is found as a considerable value in this case.

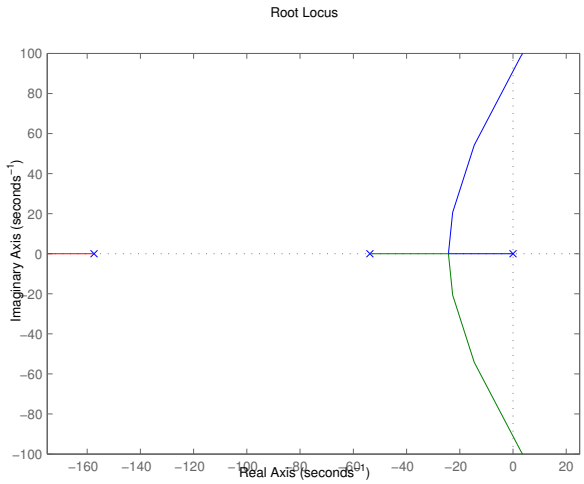

Figure 4-27: Rootlocus plot of simplified model brushless servomotor

The comparison of the influence of disturbance on the feedforward and feedback (estimated by the rootlocus method) technique are presented in Figure 4-28.

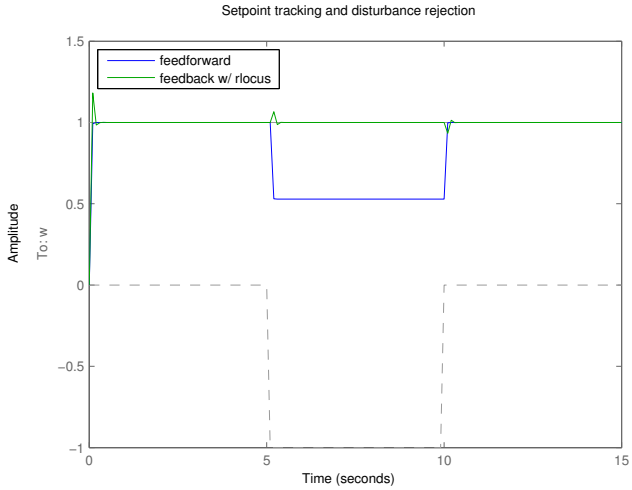

Figure 4-28: Plot of disturbance on a simplified model brushless servomotor feedback and feedforward

The system dynamics of the Linear-Quadratic Regulator (LQR) Control Design described by a set of linear differential equations and the costs described by a quadratic functional is called the LQ problem. One of the main results in the theory is that the solution is provided by the Linear-Quadratic Regulator (LQR). A feedback controller is shown in Figure 4-29.

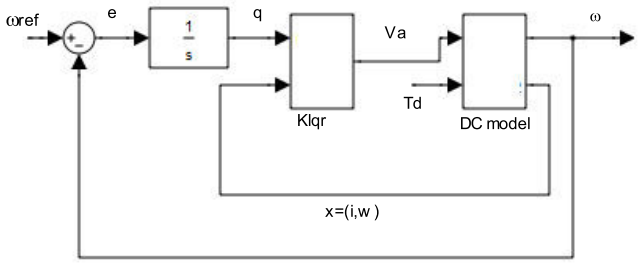

Figure 4-29: Model of linear-quadratic regulator (LQR) control

$$V_a = K_1 \cdot \omega + K_2 \cdot \omega/s + K_3 \cdot i \tag{4-10}$$

i is the armature current. Found the value K_1=44.721, K_2=20.934, K_3=3.389 for the LQR design. The comparison of the closed loop Bode diagrams for the three designs is shown on Figure 4-30.

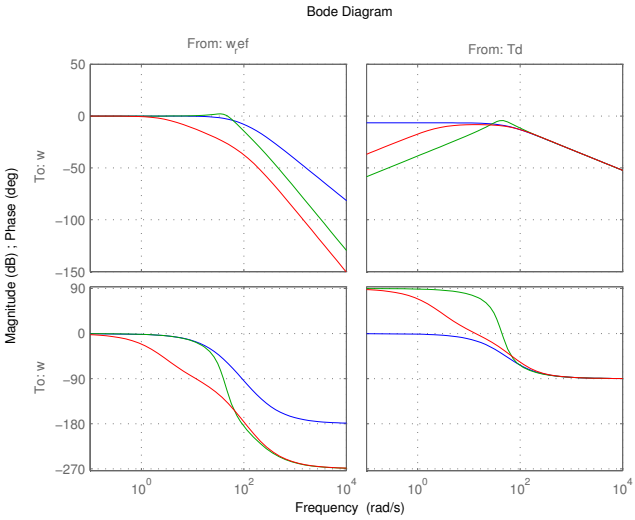

Figure 4-30: Bodeplot of design of a simplified model brushless servomotor

The -3 dB frequency is at 48.6 rad/s or 7.7 Hz the dominant pole. A First or second order model is a proper model for simulation in our case and a consistent solution. Finally the three designs on our simulation test case with disturbance are compared.

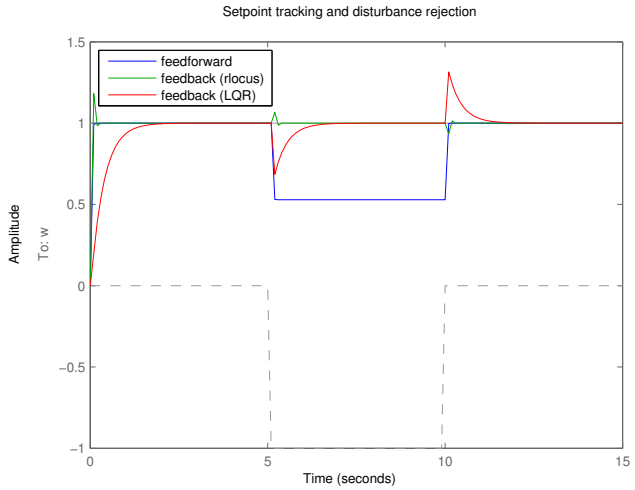

Figure 4-31: Plot of disturbance on a simplified model brushless servomotor LQR

4-4-3 Simplified synchronous brushless servomotor model

The results of the early presented brushless DC motor with and without additional gain controller does not correspond with the actual servo motor. It is not easy to produce a valid model for the selected servo motor. In the SimPowerSystems toolbox of Matlab Simulink is a reliable synchronous machine model available. This model fit the synchronous motor very well. The model is presented in Figure 4-32. The selected velocity input of the motor show a

complete fit with the FCS model. The torque option does not fit very well, every alteration of the input results in an over reaction, this can be seen in Figure 4-37. There is a enormous peak torque at the start.

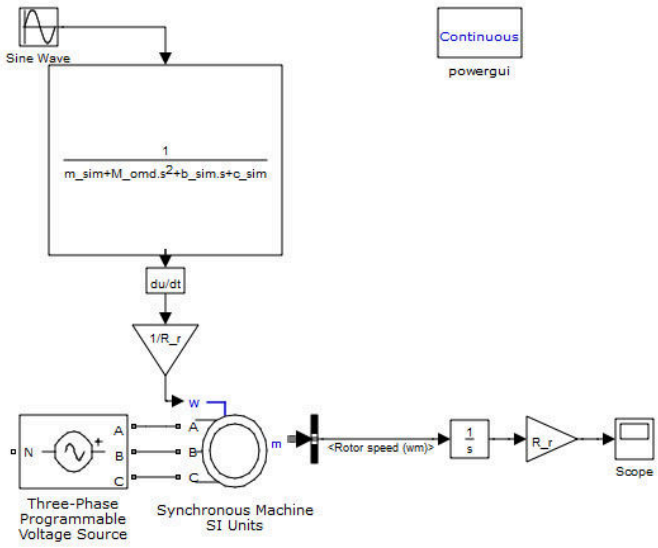

Figure 4-32: Design of a simplified synchronous brushless servomotor model

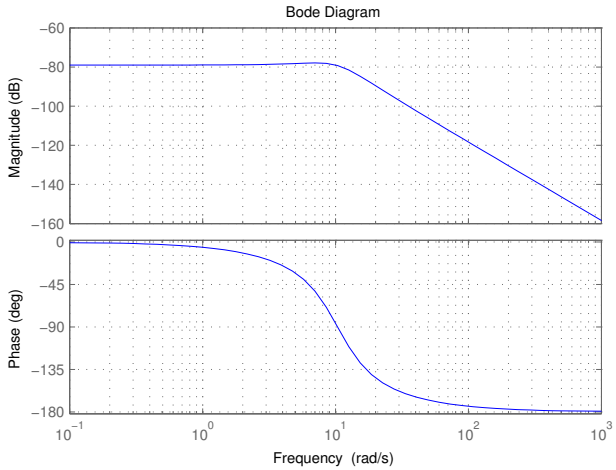

Figure 4-33: Bodeplot of velocity control loop synchronous servomotor model

4-4-4 Simulated Acceleration Bandwidth

Simulink model motor hard stop with load

For the simulation of hard end stop the acceleration is demanded at a certain force/moment. A force input is simulated as a step feed to a FCS model and he desired acceleration by two

acting forces have been calculated. The forces that have been calculated are 325 N and 750 N. The results of these calculations are shown in Figure 4-34 and 4-35

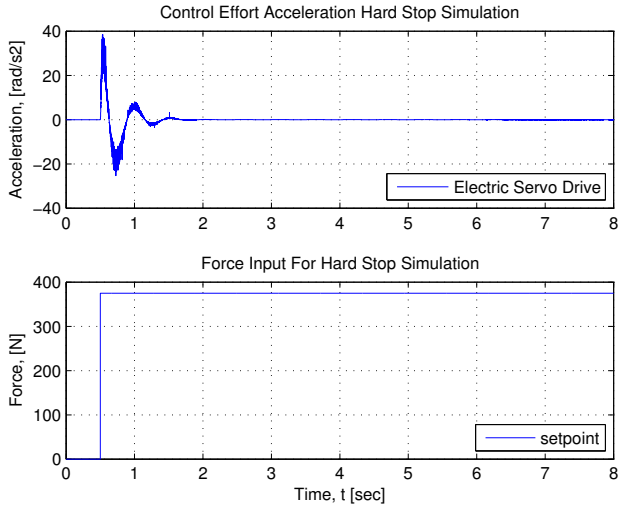

Figure 4-34: Acceleration during hard end stop simulation of the electrical servo system 375 N

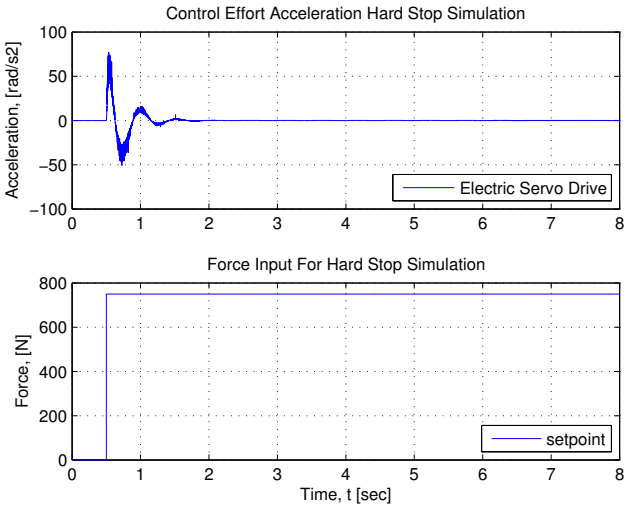

Figure 4-35: Acceleration during hard end stop simulation of the electrical servo system 750 N

In the figures an acceleration value of 35 rad/s^2 at 375 N acting force and an acceleration value of 70 rad/s^2 at 750 N acting force can be found.

Simulated acceleration bandwidth of performed electrical servo motor

In Figure 4-36 the result of the sinusoidal cyclic bandwidth is shown. When the Equation 3-9, J_t is taken for the bare motor, for the upper graph and J_t with added mass of limb in the lower graph, the maximum acceleration rate can be calculated. The rated angular acceleration

torque is 4190 rad/s. The results of the evaluated experiment show a slightly higher result, this is due to RMS value and also 15% additional performance. The simulated results present the continuous acceleration. The maximum acceleration rate is presented in Figure 4-36 and limited by the maximum revolutions of the motor and the calculated acceleration rate. For a pure sinusoidal signal the limits are presented in Figure 4-36. The calculated values are used for the other simulations and keep the additional performance in mind. In Figure 4-36 can be seen that the sinusoidal performance bandwidth of half the velocity amplitude is around 30 rad/s or 5 Hz. The calculated bandwidth limits of the performed solution are acceptable for the simulation task and within the limitations of a human person.

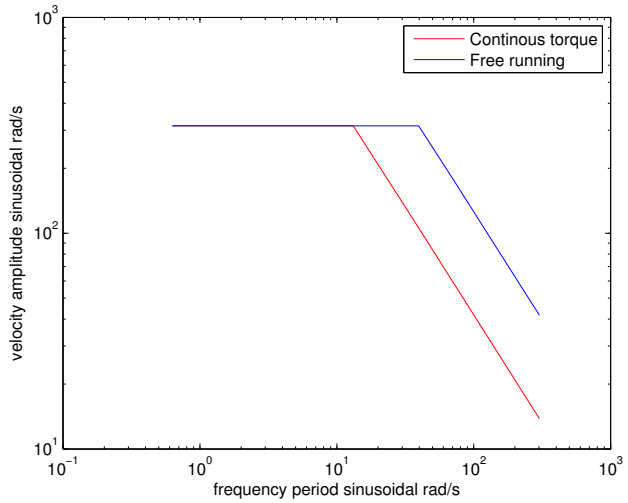

Figure 4-36: Bandwidth of sinusoidal cyclic velocity based on maximum acceleration

$$T_a = J_l \cdot \alpha \tag{4-11}$$

The acceleration rate is calculated by suggesting the specified rated torque and inertia of the motor and also the motor include load as constant. See also Equation 4-11. When applying the calculated acceleration rate and the limitations of the servo motor into a sinusoidal cyclic signal, the limited bandwidth can be established.

4-5 Comparison Hydraulic and Electrical Servo Simulation

In Figure 4-37 several methods of the control loop are presented. The earlier presented bode plots do not show very large effects on the lower frequencies. The effect is larger for the higher frequencies. The difference between the velocity and torque control loop can be inspected. The torque control loop does show a lot of lead compensation. Too much lead can cause oscillations, therefore the velocity control loop is the best solution to avoid too much lead compensation. The hydraulic velocity loop shows a little lead compensation, but the effect is marginal. The electric torque loop shows a oscillation at the start of each disturbance of the reference signal.

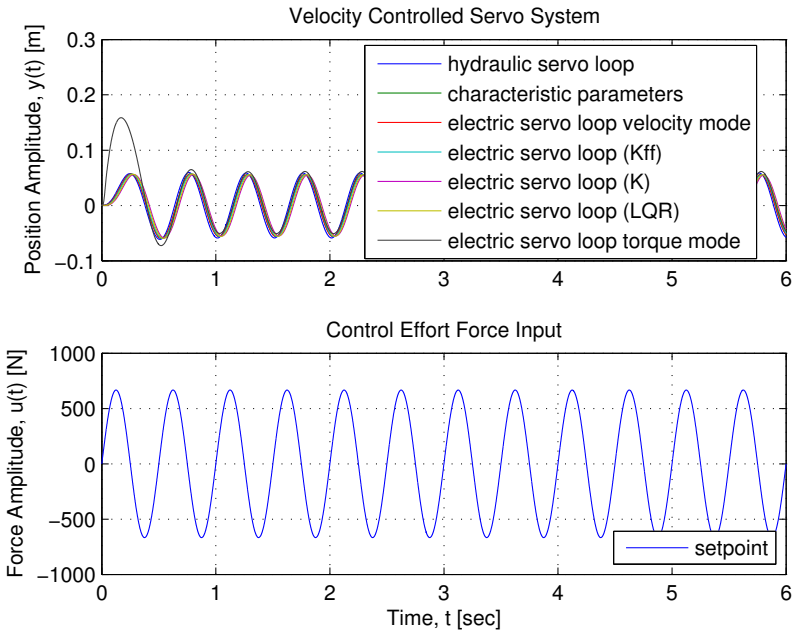

Figure 4-37: Comparison of a force sinus input response of a hydraulic and electrical servo system

In Figure 4-38 the zoomed comparison between the several control loops is shown.

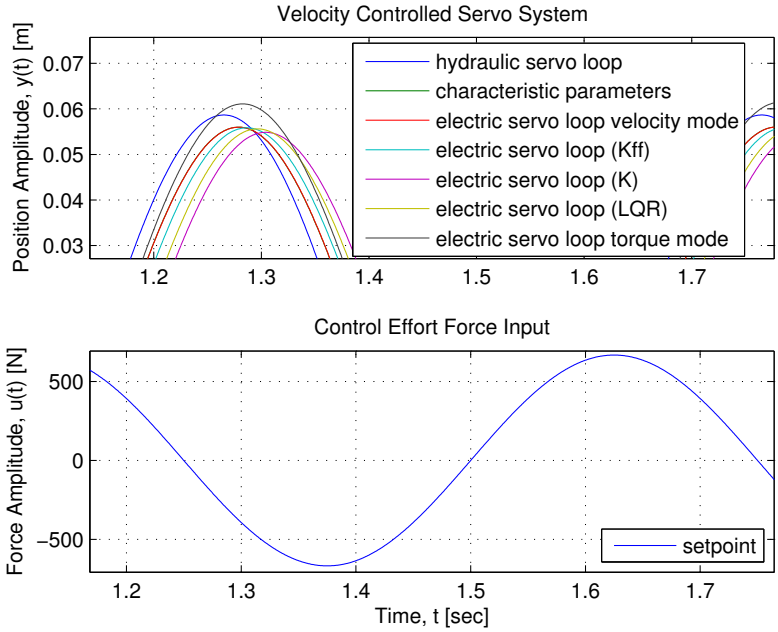

Figure 4-38: Zoomed comparison of a force sinus input response of a hydraulic and electrical servo system

In Figure 4-37 and 4-38, can be seen that the simple feedforward is a quite good solution.

What type of controller is used for the servo pack is not known. A LQR controller is a reliable controller in reaction aspect. The velocity loop of the standard synchronous motor in Matlab Simulink does not show any difference between with the reference input signal. This is a very good result, how the control loop will behave in practice is a relevant question.

4-6 Implementation possibilities for the selected servo drive

The selected servo drive can be set into several position related and force related modes. The force related option is not very accurate and has to be seen more to prevent overload. The two left over control modes are position and velocity. The velocity is more accurate when looking at the error signal. For further information about the control modes of the servo drive, please refer to the Appendix B.

4-7 Chapter summary

In this chapter the modeling of the original hydraulic driven actuators in three different (PVF) control loops is first explained. The second simulation is an electric driven actuator in the control loop, this is decided for several reasons. The simulation of the electric servo motor is difficult to establish because the lag of information of the servo pack. This has to be seen more as an estimation of the limitations of the servo system.

The input signal for the system identification is a sinus profile in the stationary part of the oscillation. The start up and stop of the oscillation is not acquainted with the simulation. The reason is the interference at the inrush oscillation and the abrupt stopping of the oscillation.

A sinusoidal input signal is achieved to inspect the response, the reason why there has been chosen for a sinusoidal input signal is the limitation on the travel and the mechanical system. It is not really a good solution to run a step profile or a trapezium pattern where the angle is less steep as in a step response. The jerk will have effect on the system like vibrating the rigid frame construction and so on. A sinus is maybe not the ideal identification method in terms of workload, however it is a smooth method for identification.

In the Chapter Flight Control System the dynamic behavior of the system is described. The components that are used for simulation is supposed as a linear system. The most important elements of the simulated model can be described as a second order mass-spring-damper system. In the Figure 4-1 the different elements of the mass-spring-damper system what is model for the simulation is shown. The ζ is supposed as a value of 0.7. The velocity loop is the best practical solution. The accuracy of the velocity loop is reasonable and a delay of calculation does not occur.

Chapter 5

Performance evaluation experiment

5-1 Rudder pedal Impression

First an impression of the result of the installed rudder pedals. A few pictures are taken to give an impression of the implemented system. The HMI-laboratory is separated by a glass wall into 2 locations, one control room and a experiment room. The picture 5-1 is taken from the projection screen to the subject place. Picture 5-2 is taken to get an impression of the electrical installation with the filters inside 5-3 and the EMC HF-shielding clamp 5-4.

Figure 5-1: Impression of the experiment room

Figure 5-2: Impression wiring electrical cabinet

On the right hand side in the picture 5-2, the power filter can be seen, left the additional connections POT (positive over travel) and NOT (negative over travel) and HOME proximity switches are situated. It is important to keep the signal cables as far as possible from the motor cable. At the bottom are the automatic fuse and earth leakage circuit breaker, safety relays and 24 VDC power supply for the servo and EtherCAT controller for communication.

Figure 5-3: Impression EMC filter

Figure 5-4: Impression circular EMC clamp

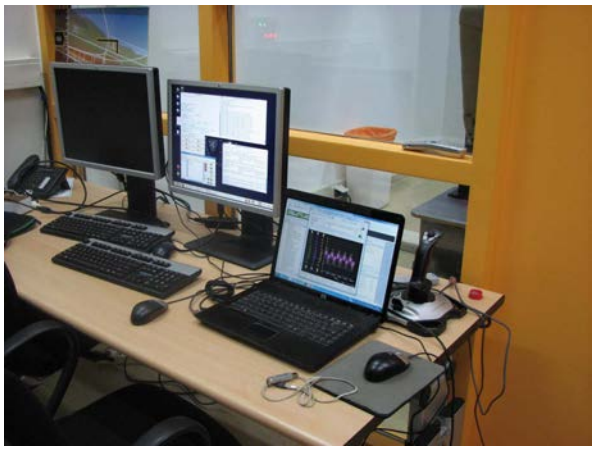

Figure 5-5: Impression of the controlroom

The picture 5-5 of the control room is taken from the side of the operator to the experiment room. An impression of the simulated mass is shown in Figure 5-6

Figure 5-6: Impression of the installed added mass 2 x 7.50 kg

5-2 Results of the velocity control loop

The implementation of the velocity control loop is realized by taking into account the hardware limits via over-travel sensors and also limited in software for position and velocity rate. To set up the communication, the middle-layer software DUECA is used. This program runs on a real time Linux kernel system 2.6. The communication protocol between the Yaskawa controller and de middle layer software is EtherCAT. The EtherCAT state machine handles the coordination of the master and slave applications during start up and operation. In Figures 5-12 till Figure 5-16 the most interesting acknowledgments, during the tests, are presented.

The first performance evaluation measurements are performed and monitored on two sides. One at the servo drive side and the other on the side of the torque transducer. The simulated

torque signal produced by the servo pack is not very accurate as mentioned before. The attached torque sensor is used for the control loop and not the torque signal produced by the servo pack. However the signal shows us the behavior of the current signal send to the motor.

5-2-1 Start stop input response

The start stop input response is a step response and is feasible for inspection of the behavior of the acceleration and deceleration time. In Figure 5-7 the start stop sequence from 0 to maximum velocity is shown. A delay between the actual velocity and the demanded velocity can be inspected.

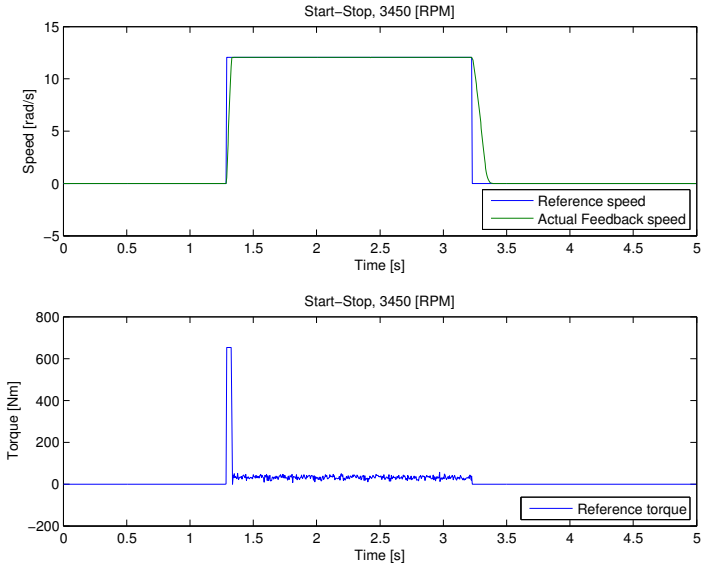

Figure 5-7: Results of measurement start stop mode

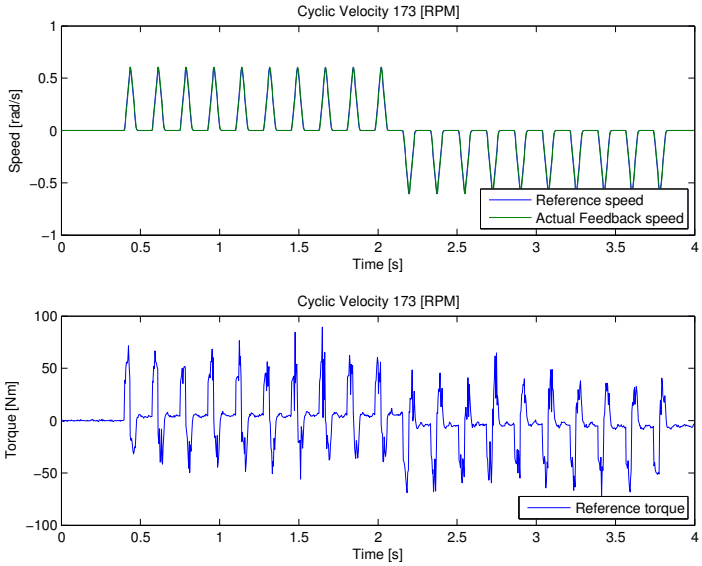

Figure 5-8: Results of measurement cyclic without torque

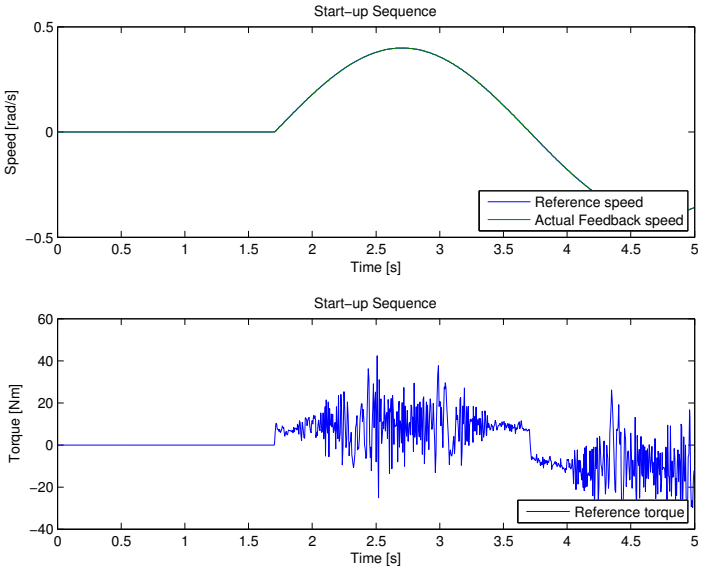

Figure 5-9: Results of measurement start-up without torque

5-2-2 Sinusoidal cyclic signal

To avoid reaching the hard end stop of the rudder pedals, a sinusoidal velocity profile is chosen over a commonly trapezoid profile. In Figure 5-11 the maximum sinusoidal frequency what can be reached at the desired maximum velocity is shown. A value of 12 Hz sinusoidal cycles can be reached. With a higher frequency (for example 16 Hz) the desired velocity can not be reached anymore. However reducing the amplitude of the maximum velocity will bring it back in the control range.

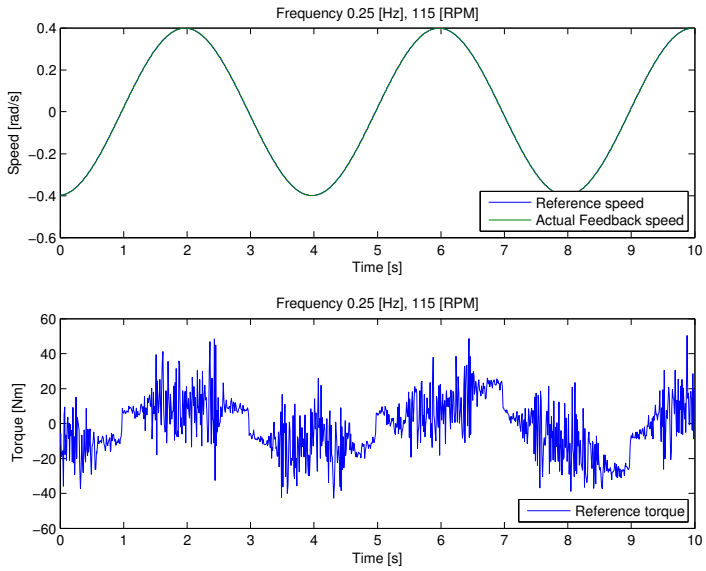

Figure 5-10: Results of measurement without torque in sinus mode

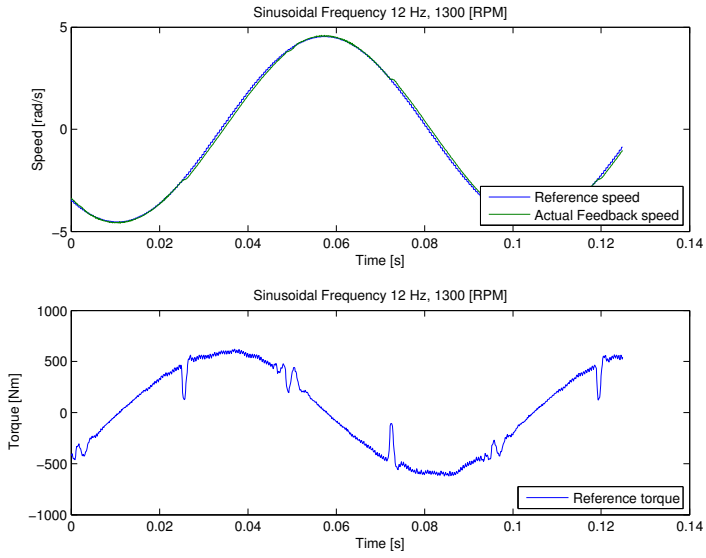

Figure 5-11: Results of measurement frequency response at 1300 RPM

The effect of without load at the rudder pedals and without added limp mass will have an oscillating effect on the torque signal. This is shown in Figure 5-10. Another imperfection on the torque signal can be seen in Figure 5-11. This disturbance effect is caused by the non synchronized Distributed Clock. A time delay will cause a disturbance, what also can be seen in the velocity signal when zoomed in at the specific point. A synchronized Distributed Clock will improve the results in the future. Some disturbance in the timing during the validation tests is noticed.

5-2-3 Noise on torque signal

The servo drive system influences the signal noise ratio in a negative way. The high frequency of voltage to the motor acts on the torque signal of the torque sensor. In Figure 5-12 the poor signal/noise ratio of the added torque transducer is shown. To inspect the relative noise on the bare measurement, a single ended measurement is inspected. The relative noise band without load or motion is between -5 and 13 Nm.

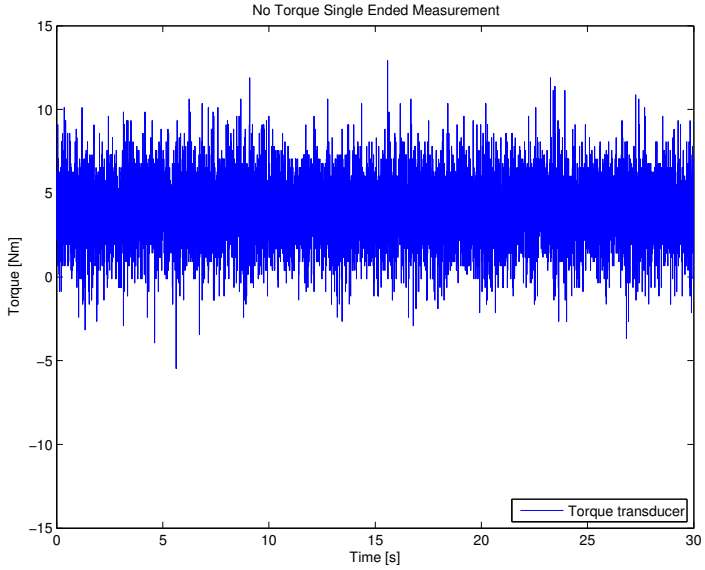

Figure 5-12: Results of measurement without torque, single ended input

To inspect the relative noise on the bare measurement, the differential input measurement is inspected. The relative noise band without load or motion is between 2 and 5 Nm.

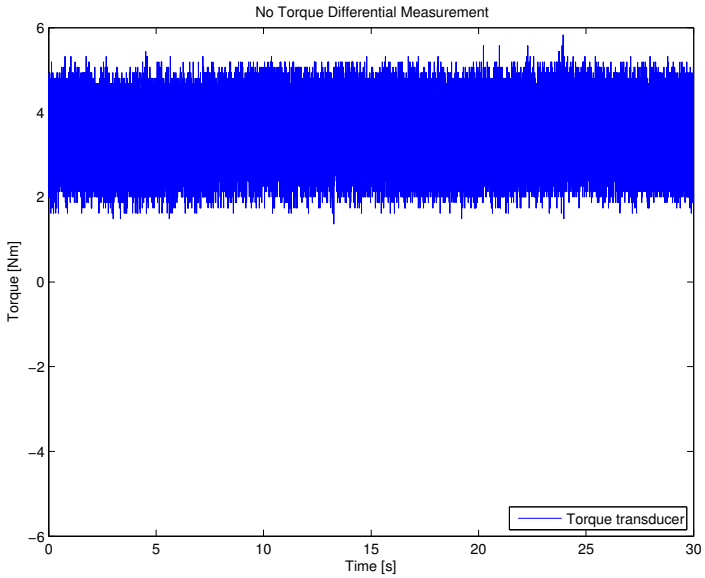

Figure 5-13: Results of measurement without torque, differential input

Another negative peculiarity of the electromagnetic compatibility (EMC) is the influence on the brake force transducer. When the servo pack is switched on, the noise on the strain gauge measuring device is increasing. The electronic strain gauge amplifier (victim) is installed in a plastic enclosure. However it is very important to reduce the radiation of the source. By using the scope on the power supply and measure signal a dominant 205.8 kHz sinus on the power is observed. The source of the radiation is the internal power supply of the Yaskawa servo pack. Another solution could be a power filter in line. This proposed solution is executed on two locations, between the power grid and the PWM power supply, and also between the power supply and the servo pack.

5-2-4 Added mass on rudder pedal

In Figure 5-16 the sinusoidal velocity response with added mass ($2 \cdot 7.50$ kg) at 2 Hz and 132 rad/s at the motor side is shown. The disturbance in the peak of the sinusoidal signal are the result of the rotation added mass around the brake shaft. This additional secondary control is added to control the brakes on the wheels of the landing gear. A spring system holds the pedal in place during flight and landing on the runway. To improve the results the pedal rotation can be fixed. When a disturbance in torque and speed is inspected, it is possible that this is due to a distinction in the timing between the slave servo-pack and the master Linux PC.

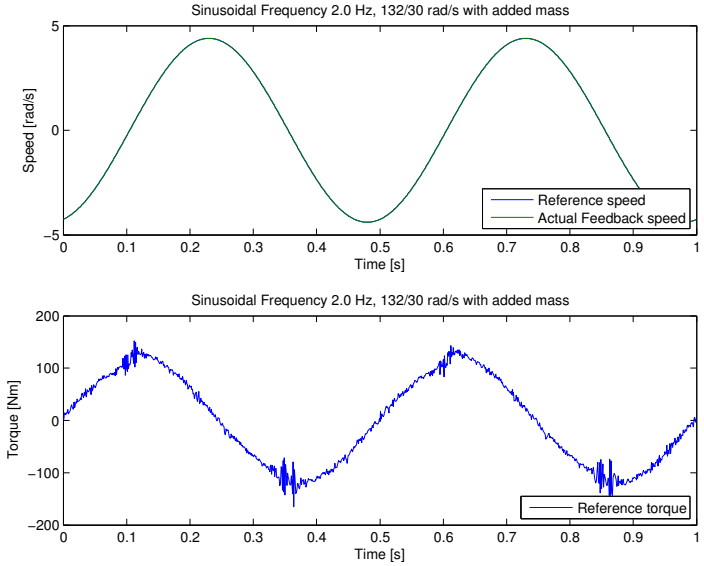

Figure 5-14: Results of sinusoidal velocity response with added mass 2Hz 132/30 rad/s

In Figure 5-15 the sinusoidal velocity response with real limb mass at 2 Hz and 132 rad/s at the motor side is shown. In this case a real limb of a human subject is taken as a load. The little hubs and hollows are the result of the inability of the subject to follow the 2 Hz sinusoidal signal in at maximum velocity as a relaxed task. The hinge effect of the pedal is also a reason of the hubs and hollows in the torque signal. The rotation is block on one side, this is the reason that the hinge effect is not symmetrical in the sinusoidal signal. The rotation movement is also spring loaded like a brake pedal in a car. The cumulative backless

at the ball joint rod end bearings has a negative contribution at the peculiarity of the system, especially when the movement is changing to the opposite direction.

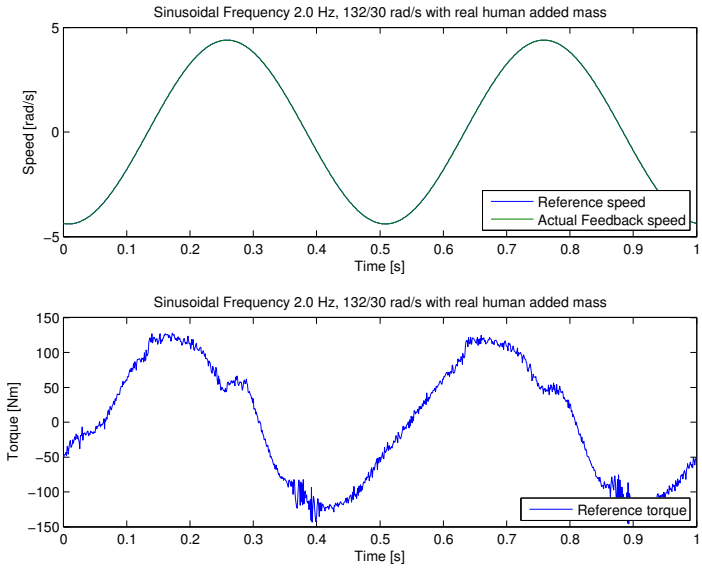

Figure 5-15: Results of sinusoidal velocity response with real human added mass 2Hz 132/30 rad/s

In Figure 5-16 the sinusoidal velocity response with real limb mass at 2 Hz and 132 rad/s at the motor side is shown. In this case a real limb of a human subject is taken as a load.

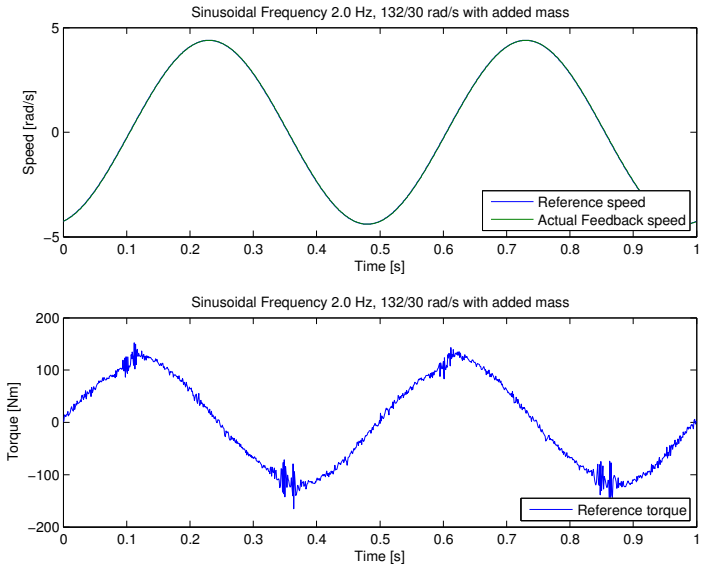

Figure 5-16: Results of sinusoidal velocity response with added mass 2Hz 132/30 rad/s

The influence of putting full torque left on the pedal is shown in Figure 5-17.

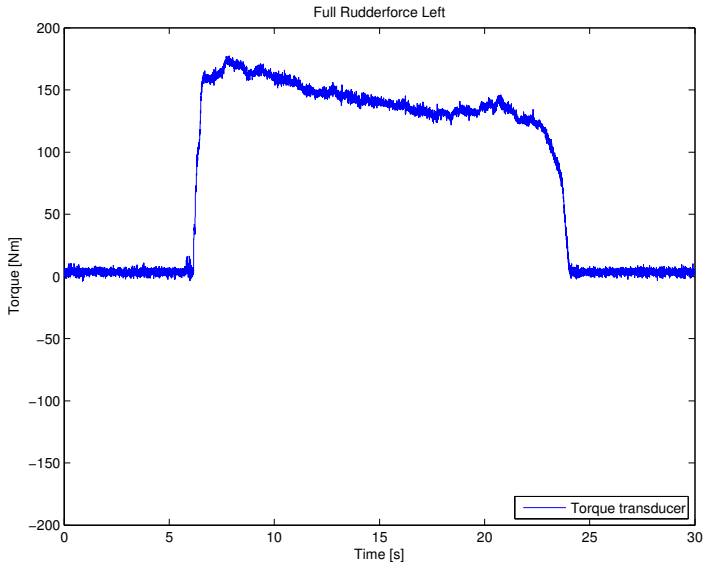

Figure 5-17: Results of measurement with full torque only left hand side

The influence of added mass with force is shown in Figure 5-18.

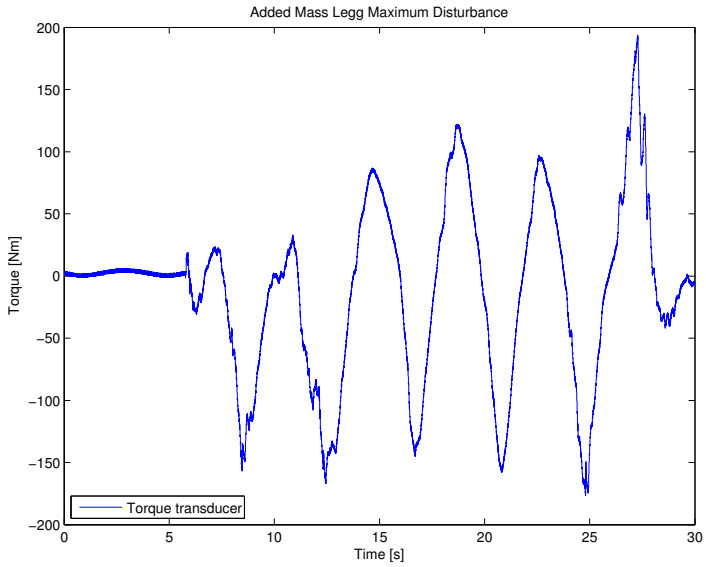

Figure 5-18: Results of measurement with added mass of limb

The influence of added mass without force (relaxed following task) is shown in Figure 5-19.

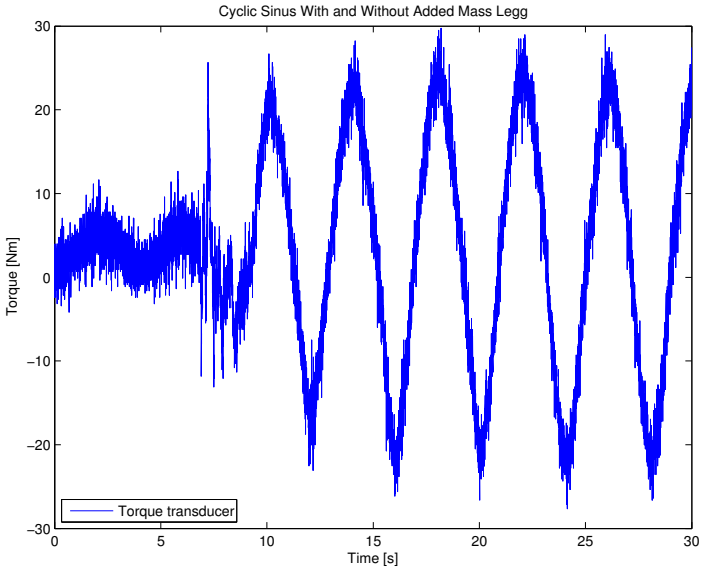

Figure 5-19: Results of measurement with added mass of limb following the sinus mode relaxed

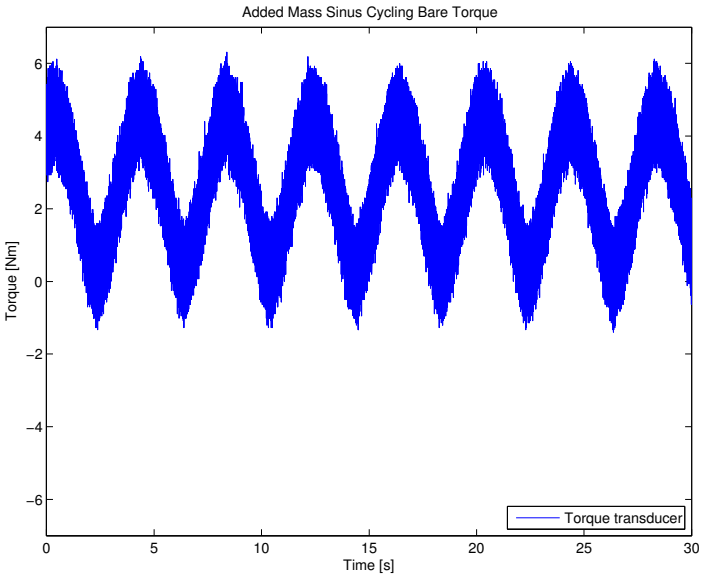

Figure 5-20: Results of measurement without torque in sinus mode

5-2-5 Bode plot velocity control loop

To check the results of the total rudder pedal system according to the required velocity bandwidth, a multi sine input signal is applied to the system. The reference signal and the actual signal for velocity are compared to each other in a bode plot. In Figure 5-25 the control loop is schematically presented. A remark about the summation point at the input-side is the + + summing point, this is because the reaction torque is measured.

The multi sine is composed by summing sinus signals with a reduced amplitude and can be divided by an n-number of the fundamental frequency. In the next 3 figures the idea of the multi sinus signal is explained. In Figure 5-21 the base frequency and his multiple numbers of this fundamental sinus signal is shown. The sinus signals are shifted in phase to avoid cumulative amplitude of the displacement and the steep acceleration at the start. The number of divided sinus signals is chosen as a prime number of oscillations, to avoid also cumulative difficulties in the Fast Fourier Transformation (FFT) analysis.

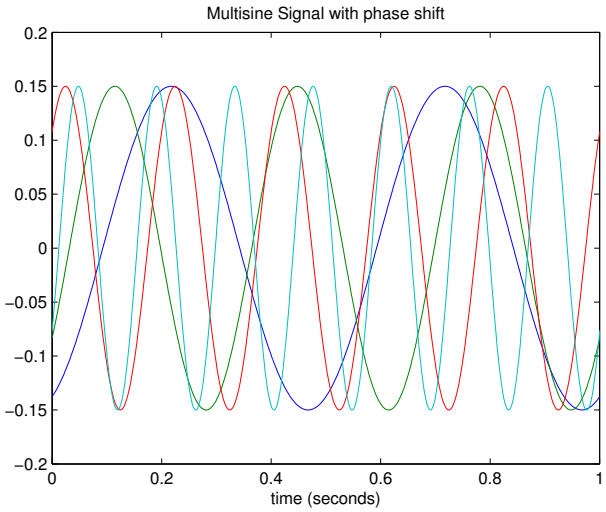

Figure 5-21: The fundamental sinus and the following sinus signals with phase shift

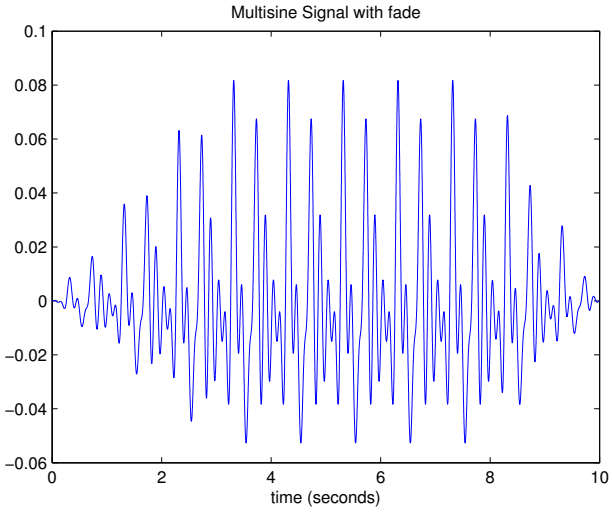

Figure 5-22: Multi sinus repeated input signal with fade in and fade out

In Figure 5-22 the signal with fade in and fade out is shown. The set of multi sinus signal is repeated 10 times. The first 3 seconds are used for fade in and the last 2 seconds of the 10 second total length is used for the fade out. In this particular example, the range from 5

till 8 seconds is a good representation for the FFT-analysis of the system. The chosen range needs to be a few seconds after reaching the desired amplitude, so the measurement starts when the system is settled.

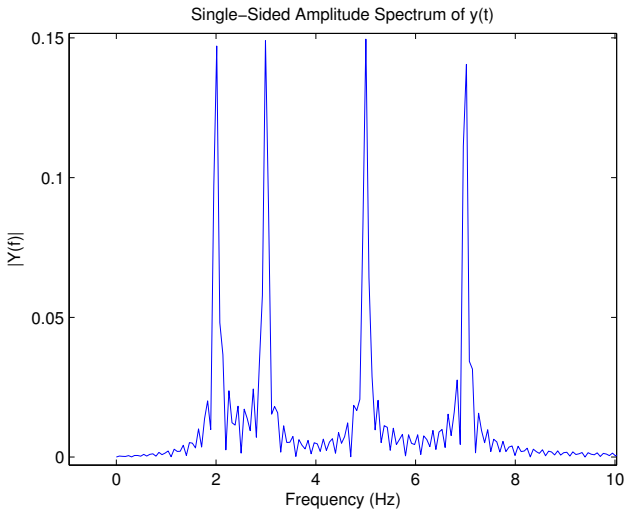

Figure 5-23: FFT of a multi sinus input signal of the relevant range

In Figure 5-23 the FFT-plot of the input signal is shown. In this particular example, the amplitude is taken 0.15. The dominant frequencies can be seen very easily.

Such a multi sine as described above is fed through the system. A FFT is obligated and the results are presented in Figure 5-26. The cross hairs and circles are the input sinuses of the multi sine and the response. The noise band is a result of the low power in the input signal to avoid reaching the end stops. For a gain plot the graph must be drawn between the cross hair points. The transfer function up till 24 Hz is a straight line. The amplitude for the higher frequency sinus signals is reduced to avoid reaching the hard end stops and overload in temperature of the servo pack. The system is not exploited to the maximum to avoid damaging the rudder pedals. Normally a narrow safety band is build around the maximum levels of position, velocity, acceleration and torque. These maximum levels take care of the system and the subject, but this is omitted for the evaluation test.

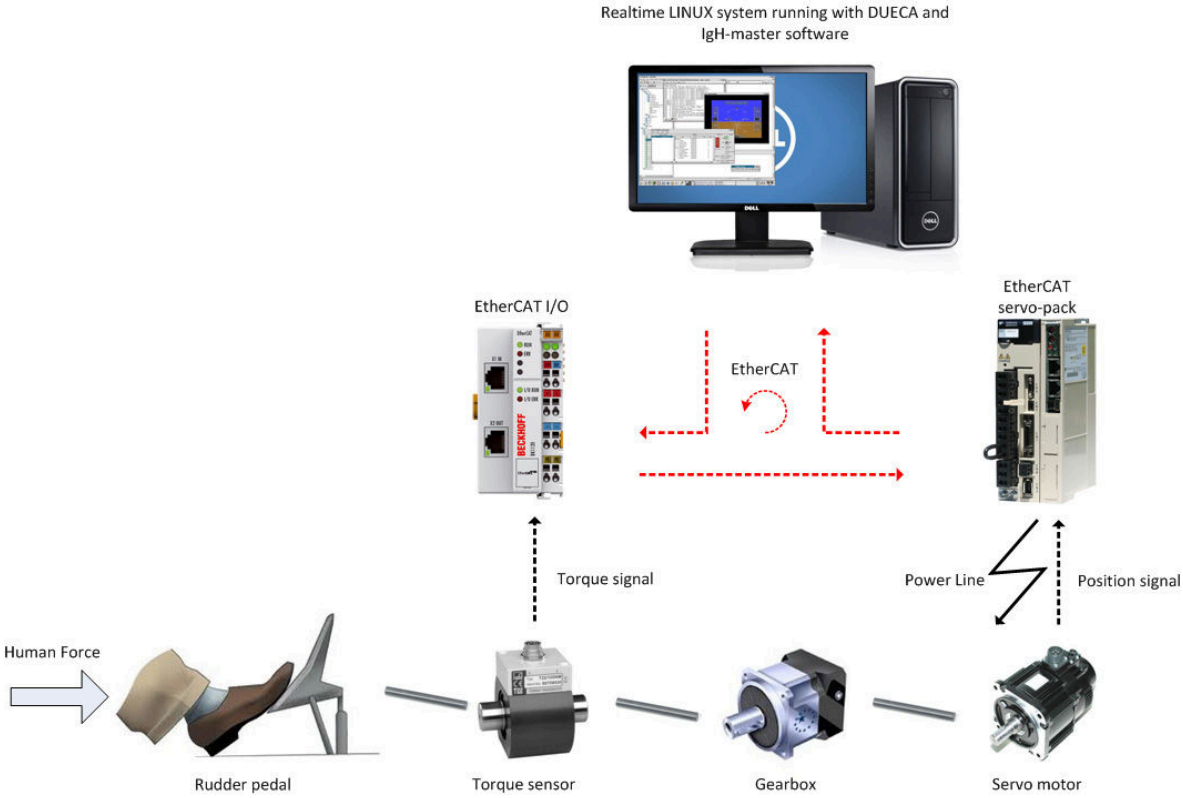

Figure 5-24: Control loop electric servo system with used components

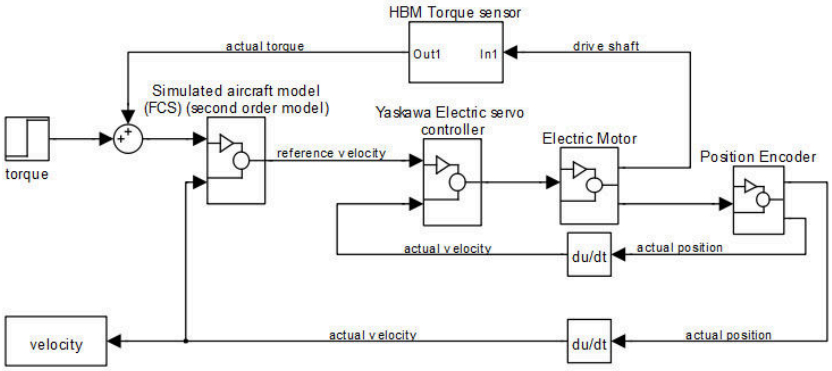

Figure 5-25: Control loop servo system schematic flow

The chosen control loop looks similar to the control they use for general haptic simulation. An example for haptic simulation is the HapticMaster at the TU Twente. The implemented control loop of the rudder pedal is similar to the HapticMaster. [19] The force feedback is really important for the haptic experience. Haptic technology, is a tactile feedback technology which takes advantage of the sense of touch by applying forces, vibrations, or motions to the user. For more results of the performance evaluation tests, please refer to the appendix.

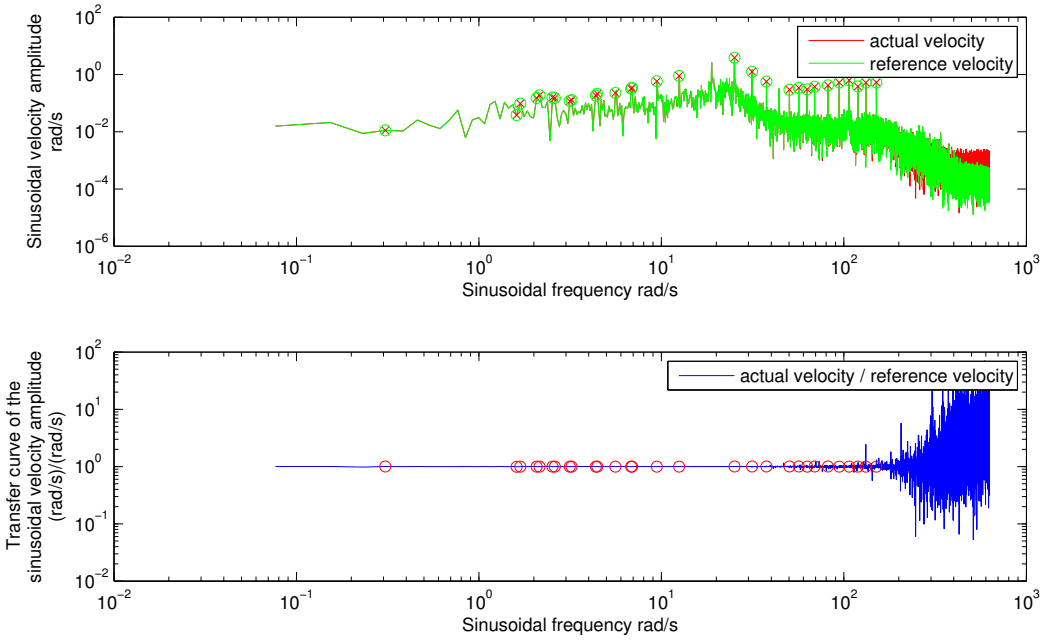

Figure 5-26: Results of multi sine velocity response

5-3 Chapter summary

The results of the velocity control loop are good for simulation of the rudder pedals. The EtherCAT communication is a good solution to avoid noise on the desired value and the actual position feedback. There is an annoying noise with a wavelength of 105.8 kHz. The action with litze cable on the ground plate did not have much effect on the acquired signal. The action with a filter in the power line does have effect on the noise. The noise is reduced to a reliable level. The remaining noise is in the MHz bandwidth. This possibly can be shifted away by ferrite cores around the cable. There is not much effect expected in reducing the noise level any more, and a certain side effect on the nearest cables can occur.

The bodeplot till 24 Hz shows a very nice result. A added white noise signal on the reference signal is actually not a correct way to identify the actuator. There is not enough power in the signal to obtain the bandwidth. The number of sinuses is not an integer number of the fundamental frequency. The peak levels in the FFT-plot will not show as a sharp desired level.

Chapter 6

Discussion

6-1 Discussion

When the results of the simulated model and the evaluation experiment are inspected, It can be noticed that the simulated results are optimistic in comparison to the evaluation measurements. The many (estimated) unknown variables do have influence on the total system. The proposed solution to design the system completely in the continuous range of the motor is a proper solution in this case.

The required 25 Hz bandwidth at maximum velocity can not be reached unfortunately. 14 Hz is reachable at maximum velocity. An additional brake resistor can enlarge the bandwidth. At a sinusoidal mode at 25 Hz, the maximum velocity of 26 rad/s can be reached at a maximum continuous torque of 208 Nm at the drive shaft of the gearbox. The maximum acceleration of 4190 rad/s^2 is the limited value in this particular situation.

The force control loop is better but not realistic to implement. The preferred control loop is the velocity control loop, there are several reason for it, the most important reason is the unsatisfying force signal and second, the difficulties to implement a force estimation model in the FCS.

The force signal with added mass seems more realistic for the motor controller inside and the current to the motor. The attached torque transducer reproduces a reliable signal, however the noise / signal ratio is poor.

The difference in the three hydraulic models (velocity, position and force) can be seen by the difference in settling time. A bode plot is obtained to inspect the differences. The influence of the system inertia has a relevant effect on the results and this can not be scaled by only a gain factor.

Chapter 7

Conclusions

7-1 Conclusions

When the requirements with the validation results are checked we could answer the research question sizing and designs as followed:

The choice of a gear ratio of 1:30 is a good opportunity, speed and torque requirement can be met. By reducing the torque via a gearbox, the inertia can also be reduced. For the inertia ratio of the drive system J_l/J_m maximum 5 is preferred. Our gear ratio is in the range of 1/5 of the motor inertia and gives a safety factor to compensate for possible mechanical construction complaints in the system.

Check with requirements:
Maximum force/moment is 250.2 Nm or 801.9 Nm. For a short period of 5 seconds by natural heat convection, the motor can produce 3 times the continuous value. The continuous value is already in specification and a safety factor is build in.

The travel range has not changed and a adjustment sensor is attached for correction

Velocity of 2 Hz sinusoidal cycling is possible and also at the maximum velocity of 1.3 m/s. The maximum frequency at maximum velocity is around 12 Hz. Lower velocity of the sinusoidal cyclic bandwidth of 24 Hz is validated and reachable. An additional brake resistor can enlarge the bandwidth, however is not necessary in this case.

The inertia ratio of the drive system 1.08 is reached in this case and for high performance the maximum value of 2 is allowed.

Chosen control loop:
The implemented velocity control loop works very well for this system. The force control loop is for several reason not the best solution for this situation. The lead compensation is too much and an oscillation can arise. The practical obstacle is the low accuracy of the derived torque value by the servo pack. This 0.1 % of the rated torque value and 0.25 Nm at the pedal shaft. The derived torque value of the servo is reliable for overload indication and safety, but is not useful as control signal. The translated current signal is oscillating heavily.

The position and velocity loop are feasible for implementation. The choice is made for the velocity loop, so to translate the signal to acceleration takes one integration an one derivation to the position.

The preferred control loop is velocity, there are several reason for it. The most important reason is the unsatisfied force signal and second the difficulties to implement a force estimation model in the FCS. The force signal with added mass seems more realistic for the motor controller inside and the current to the motor. The attached torque transducer reproduces a reliable signal, however the signal / noise ratio is poor.

There is no need to implement an additional control loop between the actual velocity and the reference (target) velocity. The build in controller of the Yaskawa drive is sufficient enough to control the velocity of the rudder pedals.

The requirements can be reached in a proper way with an electrical servo drive, this is proven by the validation tests. The safety environment is improved in comparison with the hydraulic actuator.

Appendix A

Alternative Solutions

A-1 Alternative Solution 1

A proposed solution is to exchange the hydraulic actuator for an electric servo direct drive as shown in the figure below.

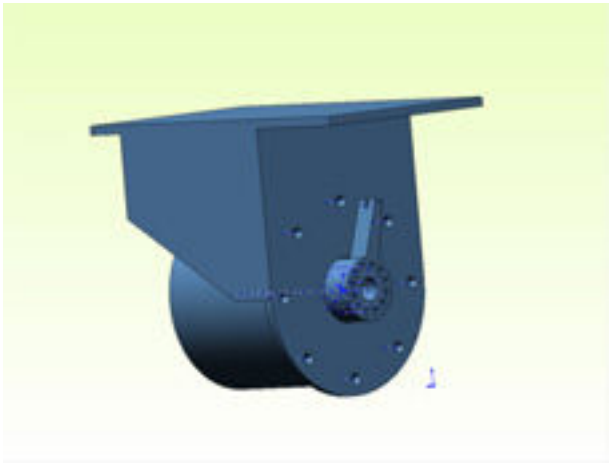

Figure A-1: Alternative solution 1 proposed exchange hydraulic motor directly for an electric servo direct drive

The experience we have acquired with one of our electric servo drive systems results in a preferred direct drive solution with a high torque motor of Parker Hannifin combined with a Compax3 servo controller. The documentation and specifications of the controller Compax3 of Parker [20] is examined. The direct drive motor type ST series [21] is a suitable solution for this matter. There are two types of drives that are suitable for installation. Type of drive 300STK4M and 300STK6M, delivers continuous 170 and 235 Nm at 11.8 and 16.3 Amps. Peak torque is 774 and 1161 Nm for a short time of 5 seconds by natural heat convection. The velocity of 4.656 m/s is acceptable, however this is not the speed the system will reach in

the decided time if the inertia can be neglected. A velocity of 1.3 m/s is the design criteria. Choice of angle encoder is single turn and absolute, the reason is the simple and accurate implementation. So choose Parker resolver and shaft type 1.
Parker motor selection: 300ST4M111K01CX
Servo Controller: C3S300V4F10I10T10M00

Maximum resolution for encoder on the controller side is: 14 bit (= 2^{14} = 16384 increments), so a standard resolver of Alxion has a resolution of 21600 increments per single turn and is accurate enough. The cycle time in communication via an Ethernet-variant is more than 1 ms. This is not acceptable and we prefer to increase this value by an analog version of the servo controller. The cycle time of the inner loop of the controller for is 8 kHz for the analog version. The resolution is 14 bit and range of +/- 10 V.

Operation mode is:
+/- 10 VDC speed command interface with encoder simulation as current value feedback.
+/- 10 VDC predefined current set point with encoder emulation for actual position value feedback and configurable holding functions.
Step/direction command input with step/direction signals as 24 VDC logic levels.
Step/direction command input with step/direction logic signals conforming to RS422 (5 VDC push-pull signal)

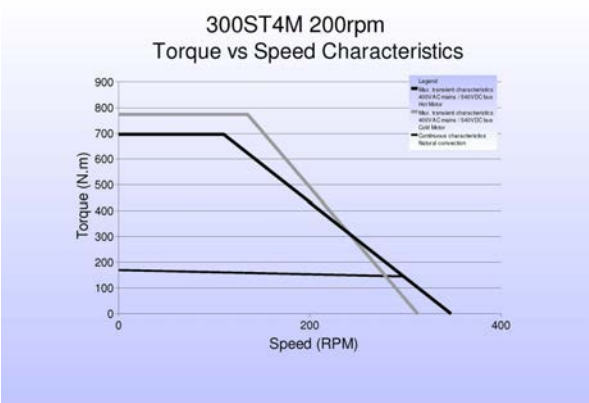

Figure A-2: Torque characteristics of the motor 300ST4M

A-1-1 Mechanical solution

The force transducer is mounted on the lever without any mechanical transition between rotor and force transducer. There could be expect a problem to control the system with a simulated position and velocity signal. This is difficult because the poor resolution getting back from the Parker servo control unit 8 bit, so 256 steps is far too low. A suggestion is to breakout the resolver encoder signal and feed back into the DAQ analog via a resolver to DC converter. Searching a good reliable converter that not exceed our financial budget was hard to find. A solution above 1500 euro is commonly asked for such a converter card. This let us to attach a secondary sensor next to the system. The sensor we like to install is a Novotechnik angle-encoder RSC 2801609111201. This is a 14 bit sensor for 90 degrees angle.

A-2 Alternative Solution 2

Suggest another transmission system and another servo drive from Yaskawa or Panasonic/Omron. By selecting another servo drive, the direct drive and a linear drive seems to be a reasonable solution. [22] A linear drive is an expensive solution due to the fact that you have 2 linear motors and also 2 servo controllers. Also the hardware setup for the rudder pedals have to be redesigned. This is not a suitable solution for our laboratory. Proposed is a solution with a direct drive. The companies Panasonic and Omron do not deliver a direct drive motor in their own product line. Of course it is possible to select a servo controller from another company, but this is not preferred to select the motor and the controller from the same supplier to avoid exchange difficulties in encoder communication. A suitable place to connect the direct drive motor on the rudder pedals is at the shaft of the second lever with the lever length of 182 mm. Now calculate back from the maximum speed what kind of motor is selectable in the torque range. T_2 is the required torque at the second pedal shaft:

$$\begin{aligned} F_{pd} &= 150lbf \approx 667N \\ T_2 &= \frac{F_{pd} \cdot i_2}{l_{i_2}} = 208Nm \end{aligned} \tag{A-1}$$

l_{i_2} = lever arm length from F_a to the second pedal shaft axis.

The selected servomotor could be a direct drive of Yaskawa SGMCS-80M with a continuous rated torque of 80 Nm, it is the first servo drive that fulfills the requirement on velocity and torque. The smallest transmission ratio for this motor is a transmission ratio of 2.6. This is a proper range for a cable transmission. The minimum drum-size is 18 times the cable diameter. With the selected motor of the 80M it is possible to reach the specified velocity of 1.3 m/s at a maximum continuous rated torque of 80 Nm and a peak torque of 240 Nm for a short time of 3 seconds by natural convection of heat. The accuracy of the absolute motor encoder is a resolution of 20 bit.

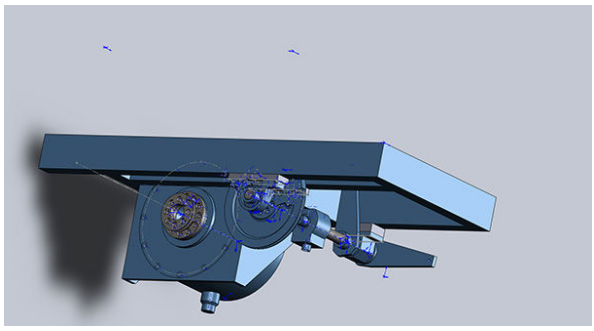

Figure A-3: Alternative solution 2 proposed gearing via a cable quadrant to an electric servo direct drive

The next step in selecting the drive is to define the servo controller. The preferred servo pack is the 15AE, which is 3 phase 230 voltage AC powered. We prefer the sigma V series if possible, because of the high bandwidth of 1.6 kHz instead of 400 Hz for the older Sigma II series. The cable size for the quadrant is calculated in according to the regulations NEN3508. [23]. Tension in the cable is around 200 kg at continuous torque, so take a work and safety

factor of 4, the break force will be 800 kg. Select a stainless steel AISI 316 cable with a maximum number of filaments according the flexibility. The construction of the cable is 7x19 filaments. Minimal drum size at the motor side is 18 times the cable diameter, according to the regulation of the norm NEN3508. A diameter of 100 mm is a acceptable suggestion, then the diameter of the quadrant becomes 260 mm. The static tension has to be taken as 0.5 times the maximum tension during continuous torque.

The tension in the cable can be measured with a cable tension measure tool. A proper bearing construction which can deliver the torque to the system without bucking of the shaft is necessary. A Suggestion is a bearing on both sides of the quadrant to avoid bucking of the shaft. Another suggestion is one full winding around the drum to avoid skidding of the cable. Check for minimal skid length for the cable, around 50 degrees contact length. Use a torque transducer. The T22 of Hottinger Baldwing is supposed to be a good transducer. Check the accuracy of the transducer, this is 0.2 percentage for this sensor, so the absolute accuracy becomes 1 Nm. The absolute force accuracy due to the torque sensor is 0.0312 N at the rudder pedals. The cost of a direct driven servomotor is over 8.000 Euro and this is over budget for this project. Proposed is to select another drive line system to connect the pedal axis to the servomotor via a gearbox with very low backlash.

A-3 Alternative Solution 3

Proposed alternative solution 3 is almost the same solution as the presented alternative solution 2, where the expensive direct motor is exchanged by a standard motor SGMGV-1EA. This is a standard motor 1500 RPM and needs to be connected to a power supply of 15 kW. This is pretty high for the small range we will use the motor for. An important disadvantage is the drift of the current in the windings of the servo motor when switching off the current to the motor. This is not acceptable for the other installed equipment in the HMI laboratory. Alternative solution 3 is a solution, however not a preferred solution.

A-4 Alternative Solution 4

For the next proposed solution, the selected motor size is made on the basis of the maximum speed in revolutions per minute. The selected range of servo motor the SGMGV-13D [9] has a nominal rated speed of 1500 RPM, which means 157.08 rad/sec. The maximum required speed is 4.54 rad/s; the maximum gear ratio that can be applied is 34.6. From torque respect, take 1:30. The maximum required torque is 208 Nm and gear ratio = 1:30 becomes 6.93 Nm required without any lose. A reasonable value for efficiency is 0.85. The torque at the motor shaft is 8.16 Nm. The maximum introduced backlash is 3 arc minute instead of 4 by an angled gearbox. [10] The nearest motor is a 8.34 Nm continuous torque. The next step is to design the selected drive line.

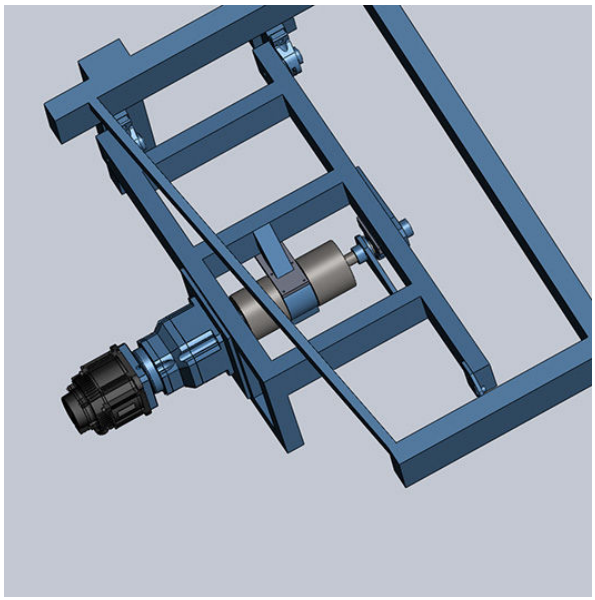

Figure A-4: Alternative solution 4 proposed gearing via planetary gearbox on an electric servo direct drive

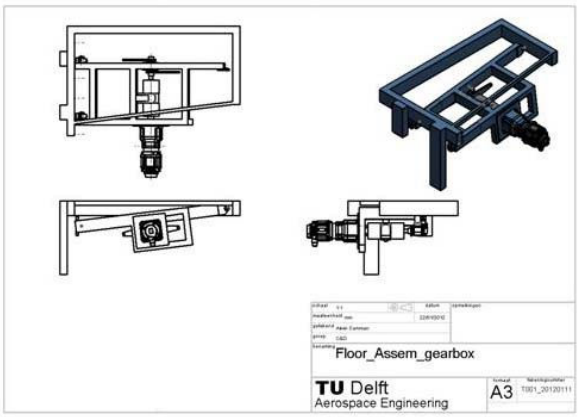

Figure A-5: Drawing alternative solution 4

A-5 Cost Analysis

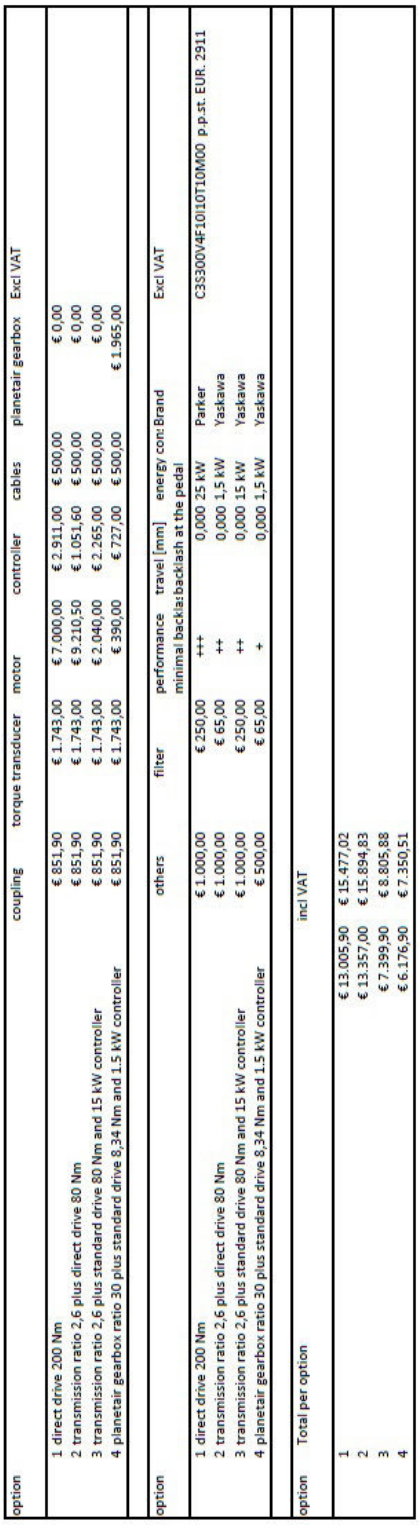

option		coupling	torque transducer	motor	controller	cables	planetair gearbox	Excl VAT
	1 direct drive 200 Nm	€ 851,90	€ 1.743,00	€ 7.000,00	€ 2.911,00	€ 500,00	€ 0,00	
	2 transmission ratio 2,6 plus direct drive 80 Nm	€ 851,90	€ 1.743,00	€ 9.210,50	€ 1.051,60	€ 500,00	€ 0,00	
	3 transmission ratio 2,6 plus standard drive 80 Nm and 15 kW controller	€ 851,90	€ 1.743,00	€ 2.040,00	€ 2.265,00	€ 500,00	€ 0,00	
	4 planetair gearbox ratio 30 plus standard drive 8,34 Nm and 1.5 kW controller	€ 851,90	€ 1.743,00	€ 390,00	€ 727,00	€ 500,00	€ 1.965,00	

option		others	filter	performance minimal backlash	travel [mm] at the pedal	energy con	Brand	Excl VAT
	1 direct drive 200 Nm	€ 1.000,00	€ 250,00	+++	0,000	25 kW	Parker	C33300V4F10I10T10M00 p.p.st. EUR. 2911
	2 transmission ratio 2,6 plus direct drive 80 Nm	€ 1.000,00	€ 65,00	++	0,000	1,5 kW	Yaskawa	
	3 transmission ratio 2,6 plus standard drive 80 Nm and 15 kW controller	€ 1.000,00	€ 250,00	++	0,000	15 kW	Yaskawa	
	4 planetair gearbox ratio 30 plus standard drive 8,34 Nm and 1.5 kW controller	€ 500,00	€ 65,00	+	0,000	1,5 kW	Yaskawa	

option	Total per option	incl VAT
	1	€ 13.005,90 € 15.477,02
	2	€ 13.357,00 € 15.894,83
	3	€ 7.399,90 € 8.805,88
	4	€ 6.176,90 € 7.350,51

Figure A-6: Cost analysis of 4 offered alternative solutions

A-6 Compare 4 Alternative Solutions

A-6-1 Energy Balance

Looking at the amount of energy needed for acceleration and exceeding the maximum continuous force on the pedals, a transmission is a good solution. The range of reliable backlash that is acceptable on the rudder pedals is a maximum transmission ratio of 1:50. The maximum size for the next step in another size controller is 1.5 kW.

For maximum speed a gear ratio of 30 is required at a maximum reachable number of revolutions of 1500 at a constant torque. The maximum allowed power supply for installation in our laboratories is in cause single phase ($16 \cdot 230$ VAC = 3.7 kW) and ($16 \cdot 400$ VAC = 6.4 kW) for three phase power supply. The smallest motor to meet the speed requirement at any specified force/torque is a 1.3 kW with a transmission ratio of 1:30.

A-6-2 Supposed Solution

Inertia is important to have in mind when using a gearbox in the drive system. [8] There are two drive-line systems that can be used to do this job (alternative solution 2 and 4). 3 systems are not really suitable, because the expensive solution (alternative solution 1 and 2) and the high current floating to the windings (alternative solution 3). A high current floating to the winding will introduce other neglected difficulties on other sensors in the system. The technical drawings are made for production. alternative solution number 4 is the best solution for us. The big advantage is that the range of the selected motor size, velocity and torque match with each other. Preferred is the 3 phase model of the drive system, because of the experience with inrush current by switching the controller on, in one of our other laboratory. In fact the 20 bit alternative solution is maybe not explicit necessary, however very useful for accurate data to implement in the control system. The gearbox is the part that can cause some problems in our system performance. For your understanding the backlash in other parts of the rudder pedals are higher than the standard backlash in the gearbox, so this can be neglected. Furthermore, the backlash in the rudder pedals is behind the motor, and this has no consequences for our control loop.

Appendix B

Installation Yaskawa Servo Drive

The servo pack installation is given on the next page, our system works without break resistor. It could possibly be added at any given time.

B-1 Overview Components

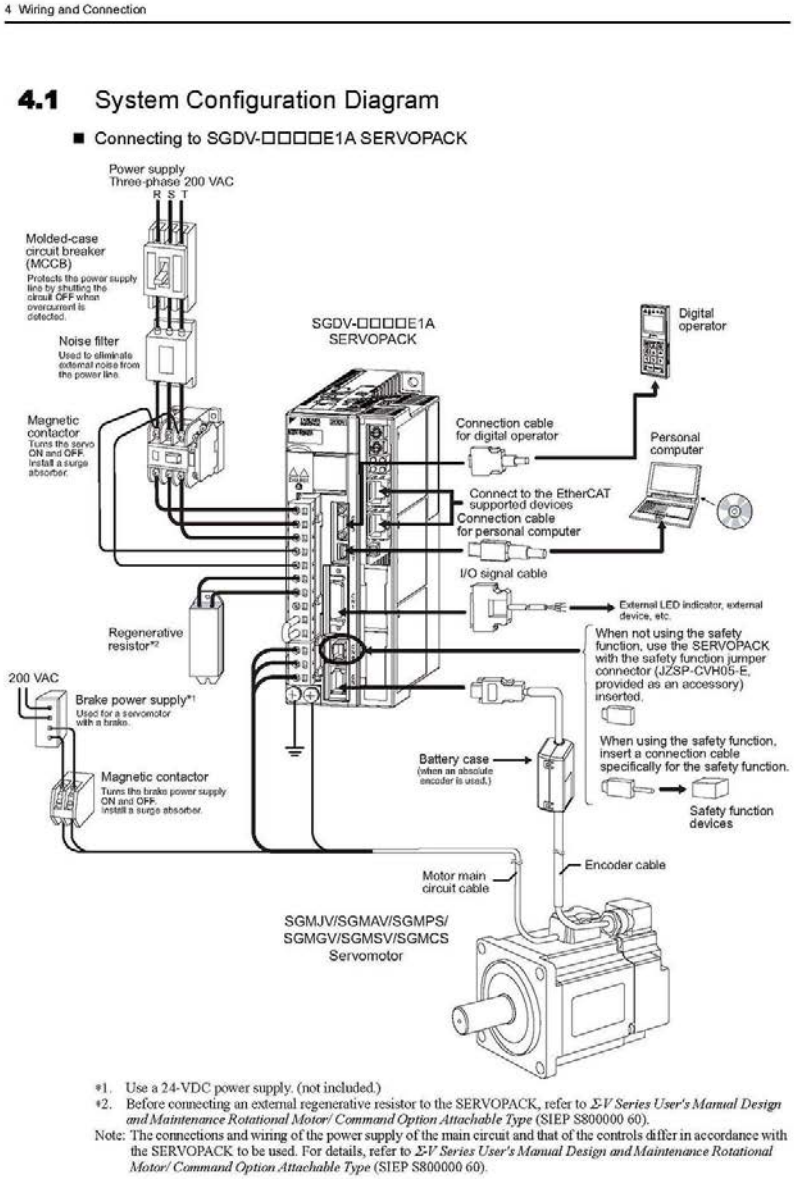

Figure B-1: Overview components Yaskawa SGMGH

Ratings and Specifications

Time Rating: Continuous
Vibration Class: V15
Insulation Resistance: 500 VDC, 10 MΩ min.
Ambient Temperature: 0 to 40°C
Excitation: Permanent magnet
Mounting: Flange-mounted
Thermal Class: F

Withstand Voltage: 1500 VAC for one minute (200-V Class)
1800 VAC for one minute (400-V Class)
Enclosure: Totally enclosed, self-cooled, IP67
(except for shaft opening)
Ambient Humidity: 20% to 80% (no condensation)
Drive Method: Direct drive
Rotation Direction: Counterclockwise (CCW) with forward run reference when viewed from the load side

200 V Class

Servomotor Model: SGMGV-□□□		03A	05A	09A	13A	20A	30A	44A	55A	75A	1AA	1EA
Rated Output*1	kW	0.3	0.45	0.85	1.3	1.8	2.9	4.4	5.5	7.5	11	15
Rated Torque*1	N·m	1.96	2.86	5.39	8.34	11.5	18.6	28.4	35.0	48.0	70.0	95.4
Instantaneous Peak Torque*1	N·m	5.88	8.92	13.8	23.3	28.7	45.1	71.1	87.6	119	175	224
Rated Current*1	A_{rms}	2.8	3.8	6.9	10.7	16.7	23.8	32.8	42.1	54.7	58.6	78
Instantaneous Max. Current*1	A_{rms}	8	11	17	28	42	56	84	110	130	140	170
Rated Speed*1	min^{-1}	1500										
Max. Speed*1	min^{-1}	3000									2000	
Torque Constant	$N·m/A_{rms}$	0.776	0.854	0.859	0.891	0.748	0.849	0.934	0.871	0.957	1.32	1.37
Rotor Moment of Inertia	$\times 10^{-4}$ kg·m²	2.48 (2.73)	3.33 (3.59)	13.9 (16)	19.9 (22)	26 (28.1)	46 (54.5)	67.5 (76.0)	89.0 (97.5)	125 (134)	242 (261)	303 (341)
Rated Power Rate*1	kW/s	15.5 (14.1)	24.6 (22.8)	20.9 (18.2)	35.0 (31.6)	50.9 (47.1)	75.2 (63.5)	119 (106)	138 (126)	184 (172)	202 (188)	300 (283)
Rated Angular Acceleration*1	rad/s²	7900 (7180)	8590 (7990)	3880 (3370)	4190 (3790)	4420 (4090)	4040 (3410)	4210 (3740)	3930 (3590)	3840 (3580)	2890 (2680)	3150 (2960)
Applicable SERVOPACK	SGDV-□□□□	3R8A	3R8A	7R6A	120A	180A	330A 220A*2	330A	470A	550A	590A	780A

*1: These items and torque-motor speed characteristics quoted in combination with a SERVOPACK are at an armature winding temperature of 20°C.
*2: Some restrictions apply when using an SGDV-200A SERVOPACK in combination with an SGMGV-30A servomotor.
Notes: 1 The values in parentheses are for servomotors with holding brakes.
2 The above specifications show the values under the cooling condition when the following heat sinks are mounted on the servomotors.
SGMGV-03A/-05A: 250 mm × 250 mm × 6 mm (aluminum)
SGMGV-09A/-13A/-20A: 400 mm × 400 mm × 20 mm (iron)
SGMGV-30A/-44A/-55A/-75A: 550 mm × 550 mm × 30 mm (iron)
SGMGV-1AA/-1EA: 650 mm × 650 mm × 35 mm (iron)

400 V Class

Servomotor Model: SGMGV-□□□		03D	05D	09D	13D	20D	30D	44D	55D	75D	1AD	1ED
Rated Output*	kW	0.3	0.45	0.85	1.3	1.8	2.9	4.4	5.5	7.5	11	15
Rated Torque*	N·m	1.96	2.86	5.39	8.34	11.5	18.6	28.4	35.0	48.0	70.0	95.4
Instantaneous Peak Torque*	N·m	5.88	8.92	13.8	23.3	28.7	45.1	71.1	87.6	119	175	224
Rated Current*	A_{rms}	1.4	1.9	3.5	5.4	8.4	11.9	16.5	20.8	25.7	28.1	37.2
Instantaneous Max. Current*	A_{rms}	4	5.5	8.5	14	20	28	40.5	52	65	70	85
Rated Speed*	min^{-1}	1500										
Max. Speed*	min^{-1}	3000									2000	
Torque Constant	$N·m/A_{rms}$	1.55	1.71	1.72	1.78	1.50	1.70	1.93	1.80	1.92	2.64	2.74
Rotor Moment of Inertia	$\times 10^{-4}$ kg·m²	2.48 (2.73)	3.33 (3.58)	13.9 (16)	19.9 (22)	26 (28.1)	46 (54.5)	67.5 (76.0)	89.0 (97.5)	125 (134)	242 (261)	303 (341)
Rated Power Rate*	kW/s	15.5 (14.1)	24.6 (22.8)	20.9 (18.2)	35.0 (31.6)	50.9 (47.1)	75.2 (63.5)	119 (106)	138 (126)	184 (172)	202 (188)	300 (283)
Rated Angular Acceleration*	rad/s²	7900 (7180)	8590 (7990)	3880 (3370)	4190 (3790)	4420 (4090)	4040 (3410)	4210 (3740)	3930 (3590)	3840 (3580)	2890 (2680)	3150 (2960)
Applicable SERVOPACK	SGDV-□□□□	1R9D	1R9D	3R5D	5R4D	8R4D	120D	170D	210D	260D	280D	370D

*: These items and torque-motor speed characteristics quoted in combination with a SERVOPACK are at an armature winding temperature of 20°C.
Notes: 1 The values in parentheses are for servomotors with holding brakes.
2 The above specifications show the values under the cooling condition when the following heat sinks are mounted on the servomotors.
SGMGV-03D/-05D: 250 mm × 250 mm × 6 mm (aluminum)
SGMGV-09D/-13D/-20D: 400 mm × 400 mm × 20 mm (iron)
SGMGV-30D/-44D/-55D/-75D: 550 mm × 550 mm × 30 mm (iron)
SGMGV-1AD/-1ED: 650 mm × 650 mm × 35 mm (iron)

49

Figure B-2: Specifications Yaskawa SGMGH 13A 400 Volt

Gearbox Performance

Model No.		Stage	Ratio	AB042	AB060	AB060A	AB090	AB090A	AB115	AB142	AB180	AB220
Nominal Output Torque T_{2N}	Nm	1	3	20	55	–	130	–	208	342	588	1,140
			4	19	50	–	140	–	290	542	1,050	1,700
			5	22	60	–	160	–	330	650	1,200	2,000
			6	20	55	–	150	–	310	600	1,100	1,900
			7	19	50	–	140	–	300	550	1,100	1,800
			8	17	45	–	120	–	260	500	1,000	1,600
			9	14	40	–	100	–	230	450	900	1,500
			10	14	40	–	100	–	230	450	900	1,500
		2	15	20	55	55	130	130	208	342	588	1,140
			20	19	50	50	140	140	290	542	1,050	1,700
			25	22	60	60	160	160	330	650	1,200	2,000
			30	20	55	55	150	150	310	600	1,100	1,900
			35	19	50	50	140	140	300	550	1,100	1,800
			40	17	45	45	120	120	260	500	1,000	1,600
			45	14	40	40	100	100	230	450	900	1,500
			50	22	60	60	160	160	330	650	1,200	2,000
			60	20	55	55	150	150	310	600	1,100	1,900
			70	19	50	50	140	140	300	550	1,100	1,800
			80	17	45	45	120	120	260	500	1,000	1,600
			90	14	40	40	100	100	230	450	900	1,500
			100	14	40	40	100	100	230	450	900	1,500
Emergency Stop Torque T_{peak}[3]	Nm	1,2	3~100	3 times of Nominal Output Torque								
Nominal Input Speed n_{1N}	rpm	1,2	3~100	5,000	5,000	5,000	4,000	4,000	4,000	3,000	3,000	2,000
Max. Input Speed n_{1a}	rpm	1,2	3~100	10,000	10,000	10,000	8,000	8,000	8,000	6,000	6,000	4,000
Micro Backlash P0	arcmin	1	3~10	–	–	–	≤1	≤1	≤1	≤1	≤1	≤1
		2	15~100	–	–	–	–	–	≤3	≤3	≤3	≤3
Reduced Backlash P1	arcmin	1	3~10	≤3	≤3	≤3	≤3	≤3	≤3	≤3	≤3	≤3
		2	15~100	≤5	≤5	≤5	≤5	≤5	≤5	≤5	≤5	≤5
Standard Backlash P2	arcmin	1	3~10	≤5	≤5	≤5	≤5	≤5	≤5	≤5	≤5	≤5
		2	15~100	≤7	≤7	≤7	≤7	≤7	≤7	≤7	≤7	≤7
Torsional Rigidity	Nm/arcmin	1,2	3~100	3	7	7	14	14	25	50	145	225
Max. Radial Load F_{2a}[3]	N	1,2	3~100	780	1,530	1,530	3,250	3,250	6,700	9,400	14,500	50,000
Max. Axial Load F_{2a}[3]	N	1,2	3~100	390	765	765	1,625	1,625	3,350	4,700	7,250	25,000
Service Life	hr	1,2	3~100	20,000+								
Efficiency η	%	1	3~10	≥97%								
		2	15~100	≥94%								
Weight	kg	1	3~10	0.6	1.3	–	3.7	–	7.8	14.5	29	48
		2	15~100	0.8	1.5	1.9	4.1	5.3	9	17.5	33	60
Operating Temp	°C	1,2	3~100	-10°C~+90°C								
Lubrication		1,2	3~100	Synthetic lubrication oils								
Degree of Gearbox Protection		1,2	3~100	IP65								
Mounting Position		1,2	3~100	all directions								
Noise Level (n_1=3000rpm, No Load)	dB(A)	1,2	3~100	≤56	≤58	≤60	≤60	≤63	≤63	≤65	≤67	≤70

Gearbox Inertia

Model No.		Stage	Ratio	AB042	AB060	AB060A	AB090	AB090A	AB115	AB142	AB180	AB220
Mass Moments of Inertia J_1	kg · cm²	1	3	0.03	0.16	–	0.61	–	3.25	9.21	28.98	69.61
			4	0.03	0.14	–	0.48	–	2.74	7.54	23.67	54.37
			5	0.03	0.13	–	0.47	–	2.71	7.42	23.29	53.27
			6	0.03	0.13	–	0.45	–	2.65	7.25	22.75	51.72
			7	0.03	0.13	–	0.45	–	2.62	7.14	22.48	50.97
			8	0.03	0.13	–	0.44	–	2.58	7.07	22.59	50.84
			9	0.03	0.13	–	0.44	–	2.57	7.04	22.53	50.63
			10	0.03	0.13	–	0.44	–	2.57	7.03	22.51	50.56
		2	15	0.03	0.03	0.13	0.13	0.47	0.47	2.71	7.42	23.29
			20	0.03	0.03	0.13	0.13	0.47	0.47	2.71	7.42	23.29
			25	0.03	0.03	0.13	0.13	0.47	0.47	2.71	7.42	23.29
			30	0.03	0.03	0.13	0.13	0.47	0.47	2.71	7.42	23.29
			35	0.03	0.03	0.13	0.13	0.47	0.47	2.71	7.42	23.29
			40	0.03	0.03	0.13	0.13	0.47	0.47	2.71	7.42	23.29
			45	0.03	0.03	0.13	0.13	0.47	0.47	2.71	7.42	23.29
			50	0.03	0.03	0.13	0.13	0.44	0.44	2.57	7.03	22.51
			60	0.03	0.03	0.13	0.13	0.44	0.44	2.57	7.03	22.51
			70	0.03	0.03	0.13	0.13	0.44	0.44	2.57	7.03	22.51
			80	0.03	0.03	0.13	0.13	0.44	0.44	2.57	7.03	22.51
			90	0.03	0.03	0.13	0.13	0.44	0.44	2.57	7.03	22.51
			100	0.03	0.03	0.13	0.13	0.44	0.44	2.57	7.03	22.51

1. Ratio (i=N_1 / N_{out}) 2. Max. acceleration torque T_{2a} = 60% of T_{2peak} 3. Applied to the output shaft center @ 100 rpm
★ S1 service life 10,000 hrs (Consult us)

APEX 3

Figure B-3: Specifications APEX gearbox AB142-030-SGMGH

B-2 Overview Wiring

4.2.3 Example of I/O Signal Connections

The following diagram shows a typical connection example.

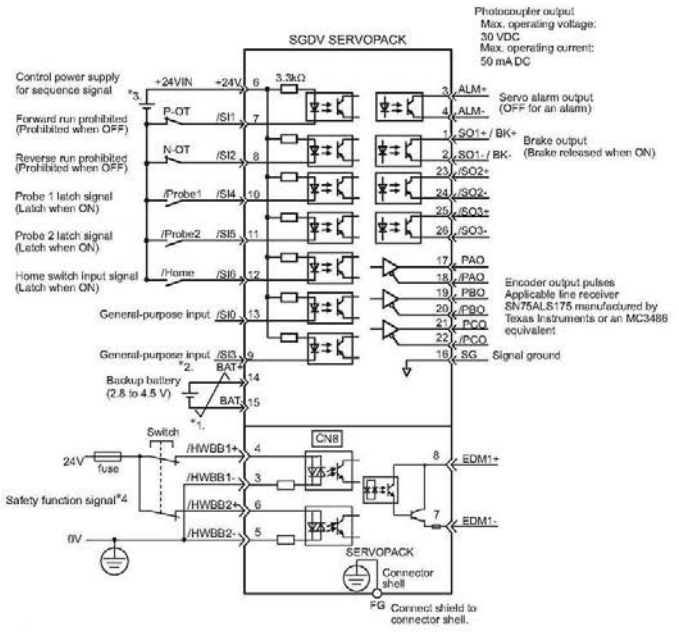

*1. represents twisted-pair wires.
*2. Connect when using an absolute encoder. When the encoder cable for the battery case is connected, do not connect a backup battery.
*3. The 24 VDC power supply is not included. Use a power supply with double insulation or reinforced insulation.
*4. To turn the servomotor power ON, a safety device must be connected and the wiring to activate the safety function must be done. When not using the safety function, use the SERVOPACK with the plug (JZSP-CVH05-E, provided as an accessory) inserted into the CN8.

Note: The functions allocated to the input signals P-OT, N-OT, /Probe1, /Probe2, and /Home and the output signals /SO1, /SO2, and /SO3 can be changed by using the parameters. Refer to *4.3.1 Input Signal Allocations* and *4.3.2 Output Signal Allocations*.

Figure B-4: Overview wiring Yaskawa SGMGH

Important is the EtherCAT state machine and it has to be followed very strictly to get the slave motor into running.

B-3 EtherCAT State flow

6 EtherCAT Communication

6.3 EtherCAT State Machine

The EtherCAT State Machine (ESM) is responsible for the coordination of master and slave applications at start up and during operation. State changes are typically initiated by requests of the master.
The states of the EtherCAT State Machine are as follows.

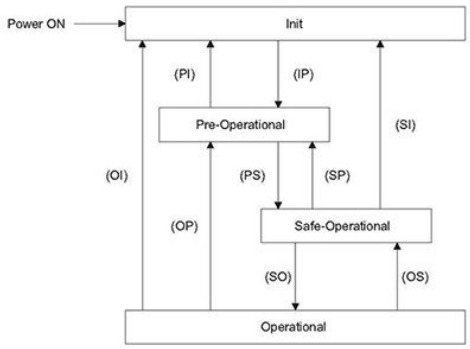

State	Description
Init	• No mailbox communication is possible. • No process data communication is possible.
Init to Pre-Op	• Master configures DL Address and SyncManager channels for Mailbox communication. • Master initializes DC clock synchronization. • Master requests 'Pre-Operational' state. • Master sets AL Control register. • Slave checks whether the mailbox was initialized correctly.
Pre-operational (Pre-Op)	• Mailbox communication is possible. • No process data communication is possible.
Pre-Op to Safe-Op	• Master configures SyncManager channels and FMMU channels for process data. • Master configures PDO mapping and the sync manager PDO assignment parameters via SDO. • Master requests 'Safe-Operational' state. • Slave checks whether the sync manager channels for process data communication and, if required, the distributed clocks settings are correct.
Safe-Operational (Safe-Op)	• Mailbox communication is possible. • Process Data communication is possible, but only Inputs are evaluated – Outputs remain in 'Safe' state.
Safe-Op to Op	• Master sends valid Outputs. • Master requests 'Operational' state.
Operational (Op)	• Mailbox communication is possible. • Process data communication is possible.

6-4

Figure B-5: EtherCAT state flow

The Yaskawa state flow can be write and read real-time via the specific addresses.

B-4 Yaskawa Drive State flow

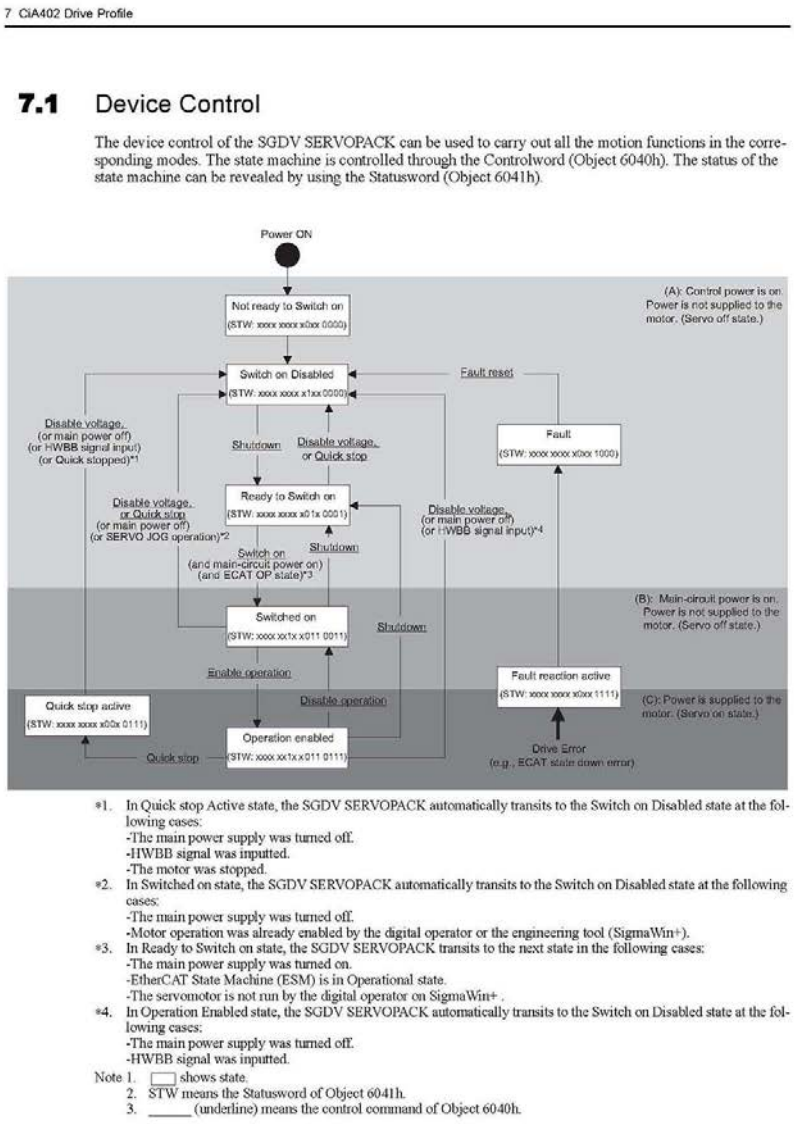

7 CiA402 Drive Profile

7.1 Device Control

The device control of the SGDV SERVOPACK can be used to carry out all the motion functions in the corresponding modes. The state machine is controlled through the Controlword (Object 6040h). The status of the state machine can be revealed by using the Statusword (Object 6041h).

*1. In Quick stop Active state, the SGDV SERVOPACK automatically transits to the Switch on Disabled state at the following cases:
-The main power supply was turned off.
-HWBB signal was inputted.
-The motor was stopped.

*2. In Switched on state, the SGDV SERVOPACK automatically transits to the Switch on Disabled state at the following cases:
-The main power supply was turned off.
-Motor operation was already enabled by the digital operator or the engineering tool (SigmaWin+).

*3. In Ready to Switch on state, the SGDV SERVOPACK transits to the next state in the following cases:
-The main power supply was turned on.
-EtherCAT State Machine (ESM) is in Operational state.
-The servomotor is not run by the digital operator on SigmaWin+ .

*4. In Operation Enabled state, the SGDV SERVOPACK automatically transits to the Switch on Disabled state at the following cases:
-The main power supply was turned off.
-HWBB signal was inputted.

Note 1. ☐ shows state.
2. STW means the Statusword of Object 6041h.
3. _____ (underline) means the control command of Object 6040h.

7-2

Figure B-6: Yaskawa drive state flow

B-5 Modes of operation SGDV servopack

The electrical servo drive (SGDV SERVOPACK) with EtherCAT communication support a set of 8 modes of operation. The chosen operation mode is the cyclic synchronous velocity

mode. These modes of operation are:

- Profile Position mode
- Interpolated Position mode
- Cyclic Synchronous Position mode
- Homing mode
- Profile Velocity mode
- Cyclic Synchronous Velocity mode
- Torque Profile mode
- Cyclic Synchronous Torque mode

B-5-1 Profile Position mode

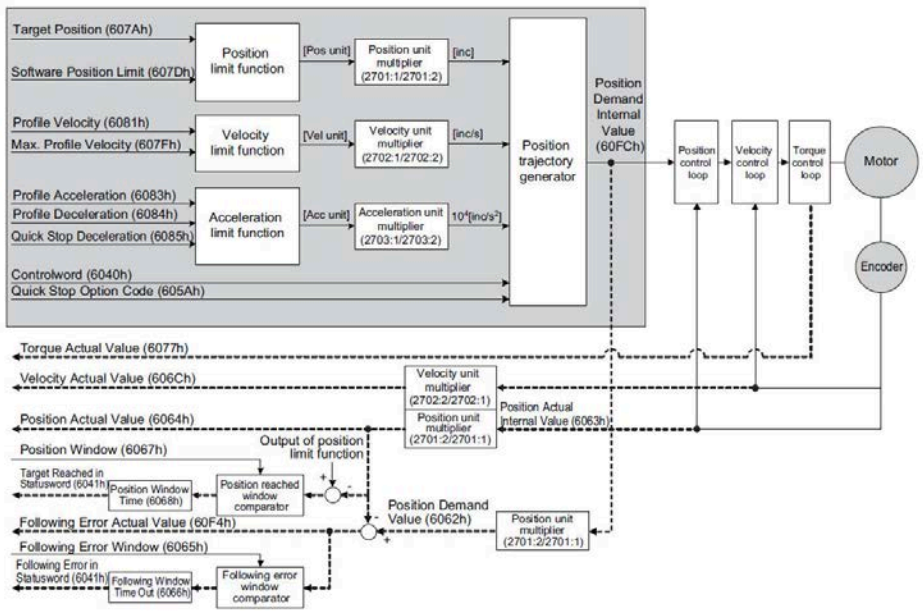

Figure B-7: Profile Position mode

B-5-2 Interpolated Position mode

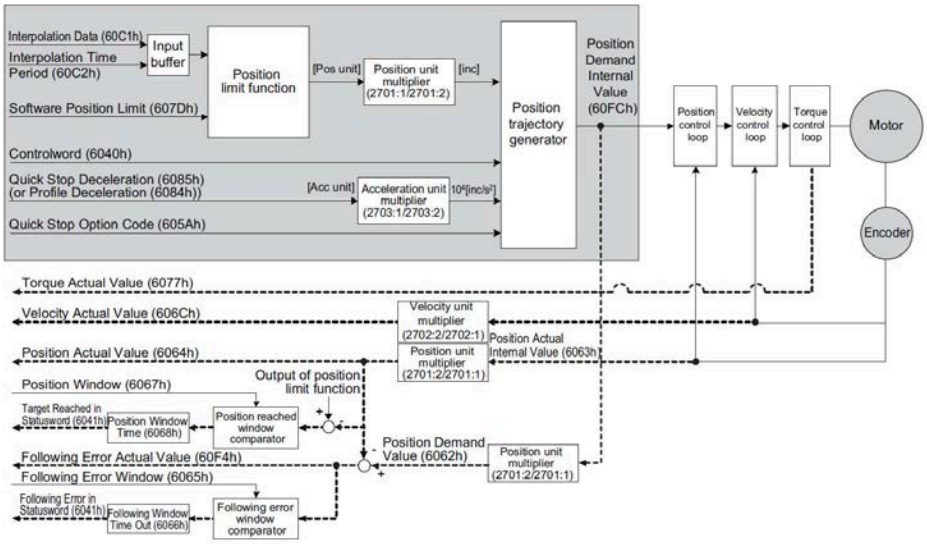

Figure B-8: Interpolated Position mode

B-5-3 Cyclic Synchronous Position mode

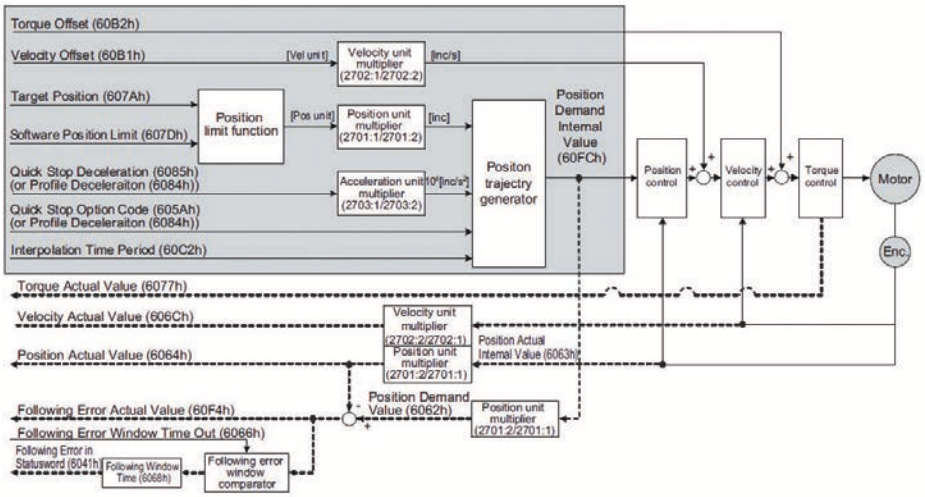

Figure B-9: Cyclic Synchronous Position mode

B-5-4 Homing mode

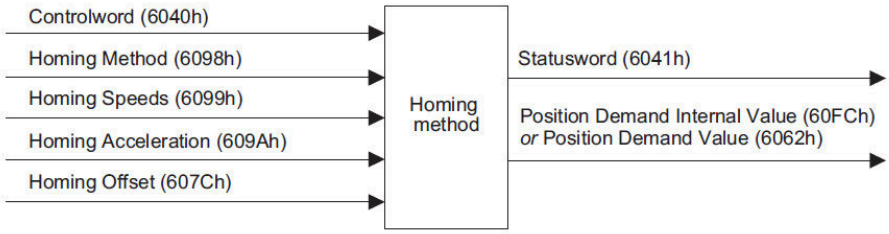

Figure B-10: Homing mode

B-5-5 Profile Velocity mode

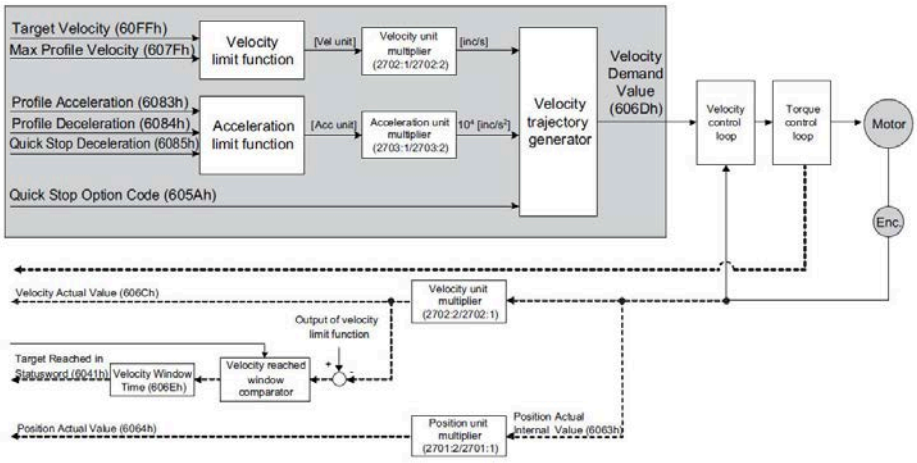

Figure B-11: Profile Velocity mode

B-5-6 Cyclic Synchronous Velocity mode

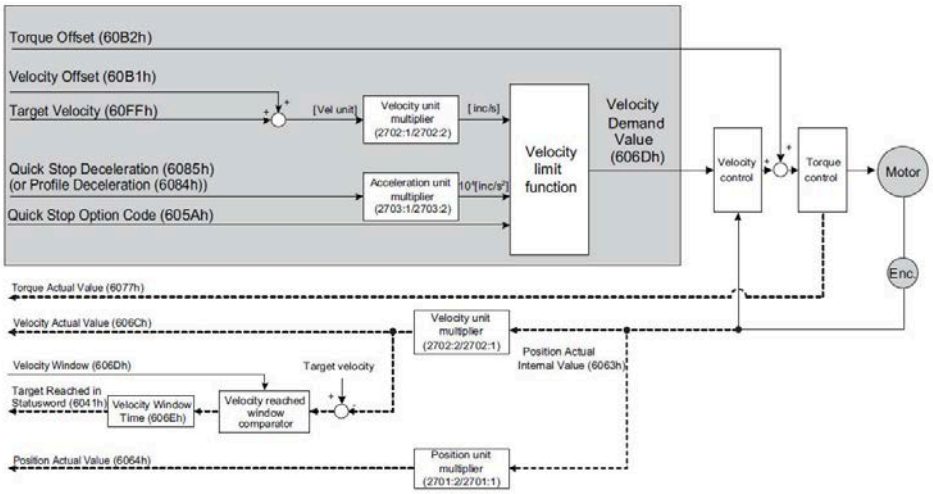

Figure B-12: Cyclic Synchronous Velocity mode

B-5-7 Torque Profile mode

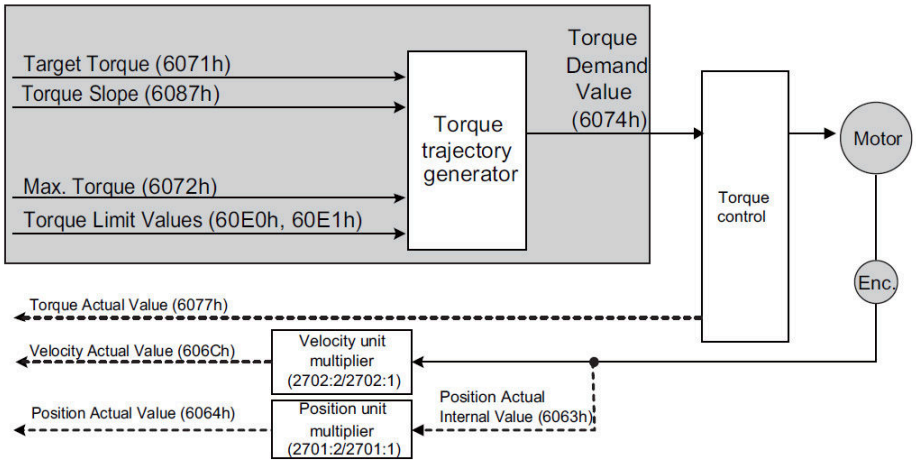

Figure B-13: Torque Profile mode

B-5-8 Cyclic Synchronous Torque mode

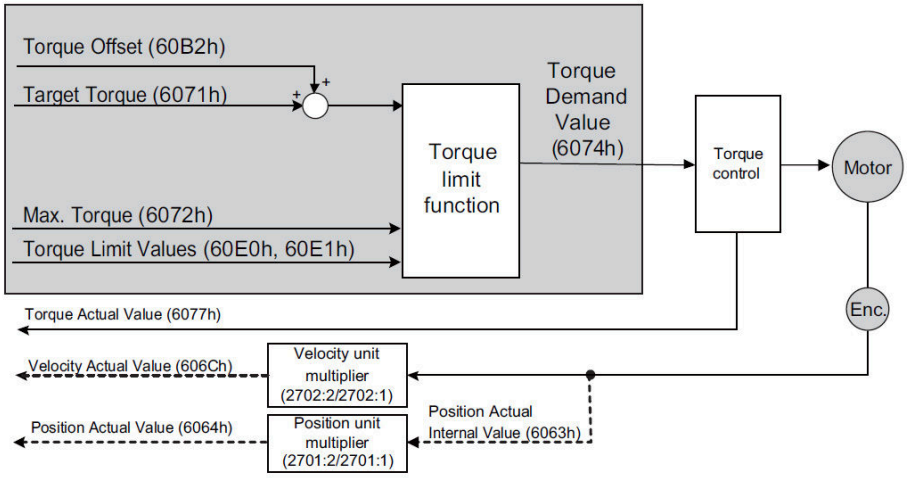

Figure B-14: Cyclic Synchronous Torque mode

According to the target torque, a cyclic synchronous torque mode could be a suitable solution. There are 2 important reasons not to choose this control mode.

1. The torque mode is an open loop and there is no coupling with the position in the servo-pack. This can be established outside the controller for example in a outer loop in DUECA. The DUECA environment is running at 4 kHz and the servo-pack on 1.6 kHz. The accuracy of the addition torque sensor and the inbuilt torque reference are not accurate enough for control.

2. Velocity mode is a closed loop in the servo-pack it self, it is more accurate also. To avoid the jerky effects on the pedal movement a smooth velocity mode is the best solution.

Appendix C

Practical Implementation

C-1 EMC

Electromagnetic compatibility EMC is the branch of electrical sciences which studies the accidental generation of electromagnetic energy with reference to the unwanted effects (Electromagnetic interference, or EMI) that such energy may induce.

EMC aims to ensure that equipment items or systems will not interfere with or prevent each other's correct operation through false emission and absorption of EMI. EMC is sometimes referred to as EMI Control, and in practice EMC and EMI are frequently referred to as a combined term "EMC/EMI". [24]

Electromagnetic interference divides several categories according to the source and signal characteristics. There are two types of interferences:

Continuous interference

Continuous, or Continuous Wave interference arises where the source continuously emits at a given range of frequencies. This type is naturally divided into sub-categories according to frequency range: Audio Frequency, Radio Frequency and Broadband noise.

Pulse or transient interference

Electromagnetic Pulse (EMP), also sometimes called Transient disturbance, arises where the source emits a short-duration pulse of energy. The energy is usually broadband by nature, although it often excites a relatively narrow-band damped sine wave response in the victim. Sources divide broadly into isolated and repetitive events.

In the servo motor situation this can be interpreted as:
Sources of isolated EMP events Switching action of electrical circuitry, including inductive loads such as relays, solenoids or electric motors power line surges/pulses
Sources of repetitive EMP events Regular pulse trains in a Electric Motor.

C-1-1 Coupling mechanisms

There are four basic coupling mechanisms: conductive, capacitive, magnetic or inductive, and radiative. Any coupling path can be broken down into one or more of these coupling mechanisms working together. For example the lower path in the diagram involves inductive, conductive and capacitive modes.

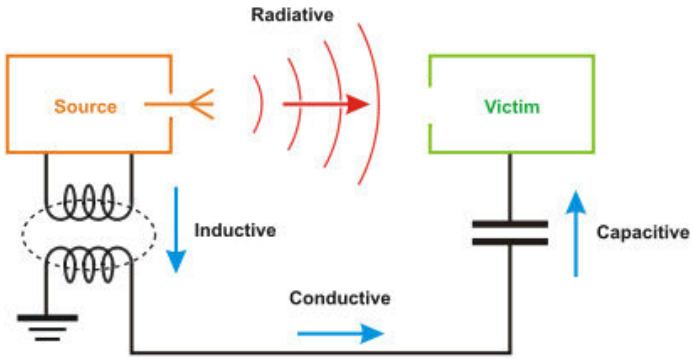

Figure C-1: The four electromagnetic interference (EMI) coupling modes

Conductive coupling

Conductive coupling occurs when the coupling path between the source and the receptor is formed by direct contact with a conducting body. For example a transmission line, wire, cable or metal enclosure. Conducted noise is also characterized by the way it appears on different conductors.

Inductive coupling

Inductive coupling occurs where the source and receiver are separated by a short distance. Strictly, "Inductive coupling" can be of two kinds; electrical induction and magnetic induction. It is common to refer to electrical induction as capacitive coupling, and to magnetic induction as inductive coupling.

Capacitive coupling

Capacitive coupling occurs when a varying electrical field exists between two adjacent conductors typically less than a wavelength apart, inducing a change in voltage across the gap.

Magnetic coupling

Inductive coupling or magnetic coupling occurs when a varying magnetic field exists between two parallel conductors typically less than a wavelength apart, inducing a change in voltage along the receiving conductor.

Radiative coupling

Radiative coupling or electromagnetic coupling occurs when source and victim are separated by a large distance, typically more than a wavelength. Source and victim act as radio antennas: the source emits or radiates an electromagnetic wave which propagates across the open space in between and is picked up or received by the victim.

C-1-2 EMC control

The damaging effects of electromagnetic interference pose unacceptable risks in many areas of technology, and it is necessary to control such interference and reduce the risks to acceptable levels. The control of electromagnetic interference (EMI) and assurance of EMC comprises a series of related disciplines.

Characterizing the threat

For characterization of the EMC, the following aspects need to be kept in mind: Interference source and signal; Coupling path to the victim; Behavior of the victim electrical and hardware malfunction.

Laws and regulators

Several international organizations work to promote international co-operation on standardization (harmonization), including publishing various EMC standards. Where possible, a standard developed by one organization may be adopted with little or no changes by others. This helps for example to harmonize national standards across Europe.

EMC design

Electromagnetic noise is produced in the source due to rapid current and voltage changes, and spread via the coupling mechanisms described earlier.

Grounding and shielding

Grounding and shielding aim to reduce emissions or divert EMI away from the victim by providing an alternative, low-impedance path. Techniques include Shielded housings. Shielded cables, where the conducting wires are surrounded by an outer conductive layer that is grounded at one or both ends.

EMC testing

Emissions are typically measured for radiated field strength and where appropriate for conducted emissions along cables and wiring. Inductive (magnetic) and capacitive (electric) field strengths are near-field effects and are only important if the device under test is designed for location close to other electrical equipment. Some pulse emissions are more usefully characterized using an oscilloscope to capture the pulse waveform in the time domain.

C-2 Skin effect

The skin effect is the phenomenon of the flow of an alternating current in a cylindrical conductor, the current density increase from inside to the outside of the conductor.

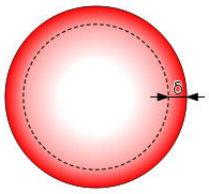

Figure C-2: Skin depth of the conductor

Distribution of current flow in a cylindrical conductor is shownn in cross sectionin Figure C-3. For alternating current, most (63%) of the electrical current flows between the surface and the skin depth, δ, which depends on the frequency of the current and the electrical and magnetic properties of the conductor. [25] Skin depth is due to the circulating eddy currents cancelling the current flow in the center of a conductor and reinforcing it in the skin.

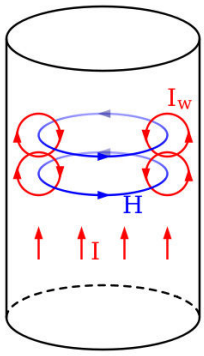

Figure C-3: Skin depth due to the circulating eddy currents

The skin effect therefore plays a particularly important role in radio frequency (RF) alternating currents, see the following figures. At a frequency of 50 Hz, the penetration depth of copper is approximately 1 cm, at 10 kHz less than 1 mm, and 10 MHz only 20 microns, this means that the current is actually run only at the surface in this latter frequency. The consequence of the skin effect is that the resistance of a conductor increases strongly at higher frequencies. Therefore it is better to work in HF technology with hollow conductors.

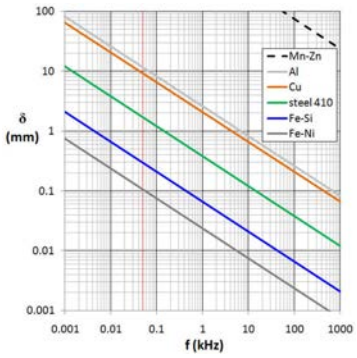

Figure C-4: Skin depth as function of frequency and thickness conductor material

The AC current density J_{AC} in a conductor decreases exponentially from its value at the surface J_S according to the depth d from the surface, as follows:

$$J_{AC} = J_S \cdot e^{-d/\delta} \tag{C-1}$$

δ = skin depth is the depth below the surface of the conductor at which the current density has fallen to 1/e of J_S [m]
J_{AC} = AC current density [A $\cdot$ m^2]
J_S = current density at the surface [A $\cdot$ m^2]
d = depth [m]

The skin depth is thus defined as the depth below the surface of the conductor at which the current density has fallen to 1/e (about 0.37) of J_S. In normal cases it is well approximated as:

$$\delta = \sqrt{\frac{2 \cdot \rho_r}{\omega \cdot \mu}} \tag{C-2}$$

ρ_r = resistivity of the conductor [$\Omega\cdot$ m]
ω = angular frequency of current [rad/s]
μ = absolute magnetic permeability of the conductor [Wb/(A $\cdot$ m)]

A proper way to solve the skin effect of the electrical servo drive is a stranded/braided wire. Stranded wire is more flexible than solid wire of the same total cross-sectional area. At high frequencies, current travels near the surface of the wire because of the skin effect, resulting in increased power loss in the wire. Stranded wire might seem to reduce this effect, since the total surface area of the strands is greater than the surface area of the equivalent solid wire, but ordinary stranded wire does not reduce the skin effect because all the strands are short-circuited together and behave as a single conductor. A stranded wire will have higher resistance than a solid wire of the same diameter because the cross-section of the stranded wire is not all copper. There are unavoidable gaps between the strands. A stranded wire with the same cross-section of conductor as a solid wire is said to have the same equivalent gauge and is always a larger diameter. For better performance at high frequencies, litz wire, which has the individual strands insulated and twisted in special patterns, may be used.

Alleviation

A type of cable called litz wire (from the German Litzendraht) is used to mitigate the skin effect for frequencies of a few kilohertz to about one megahertz. It consists of a number of insulated wire strands woven together in a carefully designed pattern, so that the overall magnetic field acts equally on all the wires and causes the total current to be distributed equally among them. With the skin effect having little effect on each of the thin strands, the bundle does not suffer the same increase in AC resistance that a solid conductor of the same cross-sectional area would due to the skin effect. Litz wire is often used in the windings of high-frequency transformers to increase their efficiency by mitigating both skin effect and proximity effect. Large power transformers are wound with stranded conductors of similar construction to litz wire, but employing a larger cross-section corresponding to the larger skin depth at mains frequencies.

C-3 Results Signal-Noise-Ratio after alleviation Skin effect

Here you can see the results of the alleviation of the skin effect. frame, back plate is grounded with a litz. The signal noise ratio of the torque sensor is $\approx 500/3 = 166.7$. The overall accuracy class of the HBM torque sensor is 0.5%. The inbuilt torque estimation in the servo pack has a little better theoretical performance of 0.1% of the rated torque. The absolute noise become theoretical 0.25 Nm.

Figure C-5: Litze (stranded wire)

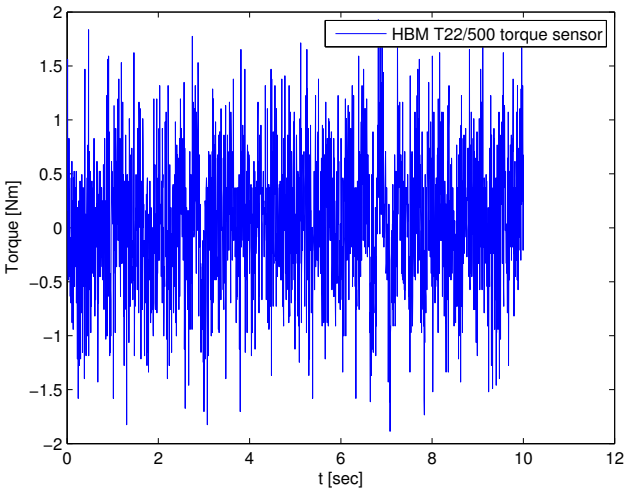

Figure C-6: Effect of ground litze on Signal-Noise-Ratio torque sensor

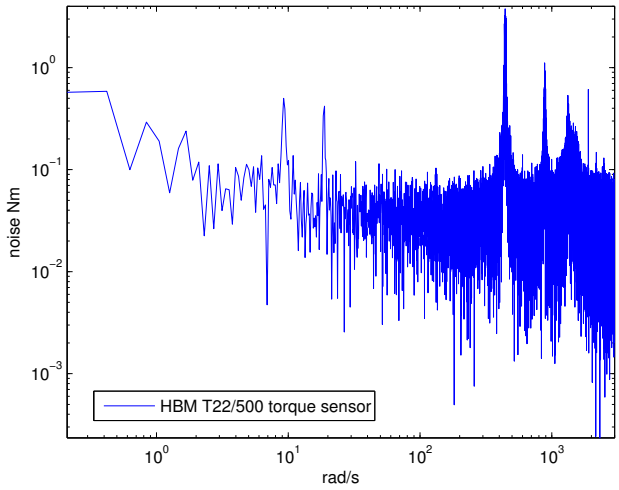

Figure C-7: fft torque sensor without litze

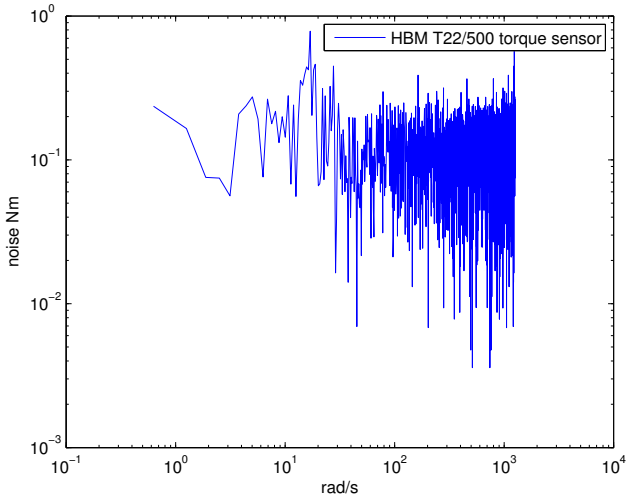

Figure C-8: fft torque sensor with litze

C-4 Data Acquisition

The sample rate of the control loop is at least 2 kHz. When we calculate the maximum allowed frequency is 20 times the dominant frequency. This specific value is proposed by Åström and Wittenmark in their work of computer control design. At 2 kHz, the maximum dominant frequency is: $((1/2000)/20)^{-1} = 100$ Hz.

A high accuracy sensor will improve the results in signal-noise-ratio effect. 4 bit noise is commonly taken as a minimum oversampling rate. In signal processing, oversampling is the process of sampling a signal with a sampling frequency significantly higher than twice the bandwidth or highest frequency of the signal being sampled. Oversampling helps avoid aliasing, improves resolution and reduces noise.

C-4-1 Oversampling factor

An oversampled signal is said to be oversampled by a factor of β, defined as

$$\beta = \frac{f_s}{2 \cdot B} \tag{C-3}$$

or

$$f_s = 2 \cdot \beta \cdot B \tag{C-4}$$

where: fs is the sampling frequency B is the bandwidth or highest frequency of the signal; the Nyquist rate is 2·B.

There are three main reasons for performing oversampling:

Anti-aliasing

Oversampling can make it easier to realize analog anti-aliasing filters. Without oversampling, it is very difficult to implement filters with the sharp cutoff necessary to maximize use of the

available bandwidth without exceeding the Nyquist limit. By increasing the bandwidth of the sampled signal, design constraints for the anti-aliasing filter may be relaxed. Once sampled, the signal can be digitally filtered and down sampled to the desired sampling frequency. In modern integrated circuit technology, digital filters are easier to implement than comparable analog filters.

Resolution

In practice, oversampling is implemented in order to achieve cheaper higher-resolution A/D and D/A conversion. For instance, to implement a 24-bit converter, it is sufficient to use a 20-bit converter that can run at 256 times the target sampling rate. Combining 256 consecutive 20-bit samples can increase the signal-to-noise ratio by a factor of 16 (the square root of the number of samples averaged), adding 4 bits to the resolution, producing a single sample with 24-bit resolution.

The number of samples required to get n bits of additional data precision is:

$$NumSamples = (2^n)^2 = 2^{2n} \tag{C-5}$$

The sum of 2^{2n} samples is divided by 2^n to get the mean sample scaled up to an integer with n additional bits:

$$result = \frac{sum(Data)}{2^n} \tag{C-6}$$

Note that this averaging is possible only if the signal contains perfect equally distributed noise which is enough to be measured by the A/D converter. If not, all 2^n samples will have the same value, the average will be identical to this value, and the oversampling will have no effect, so the conversion result will be as inaccurate as if it had been measured by the low-resolution core A/D. This is an interesting counter-intuitive example where adding some dithering noise can improve the results instead of degrading them.

Noise

If multiple samples are taken of the same quantity with uncorrelated noise added to each sample, then averaging N samples reduces the noise power by a factor of 1/N. If, for example, we oversample by a factor of 4, the signal-to-noise ratio in terms of power improves by factor of 4 which corresponds to a factor of 2 improvement in terms of voltage.

C-5 EtherCAT Implementation

The choice of digital fast communication is made to avoid noise on the input signal to the servo-pack. EtherCAT is chosen for several reasons: fast communication bus, open high performance Ethernet-based fieldbus system, require short data update times (cycle times) with low communication jitter, worldwide used and supported, low hardware costs. For setting up the EtherCAT communication, the documentation of Martin Rostan [26], Peter Domburg [27] and the EtherCAT manual of Yaskawa [28] has been consulted.

EtherCAT Introduction

Typical automation networks are characterized by short data length per node, typically less than the minimum payload of an Ethernet frame. Using one frame per node per cycle therefore leads to low bandwidth utilization and thus to poor overall network performance. EtherCAT therefore takes a different approach, called "processing on the fly".

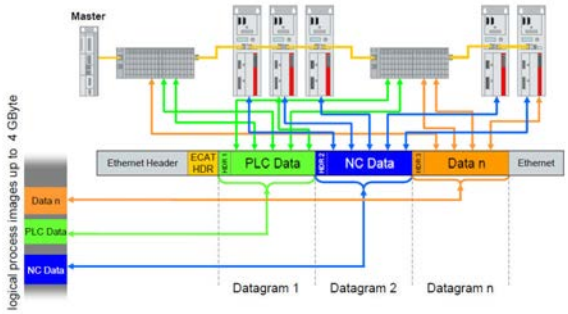

Figure C-9: EtherCAT Mapping moved into Slave Devices

The reaction time of the EtherCAT nodes is very fast within maximum 2 data tasks.

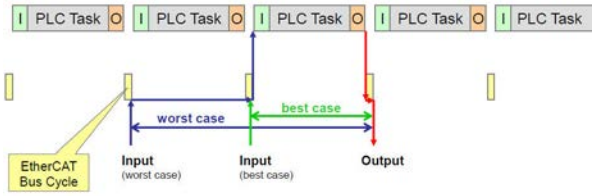

Figure C-10: Reaction time of EtherCAT

In Figure C-11 the data flow schematic is shown. It is like a train with passengers moving on and off the train. The total data length is not fixed.

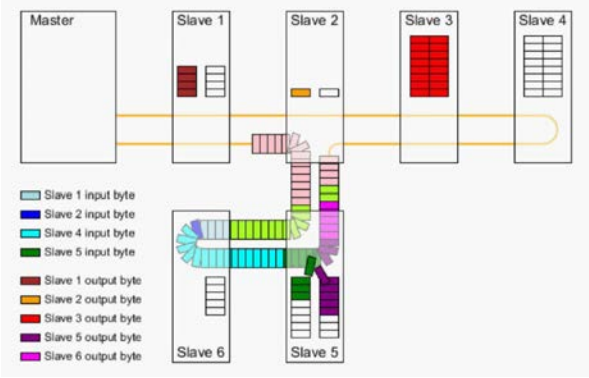

Figure C-11: Ethernet "on-the-fly", ideal bandwidth utilization for maximum performance

Functional Principle

With EtherCAT, the Ethernet packet or frame is no longer received, then interpreted and copied as process data at every node. The EtherCAT slave devices read the data addressed to them while the telegram passes through the device. Similarly, input data are inserted while the telegram passes through. The frames are only delayed by a fraction of a microsecond in each node, and many nodes - typically the entire network - can be addressed with just one frame.

EtherCAT Protocol

The EtherCAT protocol is optimized for process data and is transported directly within the standard IEEE 802.3 Ethernet frame using Ethertype 0x88a4. It may consist of several sub-telegrams, each serving a particular memory area of the logical process images that can be up to 4 gigabytes in size. The data sequence is independent of the physical order of the nodes in the network; addressing can be in any order. Broadcast, multicast and communication between slaves are possible and must be done by the master device. If IP routing is required, the EtherCAT protocol can be inserted into UDP/IP datagrams. This also enables any control with Ethernet protocol stack to address EtherCAT systems.

Performance

Short cycle times can be achieved since the host microprocessors in the slave devices are not involved in the processing of the Ethernet packets to transfer the process images. All process data communication is handled in the slave controller hardware. Combined with the functional principle this makes EtherCAT a high performance distributed I/O system.

Topology

Using full-duplex Ethernet physical layers, the EtherCAT slave controllers close an open port automatically and return the Ethernet frame if no downstream device is detected. Slave devices may have two or more ports. Due to these features EtherCAT can support almost any physical topology such as line, tree or star. The bus or line structure known from the fieldbusses thus also becomes available for Ethernet.

Synchronization

For synchronization a distributed clock mechanism is applied, which leads to very low jitters of significantly less than 1 micro second, even if the communication cycle jitters, which is equivalent to the IEEE 1588 Precision Time Protocol standard. Therefore EtherCAT does not require a special hardware in the master device and can be implemented in software on any standard Ethernet MAC, even without dedicated communication coprocessor. To keep the clocks synchronized after initialization, the master or slave must regularly send out the broadcast again to counter any effects of speed difference between the internal clocks of each slave. Each slave should adjust the speed of their internal clock or implement an internal

correction mechanism whenever they have to adjust. The system clock is specified as a 64 bit counter with a base unit of 1 ns starting at January 1, 2000, 0:00.

Device profiles

The device profiles describe the application parameters and the functional behavior of the devices including the device class-specific state machines. For many device classes, fieldbus technology already offers reliable device profiles, for example for I/O devices, drives or valves. EtherCAT supports both the CANopen device profile family as well as the drive profile known as the Sercos drive profile. Since the application view does not change when migrating from CANopen or Sercos, this assists users and device manufacturers alike.

Functional safety

The protocol enhancement called Safety over EtherCAT enables safety-related communication and control communication on the same network. The safety protocol is based on the application layer of EtherCAT, without influencing the lower layers. It is certified according to IEC 61508 and meets the requirements of Safety Integrity Level (SIL). Certified products using the Safety over EtherCAT protocol have been available since 2005.

Gateways

For integration of existing fieldbus components (e.g., CANopen, DeviceNet, Profibus) into EtherCAT networks gateway devices are available. Also other Ethernet protocols can be used in conjunction with EtherCAT: The Ethernet frames are tunneled via the EtherCAT protocol, which is the standard approach for internet applications (e.g. VPN, PPPoE (DSL) etc.). The EtherCAT network is fully transparent for the Ethernet device, and the real-time characteristics are not impaired since the master dictates exactly when the tunneled transfers are to occur and how much capacity of the 100Mbit/s media the tunneled protocols can use. All internet technologies can therefore also be used in the EtherCAT environment: integrated web server, e-mail, FTP transfer etc.

Implementation

Master can be implemented in software on any standard Ethernet MAC. Several vendors supply code for different operating systems. There are also several open and shared source implementations. For slave devices special EtherCAT slave controller chips are required in order to perform the "processing on the fly" principle. EtherCAT slave controllers are available as code for different FPGA types and are also available as ASIC implementations.

EtherCAT Technology Group

The EtherCAT Technology Group (ETG) is international user and vendor organization headquartered in Nuremberg (Germany). It was founded in November 2003 and has offices in

Tokyo (Japan), Beijing (China), Seoul (Korea), and Austin, Tx (USA). As of June 2010, it has over 1350 member companies from 50 countries. The ETG considers itself to be a forum for end users from different sectors, and for machine manufacturers and suppliers of control technology with the aim of supporting and promoting EtherCAT. The ETG provides information about EtherCAT and its application, organizes technical training classes, has technical and marketing committees, and promotes EtherCAT on trade shows in major industrial markets.

International standardization

The EtherCAT Technology Group is an official liaison partner of the IEC (International Electrotechnical Commission) working groups for digital communication. The EtherCAT specification was published as IEC/PAS 62407 in 2005, which was removed end of 2007 since EtherCAT had been integrated into the international fieldbus standards IEC 61158 and IEC 61784-2 as well as into the drive profile standard IEC 61800-7.

C-5-1 CANopen over Ethernet (CoE) in the Yaskawa drive

CANopen is the standardization in the Yaskawa drive, the figure below show the OSI layer structure.

C-5-2 Linux Etherlab Communication

The procedure to install EtherLab has to be followed very thoroughly to be able to use for OS Linux kernel 2.6. The manual of IgH is very helpful. [29] [30]

C-6 CANopen

6.1 CANopen over EtherCAT Device Architecture

The following figure shows the device architecture of the SGDV CANopen over the EtherCAT (CoE) Network Module.

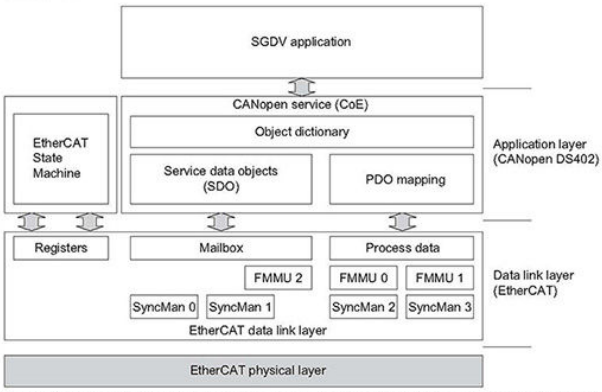

The EtherCAT (CoE) Network Module is composed of the EtherCAT communication in the data link layer and CANopen drive profile (DS402) in the application layer.
The object dictionary in the application layer includes parameters, application data, and PDO mapping information between the process data interface and the application data.

The process data object (PDO) is composed of objects in the object dictionary that can be mapped to the PDO, and the content of the process data is defined by the PDO mapping.
The process data communication is cyclic communication to write and read the PDO. The mailbox communication (SDO) is acyclic communication to write and read the data entry in the object dictionary.

Note 1. The EtherCAT (CoE) Network Module does not support EtherCAT ReadWrite commands (APRW, FPRW, BRW, LRW).
2. For SDO and PDO communication via EtherCAT data link layer, FMMU and Sync Manager have to configure as follows:

• Sync Manager Settings

Sync Manager	Assignment (Fixed)	Size	Start Address (Fixed)
Sync Manager 0	Assigned to Receive Mailbox	128byte (fixed)	0x1000
Sync Manager 1	Assigned to Transmit Mailbox	128byte (fixed)	0x1080
Sync Manager 2	Assigned to Receive PDO	0 to 200byte	0x1100
Sync Manager 3	Assigned to Transmit PDO	0 to 200byte	0x1358

• FMMU Settings

FMMU	Settings
FMMU 0	Mapped to Receive PDO
FMMU 1	Mapped to Transmit PDO
FMMU 2	Mapped to Fill Status of Transmit Mailbox

Figure C-12: CANopen over EtherCAT Device Architecture

6.3 EtherCAT State Machine

The EtherCAT State Machine (ESM) is responsible for the coordination of master and slave applications at start up and during operation. State changes are typically initiated by requests of the master.
The states of the EtherCAT State Machine are as follows.

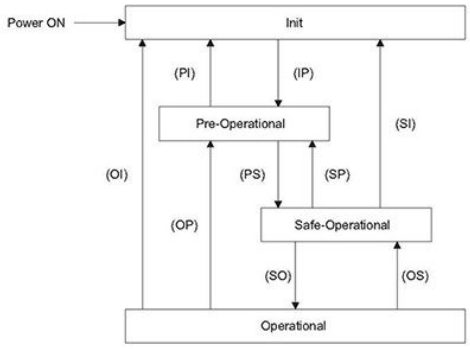

State	Description
Init	• No mailbox communication is possible. • No process data communication is possible.
Init to Pre-Op	• Master configures DL Address and SyncManager channels for Mailbox communication. • Master initializes DC clock synchronization. • Master requests 'Pre-Operational' state. • Master sets AL Control register. • Slave checks whether the mailbox was initialized correctly.
Pre-operational (Pre-Op)	• Mailbox communication is possible. • No process data communication is possible.
Pre-Op to Safe-Op	• Master configures SyncManager channels and FMMU channels for process data. • Master configures PDO mapping and the sync manager PDO assignment parameters via SDO. • Master requests 'Safe-Operational' state. • Slave checks whether the sync manager channels for process data communication and, if required, the distributed clocks settings are correct.
Safe-Operational (Safe-Op)	• Mailbox communication is possible. • Process Data communication is possible, but only Inputs are evaluated – Outputs remain in 'Safe' state.
Safe-Op to Op	• Master sends valid Outputs. • Master requests 'Operational' state.
Operational (Op)	• Mailbox communication is possible. • Process data communication is possible.

6-4

Figure C-13: EtherCAT State Machine

CANopen is a communication protocol and device profile specification for embedded systems used in automation. In terms of the OSI model, CANopen implements the layers above and including the network layer. The CANopen standard consists of an addressing scheme, several small communication protocols and an application layer defined by a device profile. The communication protocols have support for network management, device monitoring and communication between nodes, including a simple transport layer for message segmentation/desegmentation. The lower level protocol implementing the data link and physical

layers is usually Controller Area Network (CAN), although devices using some other means of communication (such as Ethernet Powerlink, EtherCAT) can also implement the CANopen device profile.

The basic CANopen device and communication profiles are given in the CiA 301 specification released by CAN in Automation. Profiles for more specialized devices are built on top of this basic profile, and are specified in numerous other standards released by CAN in Automation, such as CiA 401 for I/O-modules and CiA 402 for motion control.

Device Model

Every CANopen device has to implement certain standard features in its controlling software.

- A **communication unit** implements the protocols for messaging with the other nodes in the network
- Starting and resetting the device is controlled via a **state machine**. It must contain the states Initialization, Pre-operational, Operational and Stopped. The transitions between states are made by issuing a network management (NMT) communication object to the device.
- The **object dictionary** is an array of variables with a 16-bit index. Additionally, each variable can have an 8-bit subindex. The variables can be used to configure the device and reflect its environment, i.e. contain measurement data.
- The **application** part of the device actually performs the desired function of the device, after the state machine is set to the operational state. The application is configured by variables in the object dictionary and the data are sent and received through the communication layer.

C-6-1 Service Data Object (SDO) protocol

The SDO protocol is used to set and read values from the object dictionary of a remote device. The device whose object dictionary is accessed is the SDO server and the device accessing the remote device is the SDO client. The communication is always initiated by the SDO client. In CANopen terminology, communication is viewed from the SDO server, so that a read from an object dictionary results in an SDO upload and a write to dictionary is an SDO download.

C-6-2 Process Data Object (PDO) protocol

Too check the settings of the controller, the program Twincat is very useful. [31] The Process Data Object protocol is used to process real time data among various nodes. You can transfer up to 8 bytes (64 bits) of data per one PDO either from or to the device. One PDO can contain multiple object dictionary entries and the objects within one PDO are configurable using the mapping and parameter object dictionary entries. There are two kinds of PDOs: transmit and receive PDOs (TPDO and RPDO). In the pre-defined connection set there are identifiers for four TPDOs and four RPDOs available. With configuration 512 PDOs are possible. PDOs can be sent synchronously or asynchronously.

C-7 Safety Rudder Pedal System

The safety environment is built around the drive system. Where in the old hydraulic situation a less sufficient safety environment is taking care of the subject during the experiment, the new electric servo drive system has full control over the behavior of the pedals. This is more satisfying than the hydraulic situation. In the worst case scenario, a broken signal cable to the hydraulic valve will cause a maximal displacement in one direction at full acceleration and at maximum power. A fault in the input signal to the servo drive will cause an error detected by at least the servo pack and will result in a soft emergency stop by switching off the power to the motor directly. After the emergency stop, the mechanical system can be moved in both directions forward and backward without any motor resistance. To get an overview of the safety environment, the safety is grouped in several layers.

C-7-1 Hardware layer

First the basal, basic safety is secured by mechanical soft end bumps at the drive shaft. On the electric power side, the emergency button switches off the power contactor of the motor directly via a safety contacter. The feedback contacts (open or closed) of the power contactor provides the status of the contactor to the safety contactor. Communication with the servo pack is possible to be able to provide information of the rudder system.

C-7-2 Servo pack layer

Second by two normally open proximity end switches. When one of both switches are opened, the Hardware Base Block (HBB) in the servo pack becomes active. The servo pack inbuilt power contactor of the power line to the motor will be opened. Without any reset command to the servo pack it is not possible to change the position of the motor.

C-7-3 Software environment layer

Third, several software limitations are realized. There are software end stops at position, a rate limitation on acceleration, a maximum torque limit and so on. The last added safety function that is added is a maximum energy difference. In a moving time window, the energy of the reference signal and the actual output are compared to avoid any oppression.

Appendix D

Calibration

D-1 Calibration setup torque transducer

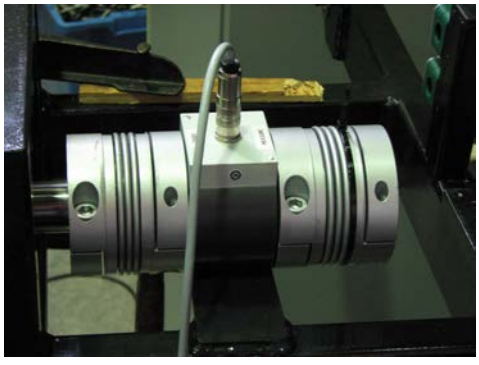

Figure D-1: Impression of the installed torque transducer

Figure D-2: Calibration of the torque transducer

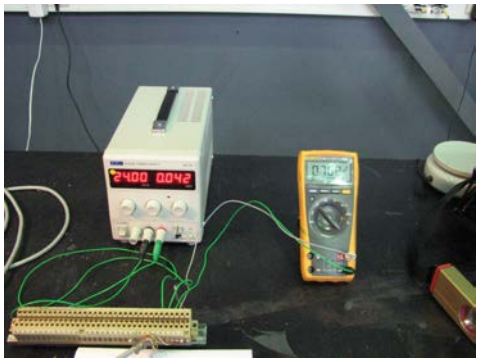

Figure D-3: Display of output during calibration

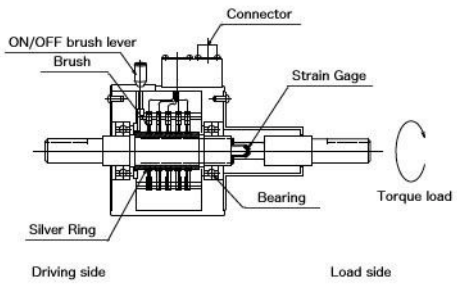

Figure D-4: Crosssection of a generic torque transducer

D-2 Calibration torque transducer

Table D-1: Torque transducer

Force [N]	Lever [m]	Torque [Nm]	Output [VDC]
0.00	0.550	0.00	0.000
4.91	0.550	2.70	0.026
9.81	0.550	5.40	0.054
14.72	0.550	8.10	0.082
19.62	0.550	10.79	0.109
24.53	0.550	13.49	0.135
29.43	0.550	16.19	0.162
34.34	0.550	18.88	0.189
39.24	0.550	21.58	0.216
44.15	0.550	24.28	0.242
49.05	0.550	26.98	0.270
53.96	0.550	29.68	0.297
58.86	0.550	32.37	0.323
63.77	0.550	35.07	0.351
68.67	0.550	37.77	0.378
73.58	0.550	40.47	0.405
78.48	0.550	43.16	0.433
83.39	0.550	45.86	0.459
88.29	0.550	48.56	0.485
93.20	0.550	51.26	0.512
98.10	0.550	53.96	0.540
103.01	0.550	56.65	0.567
107.91	0.550	59.35	0.594
112.82	0.550	62.05	0.622
117.72	0.550	64.76	0.650
122.63	0.550	67.44	0.677
127.53	0.550	70.14	0.704

Bibliography

[1] T. Oetiker, *The Not So Short Introduction to LaTeX*. Swiss Federal Institute of Technology, 2001.

[2] M. M. van Paassen, *A model of the neuromuscular system of the pilot's arm*. PhD thesis, Delft University of technology, 1994.

[3] E. C. Stewart, "A piloted simulator evaluation of transport aircraft rudder pedal force/feel characteristics," 2008.

[4] "Flight controls: How an airplane is controlled." http://www.free-online-private-pilot-ground-school.com/Flight_controls.html, cited January 2013.

[5] "http://www.navyaviation.tpub.com aviation structural mechanic." http://www.navyaviation.tpub.com/14018/css/14018_349.htm, cited January 2013.

[6] R. Hess, "Certification standards and design issues for rudder control systems in transport aircraft," 2008.

[7] R. Hess, "Metrics for the evaluation of pedal force/feel systems in transport aircraft," 2008.

[8] E. Edge, *Gear Drive Motor Moment of Inertia Equation*. engineersedge, 2012.

[9] Yaskawa, "Ac servo drives sigma-5 series, product catalog."

[10] A. Dynamics, "planetary gearbox ab-series."

[11] A. Gerretsen, "Alternative control loading architectures," 2005.

[12] A. Damman and H. Schutte, "Design of a motor controller," 2010.

[13] C. van den Eijnden, "Servo control," 2010.

[14] R. Firoozian, *Servo Motors and Industrial Control Theory*. Springer, 2009.

[15] A. Bradley, *Drives Engineering Handbook*. Rockwell Automation, 2004.

[16] E. Tazelaar, "Non linear control," 2011.

[17] Robbins and Myers, *DC Motors and Speed Controls Servo Systems*. Electro-Craft Minnesota, 1980.

[18] Mathworks, "Dc motor control," 2012.

[19] R. van der Linde, P. Lammertse, and B. Ruiter, "The hapticmaster, a new high-performance haptic interface," 2001.

[20] Parker, "Integrator servo drive compax3.".

[21] Parker, "St direct drive servomotors," 2008.

[22] Yaskawa, "Sgmcs direct drive sigma series servo product catalog."

[23] N. N. Instituut, *NEN 3508 Staalkabels, schijven en trommels voor hijs en transport-doeleinden*. NEN instituut, 1988.

[24] T. Hubing and N. Hubing, "Learn emc," 2013.

[25] W. Hayt, *Engineering Electromagnetics Seventh Edition*. McGraw Hill, New York, 2006.

[26] "Ethercat: Ethernet fieldbus for mechatronic systems." 2012.

[27] "Work shop ethernet." 2012.

[28] Yaskawa, *AC Servo Drives sigma-5 series, User's Manual Ethercat*, 2009.

[29] D. J. Barrett, *Linux pocket guide*. O'Reilly Media, 2004.

[30] F. Pose, *IgH Ethercat Master 1.5.0 Documentation*. IgH Essen, 2010.

[31] L. Theunis, "snelgids twincat," 2007.

List of Figures

1-1 Rudder pedals Fokker 50 2
1-2 Original situation rudder pedals hinge system HMI-laboratory 2
1-3 Control loop HAN 3

2-1 Rudder Control Aircraft [4] 7
2-2 Hydraulic Servo Rudder Control Aircraft [5] 9
2-3 Pedal Characteristics (Force-Deflection) [6] 10
2-4 Comparison of Pedal Force/Feel Systems, AH-64A and Airbus A300-600 [6] . . . 11
2-5 Comparison of Pedal Force/Feel Systems, UH-60A and Airbus A300-600 [6] . . . 11
2-6 Comparison of Pedal Force/Feel Systems, CH-47D and Airbus A300-600 [6] . . . 12
2-7 Comparison of Pedal Force/Feel Systems, CH-53D and Airbus A300-600 [6] . . . 12
2-8 Comparison of Pedal Force/Feel Systems, B-767 and Airbus A300-600 [6] 12
2-9 Comparison of Pedal Force/Feel Systems, Airbus A300-B2-B4 and A300-600 [6] . 13
2-10 Example of the Effect Dynamic Characteristics of Force/Feel System with Sinusoidal Inputs of Different Frequency [7] 13
2-11 Example of the Effect Dynamic Characteristics of Force/Feel System with Sinusoidal Inputs of Different Frequency [7] 14
2-12 Example of the Effect of Force/Feel System Dynamics and Rudder Actuator Characteristics on Pedal Force vs Rudder Position for Force/Feel System [7] 14

3-1 First force lever of at the rudder pedals 18
3-2 Second force lever of at the rudder pedals 18
3-3 Torque characteristics of the motor SGMGV-13D 19

3-4 Alternative solution 4 proposed gearing via planetary gearbox on an electric servo direct drive . . . 20
3-5 Drawing alternative solution 4 . . . 20
3-6 Inertia calculation of current pedal system . . . 21
3-7 Inertia calculation of drive system . . . 21
3-8 Results of measurement gainplot . . . 22
3-9 Results of measurement phaseplot . . . 22

4-1 Mass Spring Damper system . . . 26
4-2 Bodeplot of the FCS mass-spring-damper model . . . 27
4-3 Control loading system layout . . . 27
4-4 Hydraulic servo model . . . 30
4-5 Hydraulic position loop . . . 31
4-6 Hydraulic velocity loop . . . 31
4-7 Hydraulic force loop . . . 32
4-8 Schematic complete hydraulic control loop . . . 32
4-9 Bode plot bare hydraulic actuator model with a velocity loop . . . 33
4-10 Hydraulic bode plot position loop (Simulink Result) . . . 33
4-11 Hydraulic bode plot velocity loop (Simulink Result) . . . 34
4-12 Hydraulic bode plot force loop (Simulink Result) . . . 35
4-13 Hydraulic position loop (Simulink Result) . . . 36
4-14 Hydraulic velocity loop (Simulink Result) . . . 36
4-15 Hydraulic force loop (Simulink Result) . . . 37
4-16 Schematic 3 phase brushless servomotor . . . 38
4-17 Simplified model brushless servomotor conform [17] . . . 39
4-18 Results of 400 V step input feed to the simplified model of the servomotor . . . 40
4-19 Results of 400 V profile feed to the simplified model of the servomotor . . . 40
4-20 Bodeplot of design of a simplified model brushless servomotor . . . 41
4-21 Model of a DC motor . . . 42
4-22 Model of voltage control loop of a DC motor . . . 42
4-23 Step response of simplified model brushless servomotor . . . 43
4-24 Model of feedforward control . . . 44
4-25 Plot of disturbance on a simplified model brushless servomotor closed loop . . . 44
4-26 Model of feedback control . . . 45

4-27 Rootlocus plot of simplified model brushless servomotor 45
4-28 Plot of disturbance on a simplified model brushless servomotor feedback and feed-forward 46
4-29 Model of linear-quadratic regulator (LQR) control 46
4-30 Bodeplot of design of a simplified model brushless servomotor 47
4-31 Plot of disturbance on a simplified model brushless servomotor LQR 47
4-32 Design of a simplified synchronous brushless servomotor model 48
4-33 Bodeplot of velocity control loop synchronous servomotor model 48
4-34 Acceleration during hard end stop simulation of the electrical servo system 375 N 49
4-35 Acceleration during hard end stop simulation of the electrical servo system 750 N 49
4-36 Bandwidth of sinusoidal cyclic velocity based on maximum acceleration 50
4-37 Comparison of a force sinus input response of a hydraulic and electrical servo system 51
4-38 Zoomed comparison of a force sinus input response of a hydraulic and electrical servo system 51

5-1 Impression of the experiment room 54
5-2 Impression wiring electrical cabinet 54
5-3 Impression EMC filter 55
5-4 Impression circular EMC clamp 55
5-5 Impression of the controlroom 56
5-6 Impression of the installed added mass 2 x 7.50 kg 56
5-7 Results of measurement start stop mode 57
5-8 Results of measurement cyclic without torque 58
5-9 Results of measurement start-up without torque 58
5-10 Results of measurement without torque in sinus mode 59
5-11 Results of measurement frequency response at 1300 RPM 59
5-12 Results of measurement without torque, single ended input 60
5-13 Results of measurement without torque, differential input 60
5-14 Results of sinusoidal velocity response with added mass 2Hz 132/30 rad/s 61
5-15 Results of sinusoidal velocity response with real human added mass 2Hz 132/30 rad/s 62
5-16 Results of sinusoidal velocity response with added mass 2Hz 132/30 rad/s 62
5-17 Results of measurement with full torque only left hand side 63
5-18 Results of measurement with added mass of limb 63

5-19 Results of measurement with added mass of limb following the sinus mode relaxed 64
5-20 Results of measurement without torque in sinus mode 64
5-21 The fundamental sinus and the following sinus signals with phase shift 65
5-22 Multi sinus repeated input signal with fade in and fade out 65
5-23 FFT of a multi sinus input signal of the relevant range 66
5-24 Control loop electric servo system with used components 67
5-25 Control loop servo system schematic flow 67
5-26 Results of multi sine velocity response 68

A-1 Alternative solution 1 proposed exchange hydraulic motor directly for an electric servo direct drive 73
A-2 Torque characteristics of the motor 300ST4M 74
A-3 Alternative solution 2 proposed gearing via a cable quadrant to an electric servo direct drive 75
A-4 Alternative solution 4 proposed gearing via planetary gearbox on an electric servo direct drive 77
A-5 Drawing alternative solution 4 77
A-6 Cost analysis of 4 offered alternative solutions 78

B-1 Overview components Yaskawa SGMGH 82
B-2 Specifications Yaskawa SGMGH 13A 400 Volt 83
B-3 Specifications APEX gearbox AB142-030-SGMGH 84
B-4 Overview wiring Yaskawa SGMGH 85
B-5 EtherCAT state flow 86
B-6 Yaskawa drive state flow 87
B-7 Profile Position mode 88
B-8 Interpolated Position mode 89
B-9 Cyclic Synchronous Position mode 89
B-10 Homing mode 90
B-11 Profile Velocity mode 90
B-12 Cyclic Synchronous Velocity mode 91
B-13 Torque Profile mode 91
B-14 Cyclic Synchronous Torque mode 92

C-1 The four electromagnetic interference (EMI) coupling modes 94

C-2 Skin depth of the conductor 96
C-3 Skin depth due to the circulating eddy currents 96
C-4 Skin depth as function of frequency and thickness conductor material 97
C-5 Litze (stranded wire) 98
C-6 Effect of ground litze on Signal-Noise-Ratio torque sensor 99
C-7 fft torque sensor without litze 99
C-8 fft torque sensor with litze 100
C-9 EtherCAT Mapping moved into Slave Devices 102
C-10 Reaction time of EtherCAT 102
C-11 Ethernet "on-the-fly", ideal bandwidth utilization for maximum performance . . . 102
C-12 CANopen over EtherCAT Device Architecture 106
C-13 EtherCAT State Machine 107

D-1 Impression of the installed torque transducer 111
D-2 Calibration of the torque transducer 112
D-3 Display of output during calibration 112
D-4 Crosssection of a generic torque transducer 112

List of Tables

2-1 Specific rudder pedal characteristics of 6 vehicle 11

4-1 Specific values considered for hydraulic simulation 29
4-2 Specific values considered for electrical motor SGMGV-13D simulation 39
4-3 Specific constants of the Physical motor 42

D-1 Torque transducer 113